Surface Defect Detection in Optical Fiber Using Image Processing

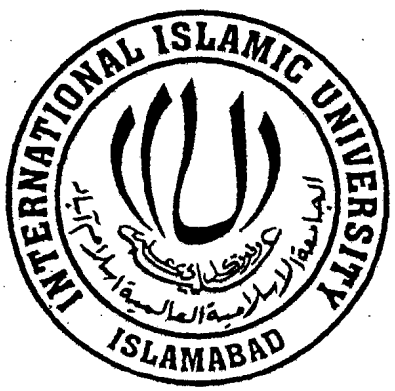

Developed by
Atique Rehman
Waheed Bin Mozaffar

Supervised by

Dr. Syed Afaq Hussain

Department of Computer Science
International Islamic University, Islamabad
(2007)

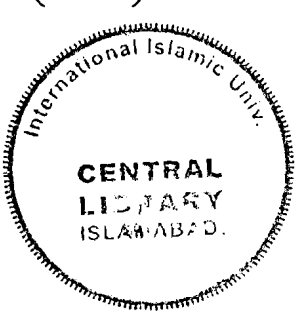

International Islamic University, Islamabad

Final Approval

It is certified that we have read the project report titled **"Surface Defect Detection in Optical Fiber Using Image Processing"** submitted by Mr. Atique Rehman and Mr. Waheed Bin Mozaffar. It is our judgment that this project is of sufficient standard to warrant its acceptance by the International Islamic University, Islamabad for the Masters of Science Degree in Computer Science (MS-CS).

Committee

Dated: 9-2-2008

External Examiner

Dr. Abdul Jalil
Associate Professor & Principal Scientist,
Dept. of Computer and Information Sciences,
PIEAS, Nilore.

Internal Examiner

Mr. Asim Munir
Assistant Professor, DCS,
International Islamic University,
Islamabad.

Supervisor

Dr. Syed Afaq Hussain
Dean (Former),
Faculty of Engineering and Technology,
International Islamic University,
Islamabad.

A dissertation submitted to the
Department of Computer Science,
International Islamic University, Islamabad
as a partial fulfillment of the requirements
for the award of the degree of
Masters of Science (MS)

DECLARATION

We, hereby declare that this research, neither as a whole nor as a part thereof has been copied out from any source. It is further declared that we have developed this Research and the accompanied report entirely on the basis of our personal efforts made under the sincere guidance of our teachers. If any part of this report is proved to be copied out or found to be reported, we shall standby the consequences. No portion of the work presented in this report has been submitted in support of any application for any other degree or qualification of this or any other university or institute of learning.

Atique Rehman
Reg # 98-CS/MS/02
Waheed Bin Mozaffar
Reg # 100-CS/MS/02

Dedication

This application is dedicated to our parents, our teachers without whose help, guidance and support, this project could not have been possible and last but not least, to the whole Muslim Ummah; may Allah enlighten our hearts to do something of even greater worth for our Ummah.

ACKNOWLEDGMENT

All praise to Almighty Allah, the most merciful and compassionate, who enabled us in completing and then presenting this project before you today.

In completing this project successfully, we were assisted by many sources, the most helpful of which came from our teachers and parents. Our teachers, especially our project supervisor Dr. Syed Afaq helped us a great deal in developing this project in a way that satisfies the standards. Our parents have always been helpful in our studies morally as well as financially but this support was more evident in this project of ours. Without their support, it would have been very difficult to complete this project with a whole hearted effort.

We would also like to acknowledge the help and guidance provided by our friends and seniors; they helped us in evaluating this project and provided us with technical support.

And last but not the least; we would like to thank Dr. Muid Mufti of University of Engineering and Technology, Texila for providing us with the images and Mr. Zia-ul-Haq Abbas of GIK Institute of Engineering Sciences and Technology, Topi for providing us with valuable help with regard to wavelets.

Atique Rehman
Reg # 98-CS/MS/02
Waheed Bin Mozaffar
Reg # 100-CS/MS/02

Project in Brief

Project Title:	Surface Defect Detection in Optical Fiber Using Image Processing
Organization:	Department of Computer Science, International Islamic University, Islamabad
Undertaken By:	Atique Rehman, Waheed Bin Mozaffar
Supervised By:	**Dr. Syed Afaq Hussain** Dean, Faculty of Engineering and Technology, International Islamic University, Islamabad
Tools Used:	C using Visual C++ 6.0 SDK and Matlab 7.0 GUIDE GUI.
Operating System:	Windows XP Professional
System Used:	IBM Compatible
Date Started:	March 2006
Date Completed:	July 2007

Abstract

In this project, a wavelet-based surface defect detection of optical fiber ferrules is proposed. Surface defects on optical fiber connectors can be detrimental to passing light signals when coupled with other optical fiber connectors. Defect free connectors are very important since these connectors couple very small cores and, unlike other connectors, do not make metal-to-metal contact. Our quality control enhancement work uses magnified images, whereby morphological operations segment the image and wavelet transforms such as Haar and the Daubechies transforms then detect defects on optical fiber connector surfaces to improve the overall acceptability of the connectors.

Table of Contents

Chapter Page no

1 INTRODUCTION

1.1 Optical Fibers

The Internet is the fastest growing technology on Earth today, and this is mainly possible because of fiber optics, the hair-thin glass wires that carry laser light communication signals around the globe.

The first commercial optical fiber network was implemented as recently as 1977. The light in the fiber optic wire is almost lossless because of the carefully calculated reflection factor between the glass core and the cladding of the fiber. While the speed of processors doubles every 18 months, and the capacity of storage double every 12 months, the speed of optical networks doubles every 9 months. The capacity for optical fiber communications is potentially 100,000 times or more that of the nearest rival for long distance, Satellite/microwave. The venture funding for optical networking in 2000 was 4 billion dollars.

Scientists have very little idea of what the actual capacity of optical communication may actually be. It is not unthinkable that with advances over the next ten or twenty years, the amount of traffic on the whole of the Internet today might be carried in a single hair-thin fiber. Fiber optics is a very important technology. Communications technologies future depends upon the effectiveness of his communications (something that we can already see a glimpse of today).

Important advances have been in the purity of the fibers themselves, so the light signal can travel as far as possible without being amplified. This has been advanced to about 80 kilometers today, something which is quite amazing considering the thinness of the fiber.

1.2 The Project

This idea of a communication system is based on the propagation of light by multiple reflections along channels formed from glass or plastic. The reflection process that is invariably employed is that of total internal reflection at a dielectric interface. This surface is very sensitive to the way light actually travels in the fiber. Much like any other communication media, optical fibers have to be cut and connected to other optical fiber ends. This introduces the role of the connector.

These specialized connectors require polishing before they can be coupled with other optical fiber connectors. But before that can happen, these connector-ends need to be polished – a fundamental process in the preparation of a connector. Incorrect polishing introduces scratches and other defects on the ferrule surface of these connectors. Such defects are harmful to the passing light signal. And in order to identify these defects we employ the use of image processing (wavelets). There are several other techniques that are used in industry to capture images, one of which is a thermographic technique and suggests one of the several ways an image may be acquired [20].

1.3 Image Processing

Image processing is now gaining integration of fundamental levels in industrial control processes. Control processes are mainly used for enhancing quality of the finished product. These mechanisms can be found in the car-manufacturing industry, the airline industry, tile-manufacturing industry, industries involving perishable and non-perishable goods, space technologies, it is also used by law-enforcement agencies etc. In fact image processing is used in almost everything that we can think of today – at least of the manufacturing sector across the board [22].

By employing image processing techniques today, industries are able to speed up the production processes significantly. This has helped in maintaining a balance of supply against rising demand from consumers. It has indirectly helped in raising employment and has raised the bar by enhancing the quality of goods available in the markets today, than say a decade ago.

1.4 Wavelets

There are several techniques and methods used to automate production and enhance quality in the overall context of image processing. Techniques vary from standalone single applications to hybrid applications that involve different methods to achieve a single task. One such discipline in image processing is wavelets. Though wavelets originally found significance in terms of its impressive image compression abilities, it has since found its way into other image-processing applications. Wavelets have also been in prominence in areas related to defect detection; since these are classified as discontinuities in the usual pattern of the image where wavelet transforms have a natural tendency of highlighting abnormalities in images and signals. This and other such techniques are largely discussed in [18].

Before any technique can be applied to images, it is often desirable to have the area of interest segmented from other regions of the image. This step reduces the overall computation time and also lays out only the significant part of the image for processing purposes.

A 2-D discrete wavelet transform will decompose the image under inspection into 4 sub-images. These are called the approximation and detail sub-images. Also called approximation and detail coefficients, they are classified as one approximation coefficient image, a horizontal detail coefficient image, one detail vertical coefficient and one as the diagonal detail coefficient.

The approximation image can then further be subdivided into four images of which one result is another approximation image, only at a lower level. This process may continue till the required level is reached.

1.5 Applied Idea

Our application involves surface defect identification of ferrule-tip ends of optical fiber connectors. The images in question have a special range of colors, distinctive from most other natural images. See Fig. 1.1.

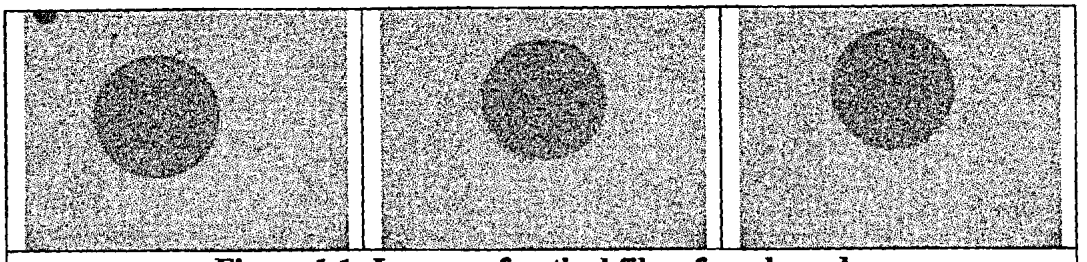

Figure 1.1: Images of optical fiber ferrule-ends.

Images in Fig. 1.1 are in a raw format. These images are then processed to enhance them, where a range of techniques are applied to segment the grayish-circular ferrule part from the image. The image is then processed for defect identification. All these techniques and more are presented in the following chapters.

An overview of how these images are segmented is briefly provided below. More detail of these techniques is provided in the literature that follows.

The images contrasting colors give the images two very distinct segments – the foreground and the background. The foreground consists of the circular ferrule, which is grayish and darker in color and also contains the central core (fiber). The background, which is relatively much lighter in color, is part of the polishing machine and holds the connector tip in place during the actual polishing. Because the image contains such distinctive segments, it also has very pronounced edges. These edges help is segmenting the circular region from the image.

And once the image has successfully been segmented it can be passed on for defect identification.

2 LITERATURE SURVEY

2.1 Optical Fiber

Optical fibers have grown tremendously over the course of the last forty years. The uses of optical fibers are quite numerous and the medium came into mainstream industrial use after the decision of the US Military to use this technology for their communication needs. Since then optical fiber technology is extensively used in telecommunications, medicine, military and the automobile industry. Telecommunications applications range from global networks to local telephone exchanges to subscribers' homes to desktop computers. These involve the transmission of voice, data, or video over distances of less than a meter to hundreds of kilometers, using one of a few standard fiber designs in one of several cable designs.

An optical fiber is a glass or plastic or a hybrid fiber designed to carry light through a process known as total internal reflection. There are several types of optical fibers. Designs include graded-index optical fibers, step-index optical fibers. There are design types that will determine the distance the fiber has to run to carry the signal which include the single-mode and the multi-mode optical fibers. Because of the mechanical properties of the more common glass optical fibers, special methods of splicing fibers and of connecting them to other equipment are needed. Optical fiber connector-ends and their defects are the theme of this report.

Before we embark on the techniques and methods used to detect the defects, an overview of the optical fiber system, its use and benefits are provided below.

An optical fiber is a thin, flexible medium capable of guiding an optical ray. Various glasses and plastics can be used to make optical fibers. The lowest losses have been obtained using fibers of ultrapure fused silica. Ultrapure fiber is difficult to manufacture. Higher-loss multi-component glass fibers are more economical and still provide better performance. Plastic fiber is even less costly and can be used for short-haul links where more loss can be tolerated [3].

An optical fiber cable has a cylindrical shape and consists of three basic sections: the core, the cladding and the jacket. The core is the inner most section and consists of one or more very thin strands, or fibers, made of glass or plastic. The core has a diameter in the range of 8 to 100 micro meters. Each fiber is surrounded by its own cladding, which is a glass or plastic coating that has optical properties different from those of the core. The interface between the core and cladding acts as a reflector to confine light that would otherwise escape the core. The jacket is the outermost layer surrounding one or a bundle of cladded fibers. The jacket is composed of plastic and other material layered to protect against moisture, abrasion, crushing and other environmental dangers. Fig. 2.1 shows a typical optical fiber.

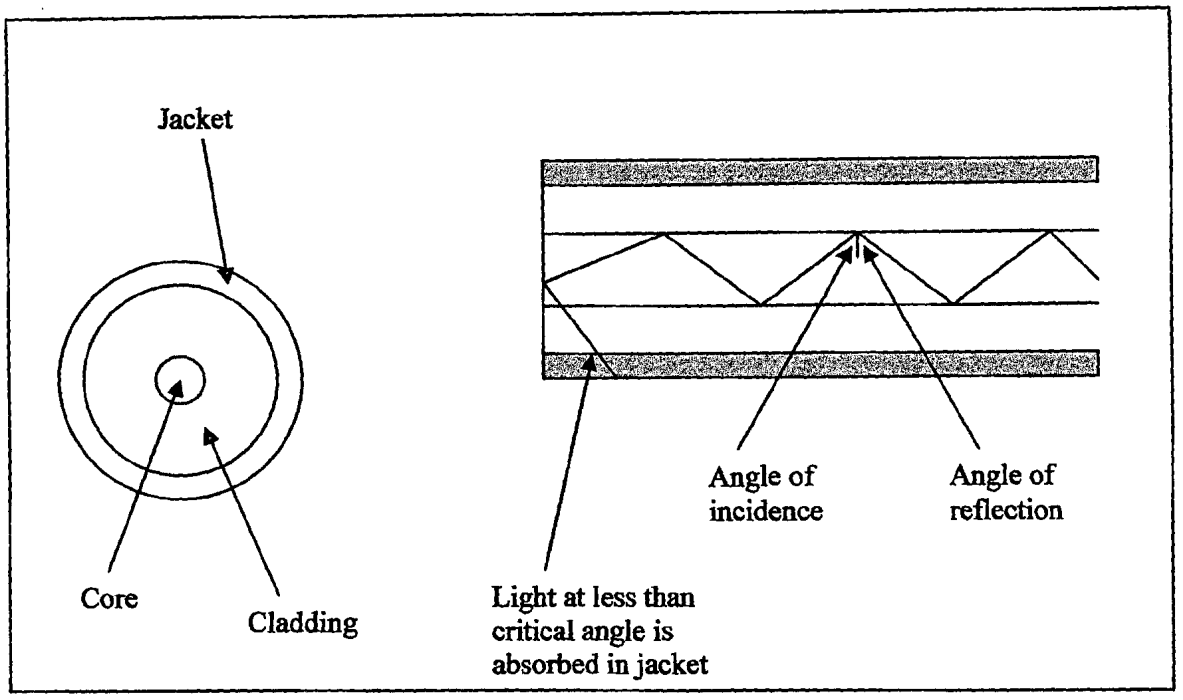

Figure 2.1: Cross sectional view of an optical fiber (left); and its corresponding longitudinal view (right)

2.1.1 Applications

One of the most significant technological breakthroughs in data transmission has been the development of practical fiber optic communications systems. Optical fibers already enjoy considerable use in long-distance telecommunications and its use in other fields is growing very rapidly. The continuing improvement in performance and decline in prices together with the inherent advantages of optical fiber, have made it increasingly attractive for local area networking. Following points highlight some of the advantages of the optical fiber technology:

- Greater capacity: The potential bandwidth and data rate of optical fibers is immense. Data rates of hundreds of Gbps over tens of kilometers have been demonstrated.

- Small and lighter: Optical fibers are considerable thinner than coaxial or twisted-pair cables. For cramped areas in buildings and underground support, the advantage of small size is considerable.

- Lower attenuation: Attenuation is significantly lower for optical fiber than for coax or twisted-pair cables and is constant over a wide range.

- Electromagnetic isolation: Optical fibers are not affected by external electromagnetic fields. Thus the system is not vulnerable to interference, impulse

noise or cross talk. Also, optical fibers do not radiate energy so there is less interference with other equipment and a high degree of security from eavesdropping and inherently are difficult to tap.

- Greater repeater spacing: With optical fibers repeater is significantly reduced. This reduction in repeater spacing also means a reduction in cost and also fewer faults. Repeater spacing in tens of kilometers for optical fibers is common and repeater spacing of hundreds of kilometers has also been demonstrated.

Categories of applications that have become important for optical fibers:

- Long-haul trunks
- Metropolitan trunks
- Rural exchange trunks
- Subscriber loops
- Local area networks

Long-haul trunks

Long-haul transmission is becoming increasingly common in the telephone network. Most of the intercontinental internet traffic (data and voice) travels over optical fiber cables under the sea. These routes average about 1500 km in length and offer high capacity (typically 20,000 to 60,000 voice channels). These systems also compete very economically with microwave systems.

Metropolitan Trunks

Metropolitan trunking circuits have an average length of 12 km and may have as many as 100,000 voice channels in a trunk group. Most such facilities are installed under the ground and are often repeaterless. Such circuits join telephone exchanges in a metropolitan or city area.

Rural exchange trunks

Rural exchange trunks have circuit lengths ranging from 40 to 160 km and link towns and villages. Most of these systems have less than 5000 voice channels. The technology used in such applications also competes with microwave facilities.

Subscriber Loop

Subscriber loop circuits are fibers that run directly from the central exchange to a subscriber. These facilities are beginning to displace twisted pair and coax cables evolving into a complete voice, data and video-carrying systems. This is overhauling the communication speed and will allow subscribers to experience faster internet access.

Local area networks

Standards have been developed and products introduced for optical fiber networks that have a total capacity of 100Mbps to 1Gbps and can support hundreds or even thousands of stations in an office building or a complex of buildings [4].

2.1.2 Transmission Characteristics

Optical fiber transmits a signal-encoded beam of light by means of total internal reflection. Total internal reflection can occur in any transparent medium that has a higher index of refraction than the surrounding medium.

Fig 2.2 shows the principle of optical fiber transmission. Light from a source enters the cylindrical glass or plastic core. Rays at shallow angles are reflected and propagated along the fiber. Other rays are absorbed by the surrounding material. This form of propagation is called **step-index multimode**, referring to a variety of angles that will reflect.

With multi-mode transmission, multiple propagation paths exist, each with a different path length and hence time to traverse the fiber. This causes signal elements (light pulses) to spread out in time, which limits the rate at which data can be accurately received. In other words, the need to leave spaces between pulses limits data rate. This type of fiber is best suited for transmissions over very short distances. When the fiber core radius is reduced, fewer angles will reflect. By reducing the radius of the core to the order of a wavelength only a single angle or mode can pass, which we refer to as the axial array.

This **single-mode** propagation provides superior performance for the following reason. Because there is a single transmission path with singlemode transmission, the distortion found in multimode cannot occur. Single –mode is typically used for long-distance applications.

However, by varying the index of refraction of the core, a third type of transmission, known as **graded-index multimode**, is possible.

Its characteristics are intermediate between the other two. The higher refractive index at the center makes the light rays moving down the axis advance more slowly than those near the cladding. Rather than zig-zagging off the cladding, light in the core curves helically because of the graded index, reducing its travel distance. The shortened path and higher speed allows light at the periphery to arrive at a receiver at about the same time as the straight rays in the core axis. Graded-index fibers are often used in local area networks.

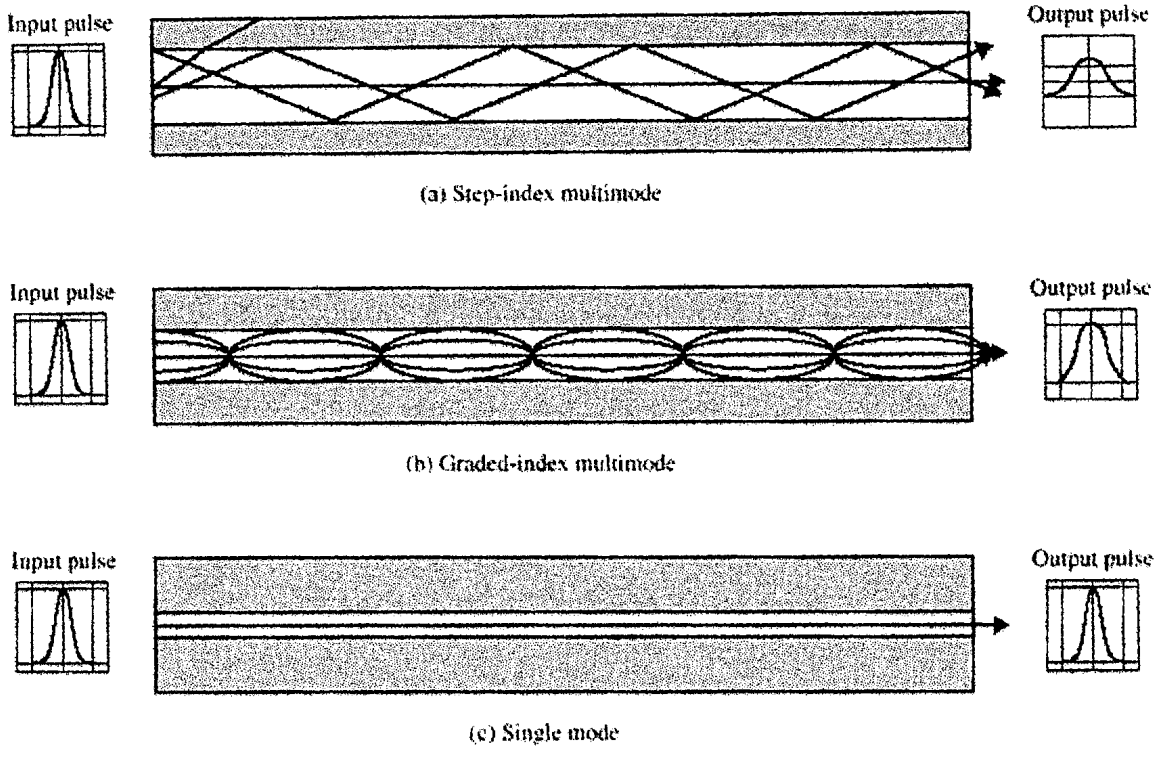

Figure 2.2: Optical Fiber Transmission Modes (diagram courtesy of Data and Computer Communications, William Stallings)

2.1.3 Light Sources

Two different types of light sources are used in fiber optic systems: the light emitting diode (LED) and the injection laser diode (ILD). Both are semiconductor devices that emit a beam of light when a voltage is applied. The LED is less costly, operates over a greater temperature range and has longer operational life. The ILD, which operates on the laser principle, is more efficient and can sustain greater data rates.

There is a relationship among wavelengths employed, the type of transmission and the achievable data rate. Both singlemode and multimode can support several different wavelengths of light and can employ laser or LED light sources. In optical fiber, light propagates best in three distinct wavelength 'windows', centered on 850, 1300 and 1550 nanometers.

Wavelength-Division Multiplexing

The true potential of optical fiber is fully exploited when multiple beams of light at different frequencies are transmitted on the same fiber. This is a form of frequency-division multiplexing (FDM), but is commonly called wavelength-division multiplexing (WDM). With WDM, the light streaming through the fiber consists of many colors, or wavelengths, each carrying a separate channel of data. Bell Labs were able to

demonstrate a WDM system with 100 beams each operating at 10GBPS which equals a trillion bits per second, or 1TBPS [4].

2.1.4 Optical Fiber Connector

Optical fibers themselves would not be of much use if they could not be connected to other optical fibers. For coupling to occur, connectors are required. The connector has an alignment mechanism, which also mounts the fiber, in a long, thin cylindrical shape, called the ferrule. The ferrule of the connector (with the fiber housed) is then polished using specialized equipment to achieve a good optical finish. This processing of the end-face is one of the most important steps in the process of preparing a connector for coupling. Diagram of a typical connector and its ferrule part is shown in Fig 2.3.

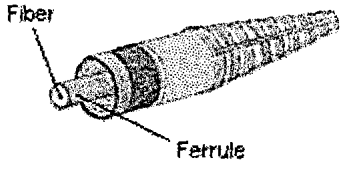

Figure 2.3: A Typical straight-tip connector.

Incorrect polishing will result in lips and hackles, blobs and scratches and other forms of defects on the surface-tip of the ferrule. Fiber cores inside the connectors are coupled very precisely to other connecting fibers and defects on the tip-surface will attenuate a passing light signal [21]. And this is the focus of our study: surface defect detection of optical fiber connectors.

2.2 Image Enhancement

Image enhancement is a very subjective term but is fundamental to the overall image processing theory. Images that scientists work on are not as glittering or clearly laid out as we see daily in magazines, television or the PC. Most images acquired are done in environments where a second chance might just not be possible e.g. NASA capturing images of exploding stars at far off distances. These images (or images in industrial applications) are prone to noise variations and usually do not have an optimal light source to lighten up the capture. This requires processing the images to make them more usable.

In other words, the principal objective of enhancement is to process an image so that the result is more suitable than the original image for a specific application. The degree of an acceptable enhancement is dependent very much on the problem at hand. Thus, for example, an enhancement technique that is used to enhance an x-ray image may not even be suitable for enhancing an image, captured in space, of a distant galaxy.

2.2.1 Image Enhancement Categories

Image enhancement falls into two broad categories: the spatial domain and the frequency domain. The spatial domain refers to the image plane itself and modification is done directly to the image pixels whereas the frequency domain technique is based on modifying the Fourier transform of an image [1].

As we have just mentioned there is no general theory of image enhancement. When an image is processed for visual interpretation, the viewer is the ultimate judge of how well a particular method works. Even when an obvious situation for enhancement is present, a certain amount of trial and error is required before an image enhancement approach is selected.

The image enhancement is pictorially summarized in figures 2.4 and 2.5.

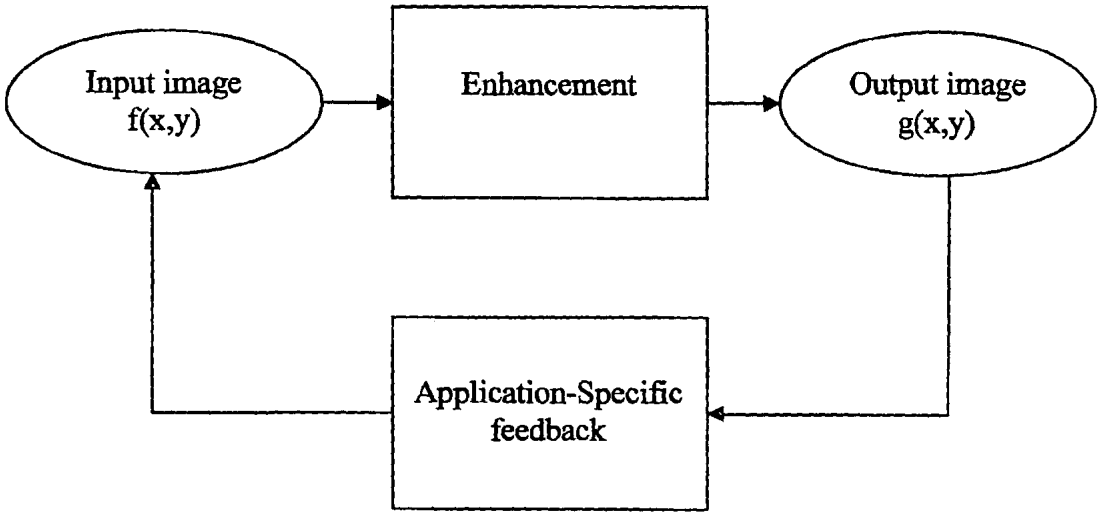

Figure 2.4: Summarized image enhancement process. f(x,y) is the input image and g(x,y) is the enhanced image

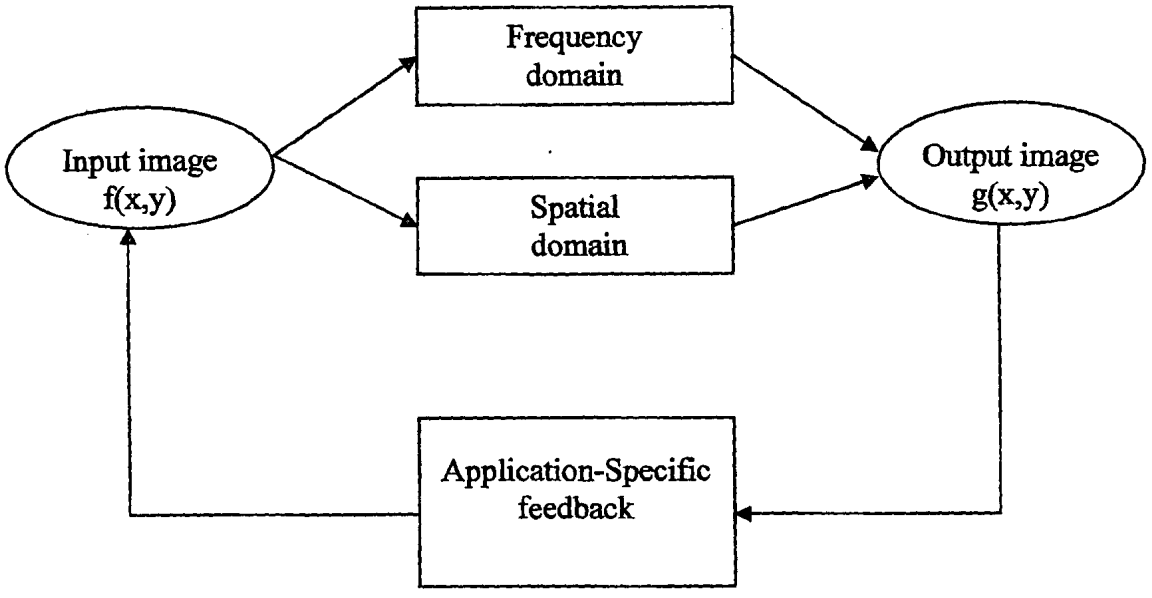

Figure 2.5: Enhancement is possible in the frequency and the spatial domain.

The enhancement field has grown very large that no single topic would be able to cover all the techniques and methods used in image enhancement. Here we provided a brief overview of some of the more popular enhancement techniques used in DIP today [5].

2.2.2 Spatial Domain

2.2.2.1 Image Negatives

This is probable the most simple enhancement technique and involves reversing the intensity levels of an image. In this manner the output produces the equivalent of a photographic negative. This type of processing is particularly suited for enhancing white or gray level detail embedded in dark regions of an image [1].

2.2.2.2 Log Transformations

Log transforms have the form $s = c\log(1+r)$, where s is the output pixel-intensity value from its corresponding input pixel-intensity value (r). c is a constant and r is ≥ 0. The output log curve, which is generated in the process, shows that this transformation maps a narrow range of gray-level values in the input image into a wider range of output levels [1].

2.2.2.3 Power-Law Transformation

Power-law transform has the basic form

$$s = cr^{\gamma} \tag{2.2-1}$$

where c and γ are positive constants. r is the input gray level and s is the output gray level. And as with log transformation, power-law curves with fractional values of γ map a narrow range of dark input values into a wider range of output values, with the opposite being true for higher values of input levels [1].

2.2.2.4 Contrast Stretching

Contrast stretching is a piecewise linear function. The idea behind contrast stretching is to increase the dynamic range of the gray levels in the image being processed. Low contrast images can result from poor illumination or lack of dynamic range in the image sensor [1][5].

2.2.2.5 Gray-level Slicing

Highlighting a specific range of gray levels in an image is often desired. Based on pervious knowledge of certain attributes in an image, certain gray levels in the range of interest are displayed while a low value for other gray levels is set. This results in a binary image. Another approach brightens the desired range of gray levels but preserves the background and gray-level tonalities in the image [1][5].

2.2.2.6 Bit-plane Slicing

Instead of highlighting gray-level ranges, highlighting the contribution made to total image appearance by specific bits might be desired. Gray level images are often represented by 8 bits per pixel. Here we imagine that the image is composed on eight 1-bit planes, ranging from bit-plane 0 for the least significant bit to bit-plane 7 for the most significant bit. In terms of an 8-bit byte, plane 0 contains all the lowest order bits in the bytes comprising the pixels in the image and plane 7 contains all the high-order bits. The higher order bits, usually, contain the majority of visually significant data. The other bit planes contribute to more subtle details in the image [5].

2.2.2.7 Histogram Equalization

The histogram equalization approach distributes evenly gray-level values across the dynamic range of an image. In other words, histogram equalization automatically determines a transformation function that seeks to produce an output image that has a uniform histogram. This method improves the overall contrast of dark and low contrast images. Histogram equalization can be applied to an image globally or locally [1].

2.2.2.8 Histogram Matching (Specification)

There are applications where a uniform histogram is not the best approach. In particular, there are instances when it is useful to be able to specify the shape of the

histogram that we wish the image to have. The method used to generate a processed image that has a specific histogram is called histogram matching [1].

2.2.2.9 Image Subtraction

Image subtraction has the form

$$g(x,y) = f(x,y) - h(x,y) \tag{2.2-2}$$

where f and h are identical images. With this approach in mind, image f and h start off as rather same images. Certain changes are made to f and after application-specific change is given the form h. g is the image that shows the difference. This approach is used extensively in an area of medical imaging called mask more radiography.

Even more popular enhancement techniques include smoothing and sharpening spatial and frequency filters. As the names imply, smoothing filters make an image more smooth and the sharpening filters make the rendering of the image sharper. The degree of the smoothness or the sharpness depends on the application at hand. In spatial enhancement the operation works with the values of the image pixels in the neighborhood and the corresponding values of the subimage. The subimage has the same dimensions as that of the neighborhood. This subimage is called a filter, a window or a mask. The values of the filter are called coefficients. The filter is convolved with the image and depending on the weights of the coefficients the convolution process determines the value of the pixel at the center of the neighborhood. A filter size of 3x3 is very common [2].

2.2.3 Frequency Domain

In the frequency domain, the mask is usually the size of the whole image itself. A discrete Fourier transform is applied to the image, the image is shifted and a frequency domain filter is applied. Once the image has been processed by a frequency-domain filter function, it is again shifted and an inverse Fourier transform is applied to obtain the transformed image. Just as the Fourier transform converts the image to a frequency domain application, the inverse Fourier transform reverts the image back to the spatial domain. The shifting process centers the low frequency components of the transforms and distributes the high frequency ones.

Fig 2.6 shows the mechanics of spatial filtering. The diagram shows a magnified drawing of a 3x3 filter and its corresponding convolution area.

It is interpreted as :

$$g(x,y) = \sum_{s=-a}^{a} \sum_{t=-b}^{b} w(s,t) f(x+s, y+t) \tag{2.2-3}$$

where

$a = \frac{m-1}{2}$ and $b = \frac{n-1}{2}$

m x n is the size of the filter.

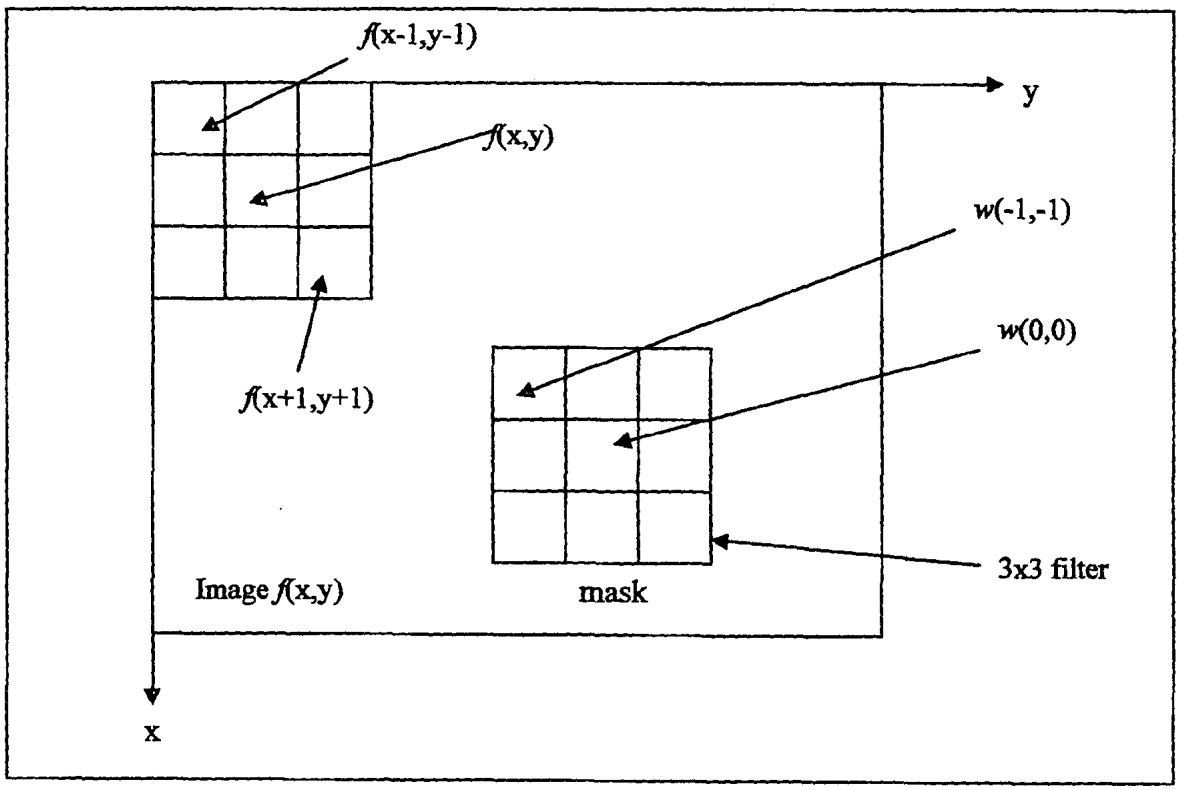

Figure 2.6: Mask coefficients showing coordinate arrangement with corresponding pixels of image section that will be convolved with the mask.

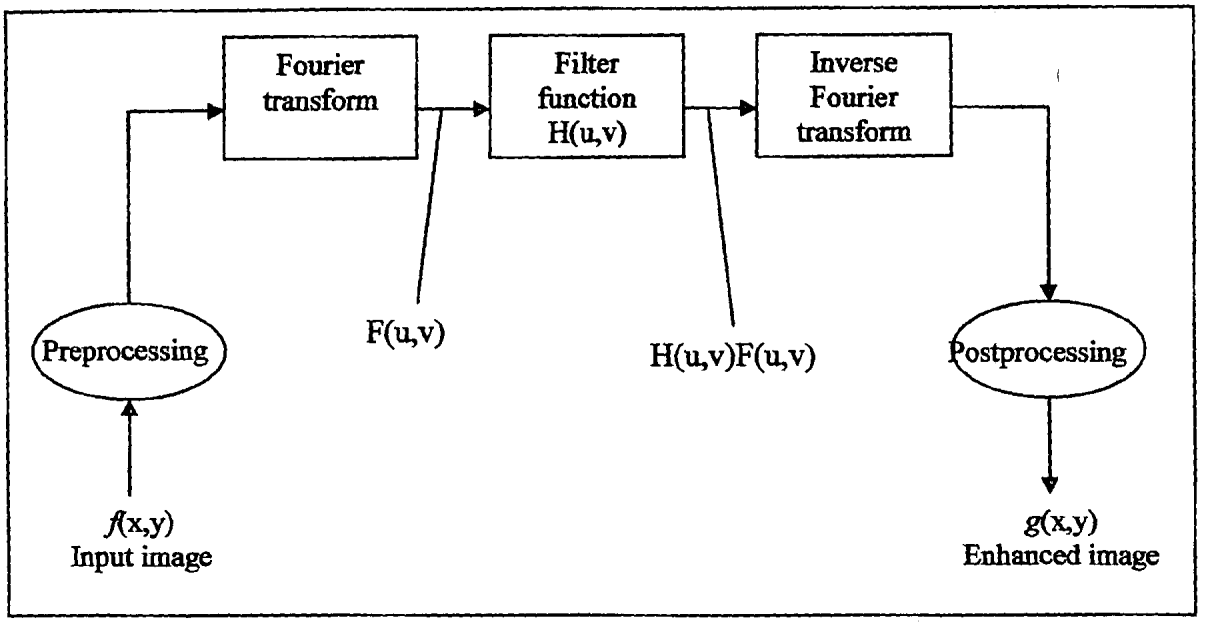

Figure 2.7: Basic steps for filtering in the frequency domain

Fig. 2.7 shows the basics of filtering in the frequency domain. These basic steps consist of the following:

1. Multiplying the input image by $(-1)^{x+y}$ to center the transform.
2. Computing F(u,v), the DFT of the image from (1).
3. Multiplying F(u,v) by a filter dunction H(u,v).
4. Computing the inverse DFT of the result in (3).
5. Obtaining the real part of the result in (4)
6. Multiplying the result from (5) by $(-1)^{x+y}$

The two-dimensional DFT and its inverse is calculated as follows

$$F(u,v) = \frac{1}{MN}\sum_{x=0}^{M-1}\sum_{y=0}^{N-1} f(x,y)e^{-j2\pi(\frac{ux}{M}+\frac{vy}{N})} \quad (2.2\text{-}4)$$

And the inverse transform is calculated as

$$f(x,y) = \sum_{u=0}^{M-1}\sum_{v=0}^{N-1} F(u,v)e^{j2\pi(\frac{ux}{M}+\frac{vy}{N})} \quad (2.2\text{-}5)$$

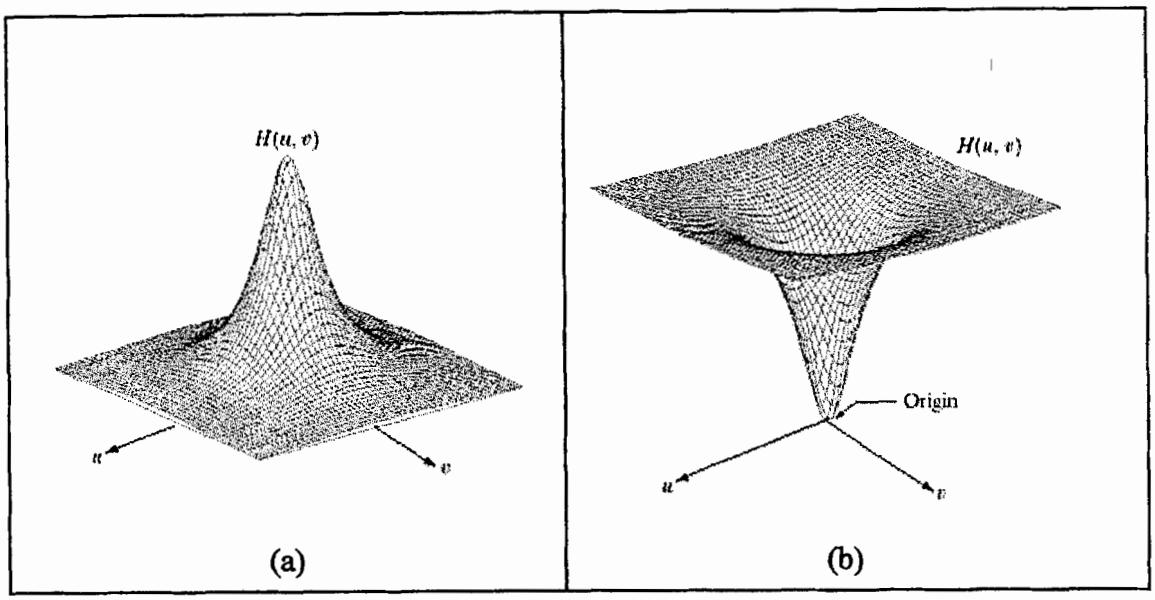

Figure 2.8: A two-dimensional frequency-domain (a) lowpass filter function; and (b) a highpass filter function

Fig 2.8a and 2.8b show two filter functions that are circularly symmetric. Their origins have been shifted to the center. Fig 2.8a shows the filter function that highlights or raises the low frequency component of the image. The outcome of this convolution is a smooth or a blurred image. Fig 2.8b, on the other hand, is a filter function that raises the high frequency portion of the input image. This will result in the output image having pronounced edge detail.

Following is a brief description of some of the popular frequency-domain filters. Here we consider the ideal, Butterworth and Gaussian filters.

2.2.3.1 Ideal Lowpass Filter

Also abbreviated as ILPS, this filter cuts off all high frequency components of the Fourier transform that are at a distance greater than a specified distance D_0 from the origin of the (centered) transform.

The filter function, H(u,v), is calculated as

$$H(u,v) = \begin{cases} 1 & if\ D(u,v) \leq D_0 \\ 0 & if\ D(u,v) > D_0 \end{cases} \quad (2.2\text{-}6)$$

Where

$$D(u,v) = \sqrt{\left(u - \frac{M}{2}\right)^2 + \left(v - \frac{N}{2}\right)^2} \quad (2.2\text{-}7)$$

D(u,v) is the distance from the point (u,v) to the origin of the frequency rectangle. D_0 is a nonnegative quantity and is usually specified by the user.

2.2.3.2 Butterworth Lowpass Filter

The transfer function of a Butterworth lowpass filter (BLPF) of order *n*, and with cutoff frequency at a distance D_0 from the origin is defined as:

$$H(u,v) = \frac{1}{1+\left[\frac{D(u,v)}{D_0}\right]^{2n}} \quad (2.2\text{-}8)$$

Where D(u,v) is calculated as mention above

And *n* is an order value that is also user defined.

2.2.3.3 Gaussian Lowpass Filter

The form of this filter (GLPF) in two dimensions is given by

$$H(u,v) = e^{\frac{-D^2(u,v)}{2\sigma^2}} \quad (2.2\text{-}9)$$

Where D(u,v) is the distance that we have calculated above and σ is the measure of the spread of the Gaussian curve.

To obtain their respective highpass filters, reciprocation would be effective.

2.2.4 High-boost Filtering

Of all these techniques our results on ferrule-ends were best achieved with high-boost filtering. High-boost filtering is a process that has been used for many years in the publishing industry to sharpen images. The method consists of subtracting a blurred

version of an image from the image itself. This process is called unsharp masking and is expressed as

$$f_s(x,y) = f(x,y) - f`(x,y) \tag{2.2-10}$$

where $f_s(x,y)$ denotes the sharpened image obtained by unsharp masking, f `(x,y) is a blurred version of f(x,y).

A slight generalization of unsharp masking is called high-boost filtering. This is expressed as

$$f_{hb}(x,y) = Af(x,y) - f`(x,y) \tag{2.2-11}$$

where $f_{hb}(x,y)$ is a high-boost filtered image and $A \geq 1$ and f.` is a blurred version of the same image.

This above equation can be written as

$$f_{hb}(x,y) = (A-1)f(x,y) + f(x,y) - f`(x,y) \tag{2.2-12}$$

and we can then obtain

$$f_{hb}(x,y) = (A-1)f(x,y) + f_s(x,y) \tag{2.2-13}$$

as the expression for computing a high-boost filtered image.

When A=1 the filter acts as a standard Laplacian sharpening filter. As the value of A is increased the processed version will be closer in its property to the original image. If the value of A is high enough, it will only have the effect of having multiplied the original image with a positive constant [1][2][5].

2.3 Image Segmentation

Image segmentation is an integral part of most image processing applications. Segmentation is a task that separates non-uniform objects in an image. Or it could be catered to carry out an operation to extract an object of interest in the image.

There are several different techniques and algorithms available to segment images. As mentioned before, image processing involves trail and error and different techniques are very much application dependent. More on information on segmentation is provided in the Segmentation chapter.

2.4 Wavelets

The fundamental idea behind wavelets is to analyze according to scale. Wavelets are functions that satisfy certain mathematical requirements and are used in representing data or other functions. In wavelet analysis, the scale that we use to look at data plays a special role. Wavelet algorithms process data at different scales or resolutions. If we look at a signal with a large "window," we would notice gross features. Similarly, if we look

at a signal with a small "window," we would notice small features. The result in wavelet analysis is to see both the forest and the trees. We have more on the "window" concept and how it differs between the wavelet transform (WT) and the Fourier transform (FT) [11].

These windows make the wavelets more useful. With wavelet analysis, we can use approximating functions that are contained neatly in finite domains. Wavelets are well-suited for approximating data with sharp discontinuities [6]. And is also one of the fundamental reasons for our choice of defect detection with wavelets.

The wavelet analysis procedure is to adopt a wavelet prototype function, called an analyzing wavelet or mother wavelet. Temporal analysis is performed with a high-frequency version of the wavelet, while frequency analysis is performed with a low-frequency version of the same wavelet. Because the original signal or function can be represented in terms of a wavelet expansion, data operations can also be performed using just the corresponding wavelet coefficients [16].

Wavelets owe their evolution, to great extent, to the Fourier transform. Therefore, before we embark on a detailed description and advantages of wavelets and their transforms an introduction to the Fourier transform is provided below.

2.4.1 Fourier Transformation

The Fourier transform's utility lies in its ability to analyze a signal in the time domain for its frequency content. An inverse Fourier transforms data from the frequency domain into the time domain.

The discrete Fourier transform (DFT) estimates the Fourier transform of a function from a finite number of its sampled points (e.g. a digital image).
The DFT has symmetry properties almost exactly the same as that of the continuous Fourier transform and in the analysis one half of the symmetry is removed. It is possible to find the surface faults from the disturbances in time and/or frequencies only, but the wavelet transform provides added benefits that elude one or the other domains. It might be useful to use a joint time and frequency method [23][25].

If f(t) is a nonperiodic signal, the summation of the periodic functions, sine and cosine, does not accurately represent the signal. Here the windowed Fourier transform (WFT) or the short time Fourier transform (STFT) is one solution to the problem of better representing the nonperiodic signal. The WFT or STFT can be used to give information about signals simultaneously in the time domain and in the frequency domain [7].

With the WFT, the input signal f(t) is chopped up into sections, and each section is analyzed for its frequency content separately. If the signal has sharp transitions, we window the input data so that the sections converge to zero at the endpoints. This windowing is accomplished via a weight function that places less emphasis near the

interval's endpoints than in the middle. The effect of the window is to localize the signal in time [8].

Fourier transforms have been the mainstay of image processing for a long time. Discrete Fourier transforms (DFT) initially, when developed for the first time, were very resource hungry and required a very long time to process specially if the size of the images was large. With the advent of the fast Fourier transform (FFT), it gained even greater popularity. FFT cut down the computational time phenomenally. FFT has since become an essential/fundamental tool in signal processing. To highlight the difference between the DFT and the FFT consider a 1-D Fourier transform of M points. The DFT transform required M^2 multiplication/addition operation. But with the FFT the same task could be achieved with $M\log_2 M$ operations. This is not all and the FFT has another advantage. The bigger the problem, the greater the computational advantage. For example if M=1024, the computation advantage between the DFT and the FFT is 100 to 1 in favor of the FFT. If M=8192, the computational advantage grows to 600 to 1.

Fourier transform is named after the French mathematician Jean Baptiste Joseph Fourier. Fouriers contribution in this particular field states that any function that periodically repeats itself can be expressed as the sum of sines and/or cosines of different frequencies, each multiplied by a different coefficient and is popularly known today, as the *Fourier series*. It does not matter how complicated the function is, as long as it is periodic and satisfies some mild mathematical conditions, it can be represented by such a sum [1].

Even functions that are not periodic (but whose area under the curve is finite) can be expressed as the integral of sines and/or cosines multiplied by a weighing function. The formulation in this case is known as the *Fourier transform*. These transforms allow us to work in the Fourier domain and then return to the original domain of the function without losing any information.

Therefore a function either a Fourier transform or a series can be reconstructed completely without any loss of information. Same is true for wavelet transforms.

And hence, briefly, the information that cannot be readily seen in the time-domain can easily be seen in the frequency domain. A signal in the time domain is easy to comprehend in its totality and its frequency information is laid out clearly in the frequency domain.

2.4.2 Wavelet Transformation

Although Fourier transform has been the mainstay of transform-based image processing since the late 1950s, a relatively recent transformation, called the wavelet transform, has made it even easier to compress, transmit and analyze many images. Unlike the Fourier transform whose basis functions are the sinusoids, wavelet transforms are based on small waves, called *wavelets*, of varying frequency and *limited duration*. This allows them to provide the equivalent of a musical score for an image, revealing not

only what notes (or frequencies) to play but also when to play them. Conventional Fourier transforms, on the other hand, provide only the notes or frequency information; temporal information is lost in the transformation process. This allows for the processing of images at more than one resolution. The appeal of such an approach is obvious – features that might go undetected at one resolution may be easy to spot at another.

2.4.2.1 Wavelet Transformation in Two Dimensions

In two dimensions, a two-dimensional scaling function, $\varphi(x,y)$ and three two-dimensional wavelets, $\psi^H(x,y)$, $\psi^V(x,y)$, *and* $\psi^D(x,y)$, are required. Terms H,V,D denote horizontal, vertical and diagonal respectively. Each is the product of a one-dimensional scaling function φ and corresponding wavelet ψ. Excluding products that produce one-dimensional results, like $\varphi(x)\psi(x)$, the four remaining products produce the separable scaling function

$$\varphi(x,y) = \varphi(x)\varphi(y) \tag{2.4-1}$$

and separable, 'directionally sensitive' wavelets

$$\psi^H(x,y) = \psi(x)\varphi(y) \tag{2.4-2}$$
$$\psi^V(x,y) = \varphi(x)\psi(y) \tag{2.4-3}$$
$$\psi^D(x,y) = \psi(x)\psi(y) \tag{2.4-4}$$

In order to provide the DWT (Discrete Wavelet Transform) of an image (or two-dimensional array) we first define the scaled and translated basis functions:

$$\varphi_{j,m,n}(x,y) = 2^{\frac{j}{2}}\varphi(2^j x - m, 2^j y - n), \tag{2.4-5}$$
$$\psi^i_{j,m,n}(x,y) = 2^{\frac{j}{2}}\psi^i(2^j x - m, 2^j y - n), \qquad i = \{H,V,D\} \tag{2.4-6}$$

where i identifies the directional wavelets in equations 2.4-2 to 2.4-4. Rather than an exponent, i is a superscript that assumes values H,V, and D. The discrete wavelet transform of function f(x,y) of size MxN is then

$$W_\varphi(j_0,m,n) = \frac{1}{\sqrt{MN}}\sum_{x=0}^{M-1}\sum_{y=0}^{N-1} f(x,y)\,\varphi_{j_0,m,n}(x,y) \tag{2.4-7}$$

$$W^i_\psi(j,m,n) = \frac{1}{\sqrt{MN}}\sum_{x=0}^{M-1}\sum_{y=0}^{N-1} f(x,y)\,\psi^i_{j,m,n}(x,y) \tag{2.4-8}$$

where j_0 is an arbitrary starting scale and $W_\varphi(j_0,m,n)$ coefficients define an approximation of f(x,y) at scale j_0. The $W^i_\psi(j,m,n)$ coefficients add horizontal, vertical and diagonal details for scales $j \geq j_0$.

And f(x,y) is obtained via the inverse discrete wavelet transform:

$$f(x,y) = \frac{1}{\sqrt{MN}} \sum_{m} \sum_{n} W_{\varphi}(j_0, m, n) \varphi_{j_0,m,n}(x,y) + \frac{1}{\sqrt{MN}} \sum_{i=H,V,D} \sum_{j=j_0}^{\infty} \sum_{m} \sum_{n} W_{\psi}^{i}(j,m,n) \psi_{j,m,n}^{i}(x,y) \quad (2.4\text{-}9)$$

2.4.3 WT Invaluable Property

Despite the Fourier transforms computational advantage and its uses, there is something that the Fourier transform lacked – time information. Since we are aware that the Fourier transform is largely responsible for representing the frequencies of say a spatial domain signal, it does not demonstrate *when* in time those certain frequencies occur. Fourier transforms only provide frequency information; temporal information is lost in the transformation process. This led to developmental work that over the course of time gave rise to *wavelets* [7].

Fourier transform was the stronghold of transform-based image processing since the late 1950s. However, wavelet transform is now making it even easier to compress, transmit and analyze many images. Unlike Fourier transform, whose basis functions are sinusoids, wavelet transforms are based on small waves, called *wavelets*, of varying frequency and *limited duration.* This allows them to provide the equivalent of a musical score for an image, revealing not only what notes (or frequencies) to play but also when to play them.

2.4.4 Basis Function

It is simpler to explain a basis function if we move into the realm of digital vectors.
Every two-dimensional vector (x; y) is a combination of the vector (1; 0) and (0; 1): These two vectors are the basis vectors for (x; y).

Notice that x multiplied by (1; 0) is the vector (x; 0); and y multiplied by (0; 1) is the vector (0; y): The sum is (x; y).

The best basis vectors have the valuable extra property that the vectors are perpendicular, or orthogonal to each other. For the basis (1; 0) and (0; 1); this criteria is satisfied [9].

2.4.5 Scale-varying Basis Functions

A basis function varies in scale by chopping up the same function or data space using different scale sizes. For example, imagine we have a signal over the domain from 0 to 1. We can divide the signal with two step functions that range from 0 to 1/2 and 1/2 to 1. Then we can divide the original signal again using four step functions from 0 to 1/4,

1/4 to 1/2, 1/2 to 3/4, and 3/4 to 1. And so on. Each set of representations code the original signal with a particular resolution or scale [9].

2.4.6 Difference between WT and FT

One of the basic dissimilarities between FT and WT is time information. WT's provide temporal information whereas FT's do not. This localization feature, along with wavelets localization of frequency, makes many functions and operators using wavelets "sparse" when transformed into the wavelet domain. This sparseness, in turn, results in a number of useful applications one of which is data compression.

One way to see the time-frequency resolution differences between the Fourier transform and the wavelet transform is to look at the basis function coverage of the time-frequency plane [10].

Fig. 2.9 shows a windowed Fourier transform, where the window is simply a square wave. The square wave window truncates the sine or cosine function to fit a window of a particular width. Because a single window is used for all frequencies in the WFT, the resolution of the analysis is the same at all locations in the time-frequency plane [11].

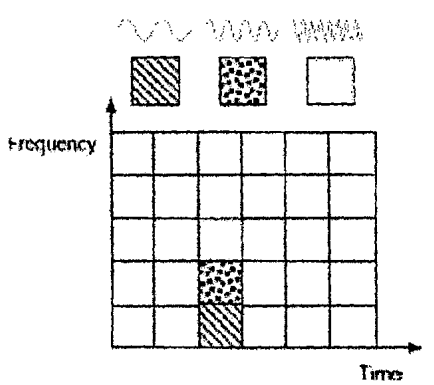

Figure 2.9: Fourier basis functions, time-frequency tiles, and coverage of the time-frequency plane.

An advantage of wavelet transforms is that the windows vary. In order to isolate signal discontinuities, one would like to have some very short basis functions. At the same time, in order to obtain detailed frequency analysis, one would like to have some very long basis functions.

A way to achieve this is to have short high-frequency basis functions and long low-frequency ones. This happy medium is exactly what you get with wavelet transforms.

Fig 2.10 shows the coverage in the time-frequency plane with one wavelet function, the Daubechies wavelet.

Unlike Fourier transforms, wavelet transforms do not have a single set of basis functions. Fourier transforms utilize only the sine and cosine functions. Wavelet transforms, on the other hand, have an infinite set of possible basis functions. Thus wavelet analysis provides immediate access to information that can be hidden by Fourier analysis [11].

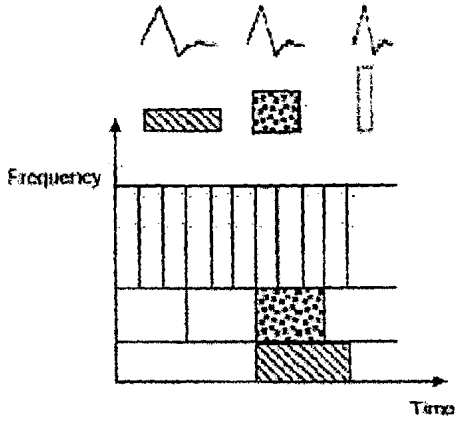

Figure 2.10: Daubechies wavelet basis functions, time-frequency tiles, and coverage of the time-frequency plane.

2.4.7 Wavelet Family

Today there are several different types of wavelets with different pros and cons. These different types of wavelets have formed a collection of wavelet classes and are referred to as a family of wavelets. Within each family of wavelets (such as the Daubechies family) are wavelet subclasses distinguished by the number of coefficients. Wavelets are classified within a family most often by the number of vanishing moments. This is an extra set of mathematical relationships for the coefficients that must be satisfied, and is directly related to the number of coefficients [6].

For example, within the Coiflet wavelet family are Coiflets with two vanishing moments, and Coiflets with three vanishing moments. Fig 2.11 illustrates several different wavelet families.

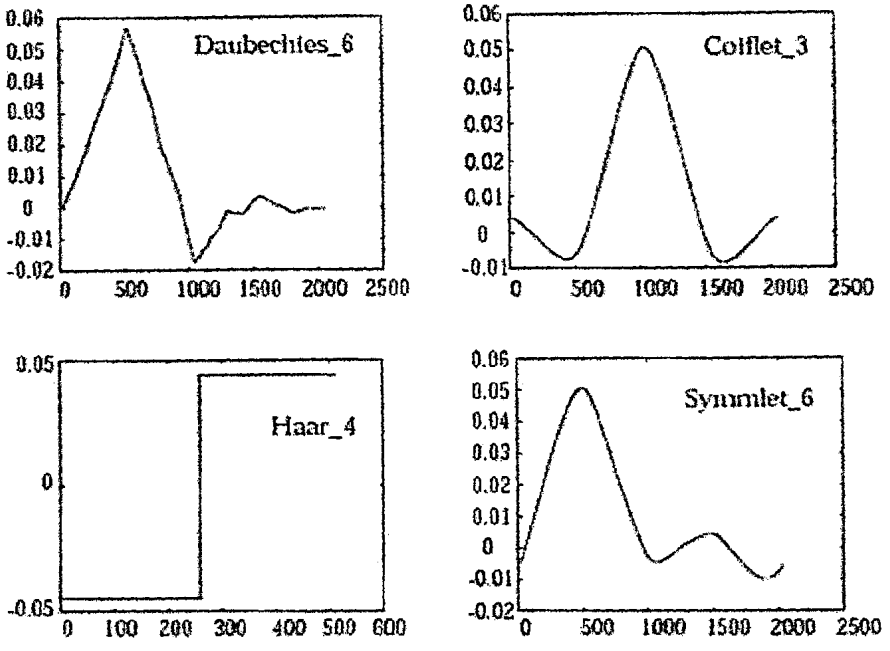

Figure 2.11: Several different families of wavelets. The number next to the wavelet name represents the number of vanishing moments (A stringent mathematical definition related to the number of wavelet coefficients) for the subclass of wavelet.

2.4.8 Multiresolution Analysis

In 1987, wavelets were first shown to be the foundation of a powerful new approach to signal processing and analysis called multiresolution theory. Multiresolution theory incorporates and unifies techniques from a variety of disciplines, including subband coding from signal processing, quadrature mirror filtering from digital speech recognition, and pyramidal image processing. As the name implies, multiresolution theory is concerned with the representation and analysis of signals (or images) at more than one resolution. This is appealing because features that might go undetected at one resolution may be easy to spot at another [12].

From this very theory we get extra information when we split all the bands. This is called as *wavelet packet decomposition* and its properties give an understanding of analysis at different resolutions which is described in detail in the next section [24].

There are two major aspects to wavelets – analyzing images at different resolutions and subband coding.

2.4.9 Image Pyramid

When we look at images, generally we see connected regions of similar texture and gray level that combine to form objects. If the objects are small in size or low in

contrast, we normally examine them at high resolutions. If they are large in size or high in contrast, a coarse view is all that is required. If both small and large object – or low and high contrast objects – are present simultaneously, it can be advantageous to study them at different resolutions. This is the fundamental motivation for multiresolution processing.

Images are two-dimensional arrays of intensity values with locally varying statistics that result from different combinations of abrupt features like edges and contrasting homogenous regions. Here we introduce image pyramids.

Image pyramids are conceptually simple structures of representing an image at more than one resolution. It was originally designed for computer vision applications and is essentially a collection of decreasing resolution images arranged in the shape of a pyramid. The base of the pyramid contains a high-resolution representation of the image, and moving upwards, the apex contains a low resolution approximation. This is conceptualized in Fig 2.12.

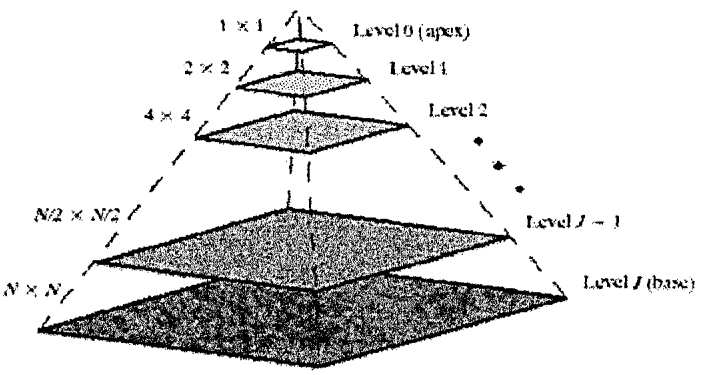

Figure 2.12: Pyramidal image structure

As we move up the pyramid both the size and the resolution decreases. Since base J is size $2^J x 2^J$ or NxN, where $J=\log_2 N$, intermediate level j is size $2^j x 2^j$, where $0 \leq j \leq J$. Fully populated pyramids are composed of J+1 resolution levels from $2^J x 2^J$ to $2^0 x 2^0$, but most pyramids are truncated to P+1 levels, where j = J-P, ..., J-2, J-1, J and $1 \leq P \leq J$.

In other words we normally limit ourselves to P reduced resolution approximations of the original image; a 1x1 or single pixel approximation of a 512x512 image, for example, is of little value [17]. The total number of elements in a P+1 level pyramid for P>0 is

$$N^2\left[1+\frac{1}{4^1}+\frac{1}{4^2}+\cdots+\frac{1}{4^P}\right] \leq \frac{4}{3}N^2 \qquad (2.4\text{-}1)$$

2.4.10 Subband Coding

Another important imaging technique with ties to multiresolution analysis is subband coding. In subband coding an image is decomposed into a set of band limited components, called subbands, which can be reassembled to reconstruct the original image without error. Originally developed for speech and image compression, each subband is generated by bandpass filtering the input. Since the bandwidth of the resulting subbands is smaller than that of the original image, the subbands can be down sampled without loss of information. Reconstruction of the original image is accomplished by up sampling, filtering and summing the individual subbands.

Fig 2.13 shows the principal components of a two-band subband coding and decoding system. The input of the system is a one-dimensional, band-limited discrete time signal x(n) = 0,1,2,...; the output sequence ,x`(n), is formed through the decomposition of x(n) into $y_0(n)$ and $y_1(n)$ via analysis filters $h_0(n)$ and $h_1(n)$. The subsequent recombination is done via synthesis filters $g_0(n)$ and $g_1(n)$. Note that filters $h_0(n)$ and $h_1(n)$ are halfband digital filters whose idealized transfer characteristics, H_0 and H_1 are shown in Fig 2.14.

Filter H_0 is a low pass filter whose output is an approximation of x(n) and filter H_1 is a highpass filter whose output is the high frequency or the detail part of x(n). All filtering is performed in the time domain by convolving each filters input with its impulse response – its response to unit amplitude impulse function, δ(n) [1].

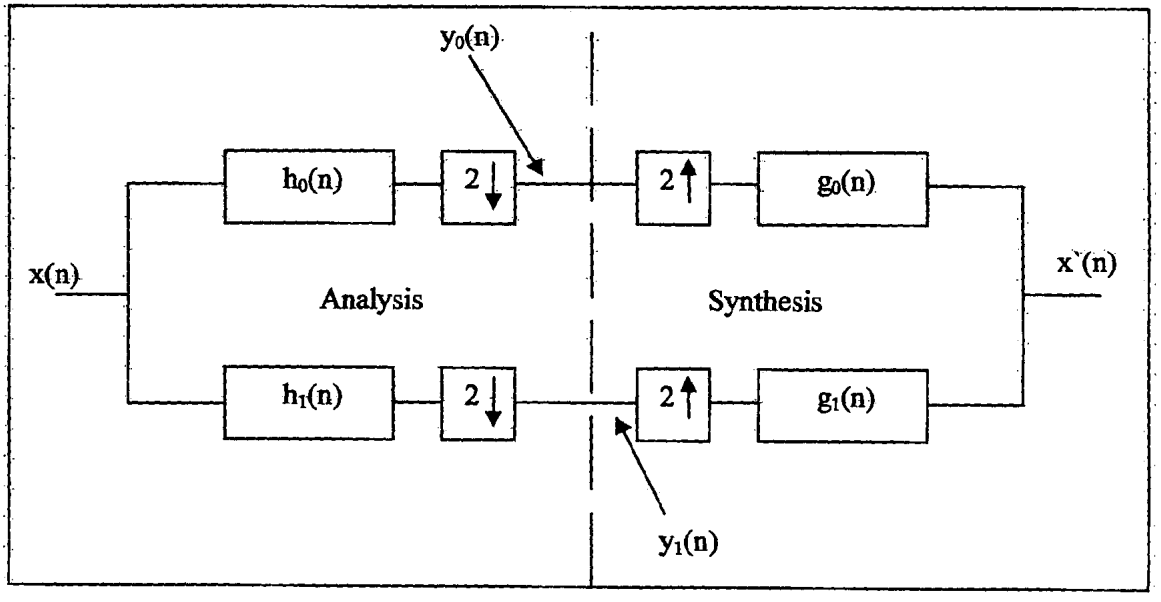

Figure 2.13: A two-band filter bank for one-dimensional subband coding and decoding; and

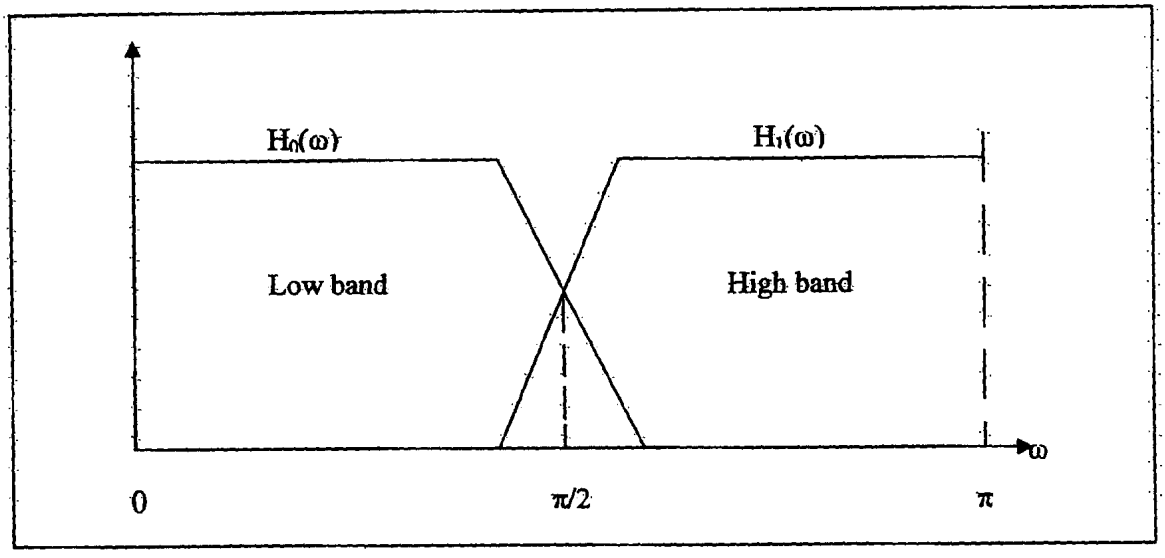

Figure 2.14: its spectrum splitting properties

This was a very basic description of the properties that wavelets take advantage of. In the case of images, which are two-dimensional instead of 1-D, the decomposition of the bands is slightly different. Images on the other hand are 2-D and the processing is slightly different (although the basics of WT remain intact). Wavelet analysis in image processing decomposes an image into approximation, horizontal, vertical and diagonal detail subbands. This is shown in Fig. 2.15.

In Fig. 2.15, x(m,n) is an input image with 'm' rows and 'n' columns. a(m,n) is the level 1 approximation detail of the image x(m,n). Similarly $d^V(m,n)$, $d^H(m,n)$ and $d^D(m,a)$ are the vertical, horizontal and diagonal level 1 details or subbands of the image x(m,n). A level-2 wavelet analysis would involve replacing x(m,n) with a(m,n) as the input. This in turn will generate another approximation, vertical, horizontal and diagonal set of details or subbands. Because of the downsampling, each corresponding output would be half its size.

The coefficients are ordered using two dominant patterns, one that works as a smoothing filter (like a moving average) the output of which here is a(m,n), and one pattern that works to bring out the images "detail" information (horizontal, vertical, diagonal). These orderings of the coefficients are called a quadrature mirror filter pair. A more detailed description of the transformation matrix can be found at [13].

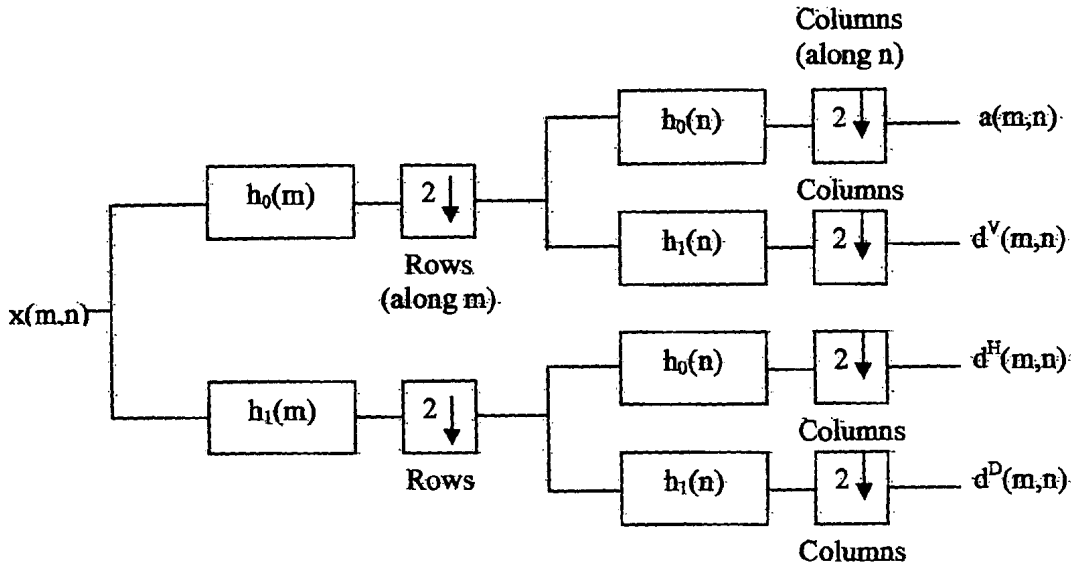

Figure 2.15: A two-dimensional four-band for subband image coding

2.5 Problem Identification

There are some similar studies on wavelet transforms but in different areas. In [14] a solution regarding tile surface defect detection using wavelets is proposed. A system developed by the researchers called TEMPLAR is described in the paper. TEMPLAR enables a large reduction of the wavelet transform data while retaining problem-specific information, which facilities an efficient pattern recognition process. In TEMPLAR the process begins with the creation of a template of the defective tile. Training data in the form of twelve identical tile images is provided to produce the artificial template.

The second stage of the process involves passing the defective tile image through a wavelet transform.

The third stage in TEMPLAR is the reconstruction operation, which is carried out using the wavelet transform toolbox in Matlab that gives the Variance result as an image, which is a black & white or Gray scale image. It contains only the difference between the artificial template image (which can be considered the original template clear, and clean image tile) and the defect tile image.

However, results are relative only to other wavelet transforms and are subjective. Defects are not quantified. In summary the study concludes that the Daubechies wavelet provides better results than Haar.

Although the results demonstrated show good identification of the tile defects, what is taken for granted is the fact that the tiles are rectangular. The application mentioned therein takes advantages of the natural 'discontinuity-highlighting' tendencies of wavelets. Resultantly any irregularity within the coefficients of the transform is labeled as a defect. Fig. 2.16 summarizes the process

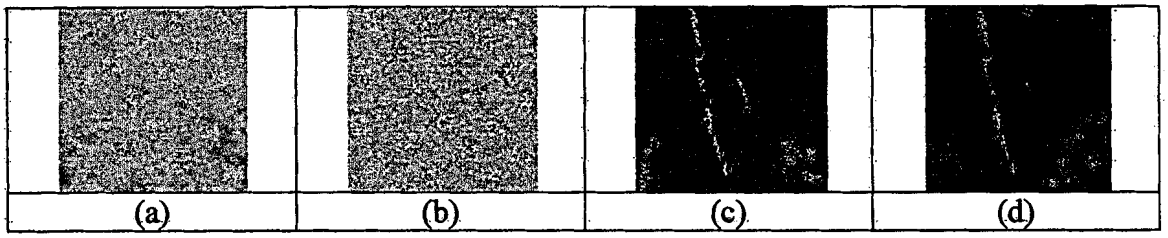

Figure 2.16: (a) Defective tile, (b) Tile template, (c) Reaction to Haar wavelet (variance), and (d) Reaction to Daubechies wavelet (variance)

Ferrule images on the other hand are circular. When passed through a wavelet transform the boundaries of the circular region are also classified as defects. The boundary pseudo-defects have to be removed before an evaluation for the classification/identification of defects can even take place. This remains the major challenge.

Unlike circular objects, these rectangular images also avoid the computational overhead of pseudo-defects.

Another similar study [22] identifies defects in images of textile surfaces. Here the technique involves feature extraction, pixel intensities calculation and analysis of wavelet coefficients. The process also involves the use of Haar and Daubechies wavelets. Their results also successfully identify defects but again were subjective and were rectangular and thus removing the overhead of having to remove pseudo-defects. See Fig. 2.17

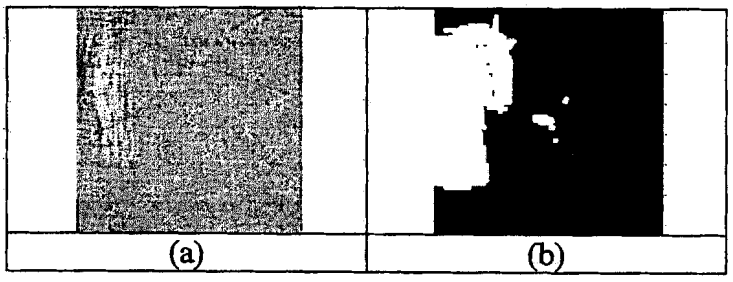

Figure 2.17: (a) Textile image with defect, (b) Wavelet transform of the image

This approach employs using feature extraction methodology that is applied to a k-level wavelet domain. The feature extraction approach considers multidimensional vectors of wavelet coefficients having as components suitably selected windows of these coefficients from their associated QMF channels.

Ferrule images in our study are circular (see fig. 2.18). They need to be segmented before a wavelet transform can be applied. Even after the transform, the detail subbands need to have pseudo-defects removed. The nature of the shape of the object in question makes it necessary to segment the image and also involves the need to remove pseudo-defects after the transform. The technique applied takes a wavelet transform of the ferrule image and also of the ferrule boundary. The ferrule boundary transform detail subbands are subtracted from the main transforms. This results in detail subbands as having only the defect details.

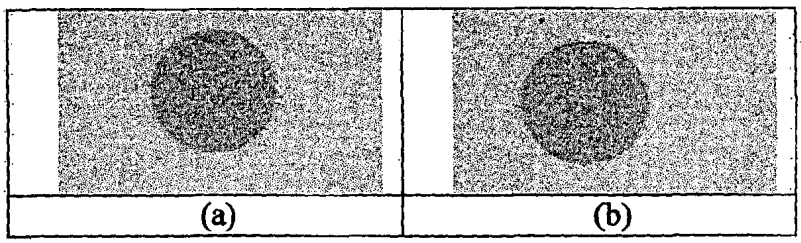

Figure 2.17: (a) A ferrule end with scratch marks and (b) a ferrule end with an obvious defect

3 IMAGE SEGMENTATION

Our method is based on selecting a threshold value to segment the images. These images have two large distinct areas based on their gray-level values – the darker foreground ferrule region and the lighter background region. These images have histograms that are bimodal, meaning that they will produce graphs with two obvious peaks. From hereon, selecting the threshold is apparently simple: choose the grey level representing the lowest point between the two peaks. Although it seems pretty simple, the histograms that were generated had several spread out grey level values between the two obvious peaks. This made the task slightly more skewed.

3.1 Image Acquisition

Images have been acquired using specialized cameras used in industrial quality control departments. Image acquisition of these connector surfaces is unfazed by gloss-related problems that may appear due to polishing or glazing operations that hamper the accurate detection of surface defects of certain items in the industry [14][19]. The captured images are converted to grayscale and binary forms to be suitable for use with various algorithms that are used to segment areas of interest in such images. There are other such similar tools that may be used to acquire these images [15].

3.2 Segmentation Method

There are also other problems involved in histogram processing like detecting the two obvious peaks where, relatively, other peaks are in close proximity. Noise variations can also produce sharp peaks. At times the second peak in the histogram is not obvious. There may also be need to spread out the histogram or to make it more smooth for the peaks to be made more distinct. And keeping all these in mind we adapted the *iterative selection* threshold method.

The idea here is to provide an estimate of the average gray level of both the background (T_b) and the objects (T_o). The average of these two values is selected as the initial threshold : $T = (T_o + T_b) / 2$. Initially these values are guesses based on the known properties of the image. Sometimes values from the four corners are assumed to be background pixels. It is even possible to use the overall mean grey-level value as the initial threshold [2].

However, in our application, since we know that the foreground ferrule region is darker and the background is lighter, we chose the initial values as $T_o = 0$ and $T_b = 255$.

The next step is to refine the values of T_b and T_o using the threshold value T. Here mean of the values below T are treated as T_o and mean value of grey levels greater than T are treated as T_b. From the new values just acquired (T_o and T_b) a second threshold value T is calculated as before $T = (T_o + T_b) / 2$. This process is repeated until the same T value is produced on two consecutive iterations. This final T value is considered to be a good threshold value.

We applied the iterative technique to our "edge-detected" images. This is demonstrated in Fig. 3.1. Image in Fig 3.1a was convolved with an edge detection kernel of size 3x3. Fig 3.1b shows the intermediate result, with prominent edges of objects, of the image after the edge detection operation. Fig 3.1c shows the result obtained after applying the iterative selection threshold method on image on Fig 3.1b. **There are more images and results in the result section of the document.**

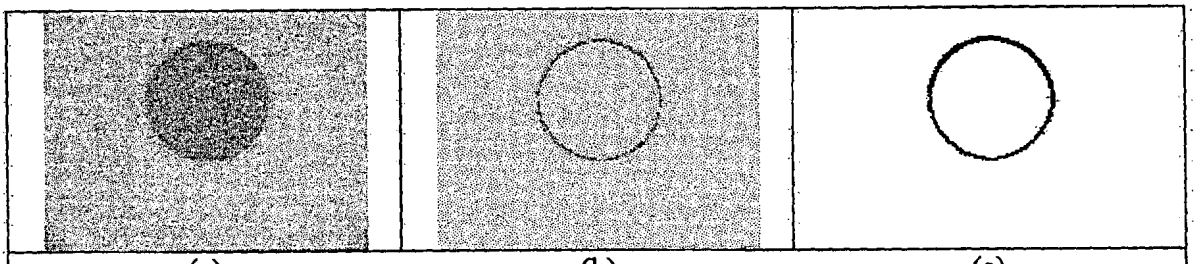

Figure 3.1: (a) the original image; (b) image convolved with an edge detector and (c) binary image obtained with the iterative selection threshold method of (b)

3.3 Edge Detection

Another objective of machine vision and image processing is edge detection. The simplest way of obtaining edges is to differentiate between gray-level values of the object and the background. An edge detection operation is primarily responsible for highlighting boundary regions of objects in images. Object and background regions usually have a distinct range of grey-level values and edge detection filters pronounce the effect of discontinuities in images. Edge detection algorithms also (usually in practice) suppress smother information of the image. However, we first enhanced the contrast of the image to make the discontinuities more viable for processing.

There are several spatial edge detection kernels available and can be classified into first- and second-order derivative categories. First-order derivatives generally produce thicker edges in the image. The second-order derivatives have a stronger response to finer detail (e.g response to thin lines).

The images in question have a special range of colors, distinctive from most other natural images. Their contrasting colors give the images two very distinct segments – the foreground and the background. The foreground consists of the circular ferrule, which is grayish and darker in color and also contains the central core (fiber.) The background, which is relatively much lighter in color, is part of the polishing machine and holds the connector tip in place during the actual polishing. Because the image contains such distinctive segments, it also has very pronounced edges.

We applied the second-order derivative and found very good results. The second-order derivative (itself called the Laplacian) results in a Laplacian image. This is an

image with edge information. The two-dimensional Laplacian is obtained by the following equation [1][2]:

$$\nabla^2 f = [f(x+1,y) + f(x-1,y) + f(x,y+1) + f(x,y-1)] - 4f(x,y) \quad (3.3\text{-}1)$$

Where $\nabla^2 f$ is the image laplacian,

f is the image.

This equation can be implemented using the following 3x3 kernels. We applied the one shown in Fig 3.2a.

0	1	0
1	-4	1
0	1	0

(a)

1	1	1
1	-8	1
1	1	1

(b)

0	-1	0
-1	4	-1
0	-1	0

(c)

-1	-1	-1
-1	8	-1
-1	-1	-1

(d)

Figure 3.2: Masks that are used to obtain the Laplacian

In Fig. 3.2 we have four Laplacian masks that can be applied to an image for the purpose of edge detection. Figures 3.2b and 3.2d also include the diagonal neighbors of the pixels in the context of the mask.

The equation given above is the last term subtracted. This is because the central weight is also negative. For masks in Fig. 3.2c and 3.2d this last term will be positive and the ones preceding it will be negative.

3.4 Region Growing

The binary image, we obtained earlier using the iterative method, is then processed based on values fundamental to circular regions. Values like circularity and center of mass play a crucial role is growing a template to extract the central ferrule region. The shape of the ferrule region is unique and consistent. The outline of the ferrule region can therefore be approximated by a circle.

Once the bi-level image is obtained, the area of the region inside the circular region is calculated using the technique, as mentioned in [2]. The center of mass *C* is also calculated as (*Cr*, *Cc*), where *Cr* is the center row and *Cc* is the center column of the circular object. *Cr* and *Cc* can be computed as:

$$Cr = \frac{\sum_{Row=1}^{NR}\sum_{Col=1}^{NC} F(row,col)row}{area(F)} \quad (3.4\text{-}1)$$

$$Cc = \frac{\sum_{Row=1}^{NR}\sum_{Col=1}^{NC} F(row,col)col}{area(F)} \quad (3.4\text{-}2)$$

(where *area (F)* is the number of pixels of the object. *NR* and *NC* are the Number or Rows and Number of Columns of the object, respectively.)

One property of the central core is that it is also the very center of the ferrule. The core is also very small in area. This information is used together with the center of mass value to establish the central point of the circular region. The lighter color of the core also aids this process. A seed pixel is then chosen that is grown outwards, recursively, towards the boundary from the center. This is shown in Fig 3.3b. Once the central circular region is fully grown, it is able to provide a form of template that is then used to extract the circular region from the main image (Fig. 3.3c).

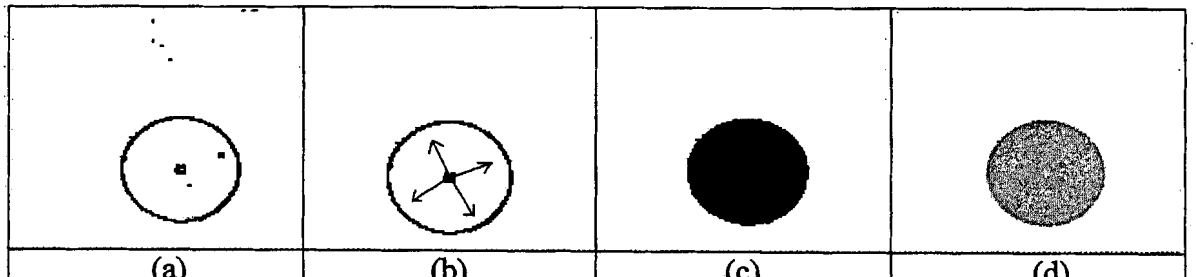

Figure 3.3: (a) Binary image obtained based on an iterative threshold; (b) the circular ferrule-area region is grown towards the boundary (c) template that has been grown; and (d) ferrule obtained based on the grown template.

Other segments that appear in the background area are highlighted and removed from the image on the basis of their overall area (see Fig. 3.3b).

Based on the template that has just been grown, the ferrule segment of the image is successfully obtained. Fig. 3.3d shows a successfully segmented ferrule region.

Fig. 3.4 shows some more results obtained by applying our technique.

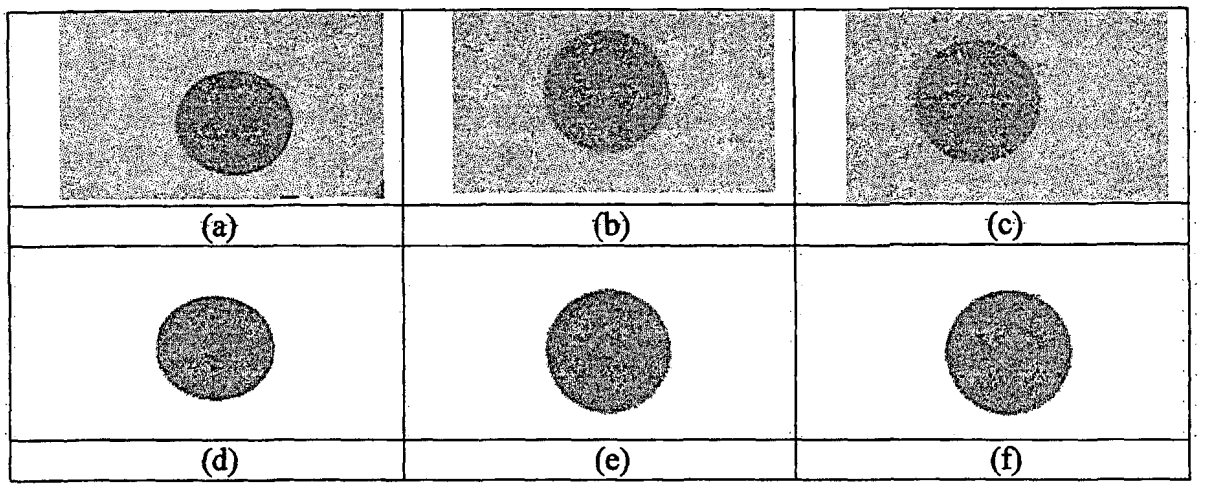

Figure 3.4: Ferrule tips of varying size with respective segmented ferrule regions (a-d, b-e, c-f)

In summary of the above mentioned techniques is the flow chart. The flowchart of the ferrule region extraction is shown in Fig 3.5.

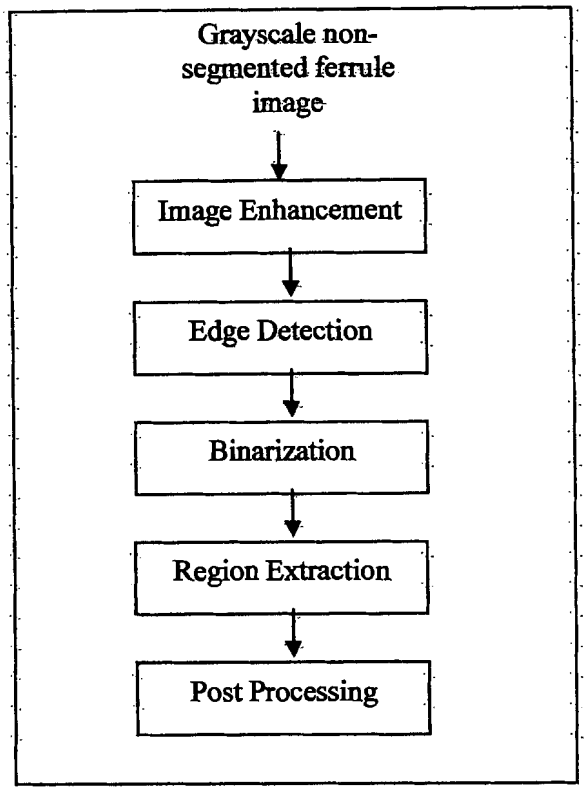

Figure 3.5: Image segmentation flowchart.

3.5 Wavelet Analysis

Fig. 3.6 summarizes the wavelet concept in the image-processing domain.

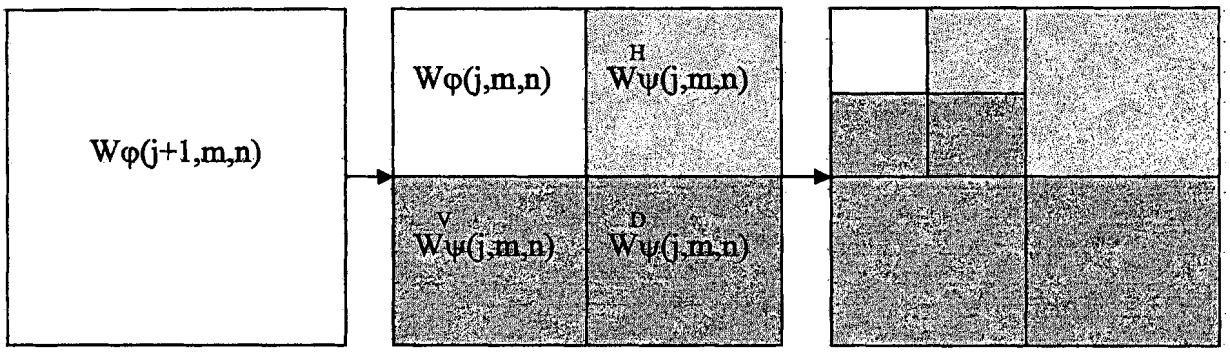

Figure 3.6: Image wavelet decomposition

And similarly our effort of a segmented ferrule images wavelet decomposition is shown in Fig 3.7.

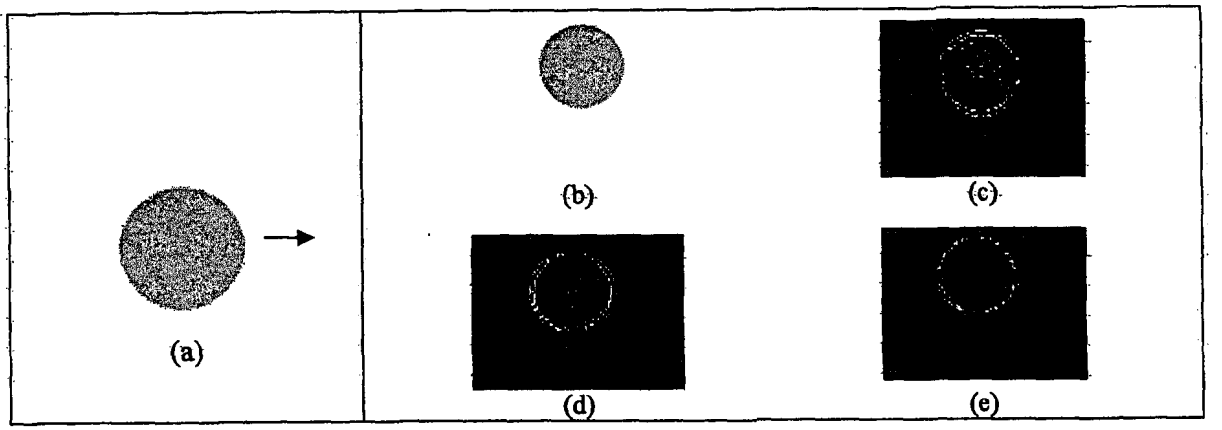

Figure 3.7: A segmented (a) ferrule image and its (b) approximation coefficient wavelet transform, and (c) horizontal detail coefficient image, (d) vertical detail coefficient image and (e) diagonal detail coefficient image obtained using the Daubechies transform.

And it is notable that the horizontal detail image brings out successfully many of the defect marks on the ferrules tip. Figures 3.8 through 3.10 show some more transforms.

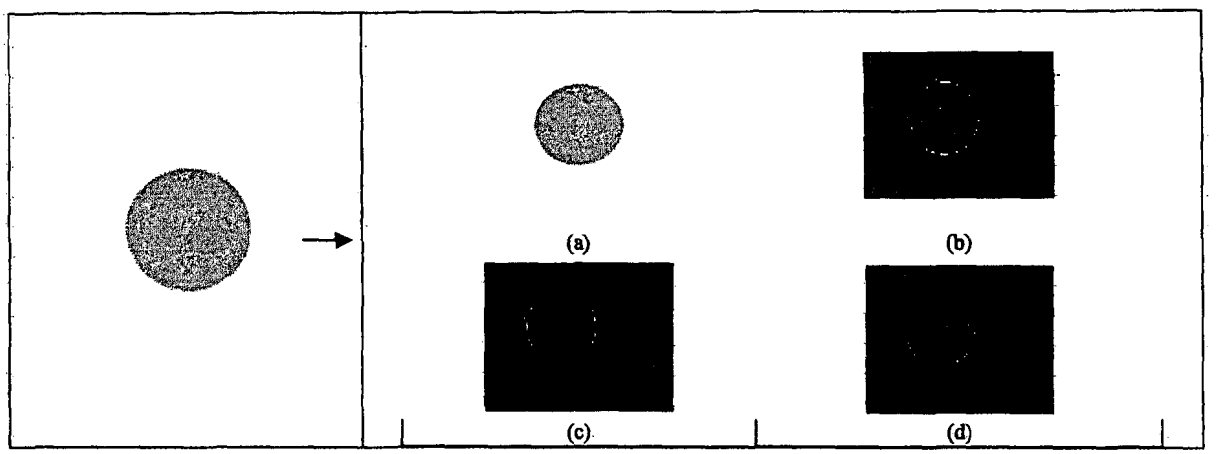

Figure 3.8: (a) Approximation image of a connector ferrule part , (b) Horizontal detail image, (c) Vertical detail and (d) Diagonal detail obtained using the Daubechies transform.

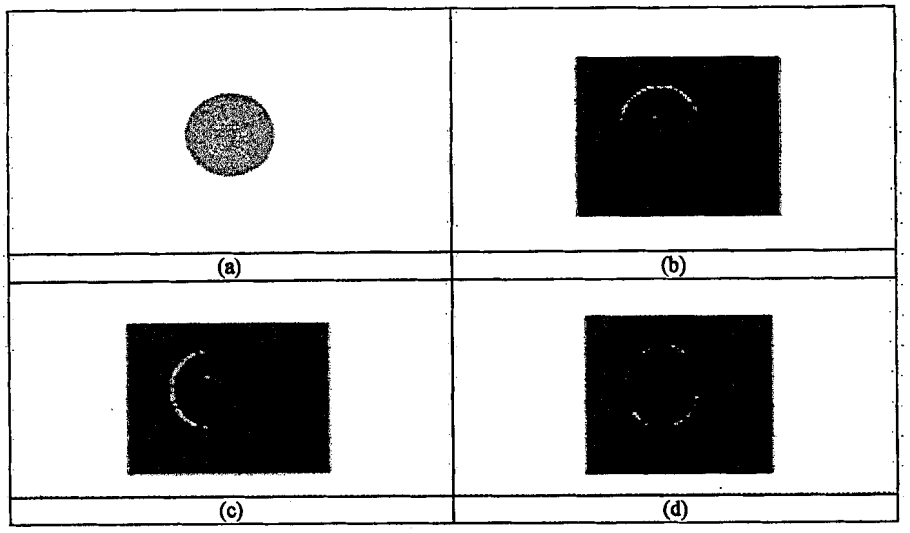

Figure 3.9: (a) Approximation image of segmented ferrule region, (b) Horizontal detail image, (c) Vertical detail and (d) Diagonal detail obtained using the Haar transform

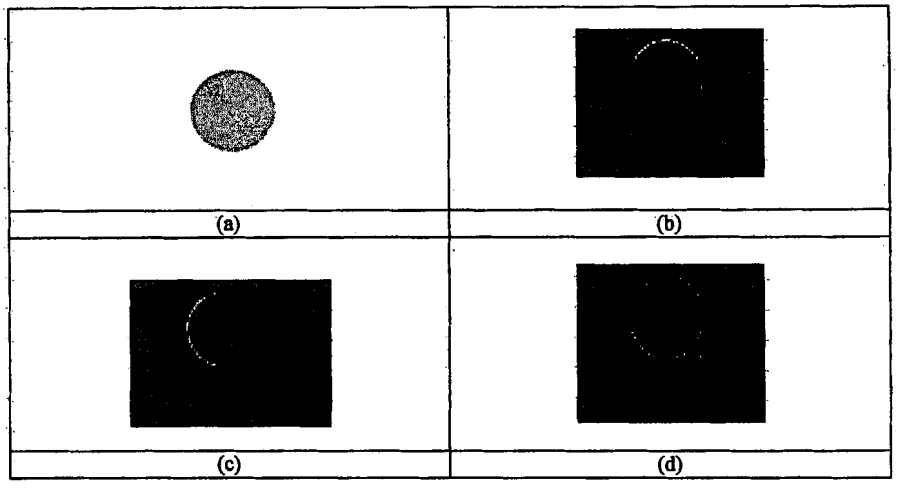

Figure 3.10: (a) Approximation image of a segmented ferrule region (b) Horizontal detail image, (c) Vertical detail and (d) Diagonal detail obtained using the Haar transform

We applied the Haar and Daubechies wavelets to our segmented images using Matlab. Both effectively identified the defects with the Daubechies giving the better of the two results. However, there is one thing to note. Although the results obtained identified the defects pretty successfully, outer boundary areas of the ferrule region also produced sharp discontinuities in the transformed version. Since these are farthest from the central core, they may be eliminated based on their radius value from the center of the ferrule.

Figures 3.8 through 3.10 show some results. Fig. 3.7 and Fig. 3.8 show the coefficients obtained using the Daubechies wavelet transform, while Fig. 3.9 and Fig. 3.10 do the same for the Haar transform.

We used our techniques on 12 images with different defects. Some of the images were without the central core. Some were plain and flawless. We found that different types of wavelets provided different results. In our scenario the Daubechies filters provided the best results. Detail coefficients of Fig. 3.9 and Fig. 3.10 (horizontal, vertical and diagonal details) were calculated using the Haar wavelets. Similarly detail coefficients of Fig. 3.7 and Fig. 3.8 were calculated using the Daubechies 4-tap wavelets. The latter have provided better results and have to quite a good extent been able to identify the defects. Image analysis was done using the Matlab software (version 7). More results are available in the Results section.

4 IMPLEMENTATION & DESIGN

Image processing and computer vision techniques are used together to segment the images. Image processing techniques are used to apply sharpening filters to bring out the detail from the image. Edge detection algorithms are then applied to highlight the boundary regions of the ferrule area. Computer vision techniques convert the edge highlighted image to a bi-level form. The circular ferrule region is then grown to form a type of template. This template is then used to extract the ferrule region from the image.

The extracted ferrule images are then passed into out Matlab application for the purpose of defect detection using the various wavelet functions provided therein. The Matlab application is a GUI and very simply highlights the defects in the ferrule region through its coefficients.

Provided below is a complete description of the several functions used to implement the two-tiered application process.

4.1 Proposed Solution

The images in our study are composed of optical fiber ferrule ends. Contrasting colors give the images two very distinct segments – the foreground and the background. The foreground consists of the circular ferrule, which is grayish and darker in color and also contains the central core (fiber). The background, which is relatively much lighter in color, is part of the polishing machine and holds the connector tip in place during the actual polishing. Because the image contains such distinctive segments, it also has very pronounced edges. These edges help is segmenting the circular region from the image.

Before segmentation the images are enhanced and fed to the segmentation method. Once the image has successfully been segmented it can be passed on for defect detection using wavelets.

4.1.1 Flowcharts

All the design process and activities to achieve the tasks are described pictorially as flowcharts below.

Flowchart to generate a high-boost filtered image

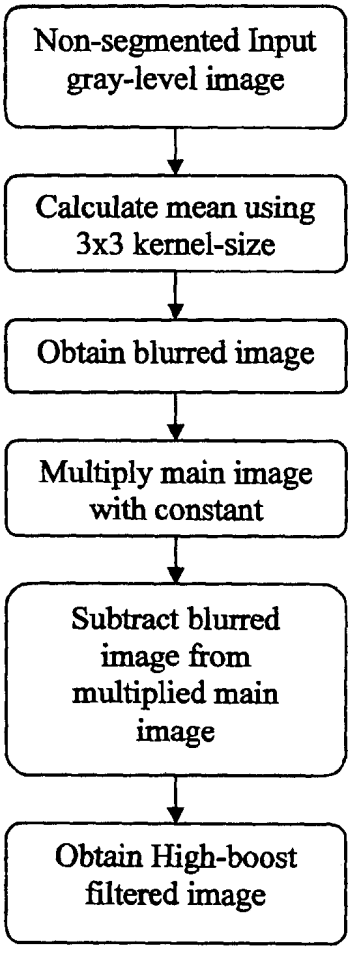

Flowchart to edge-detect the image

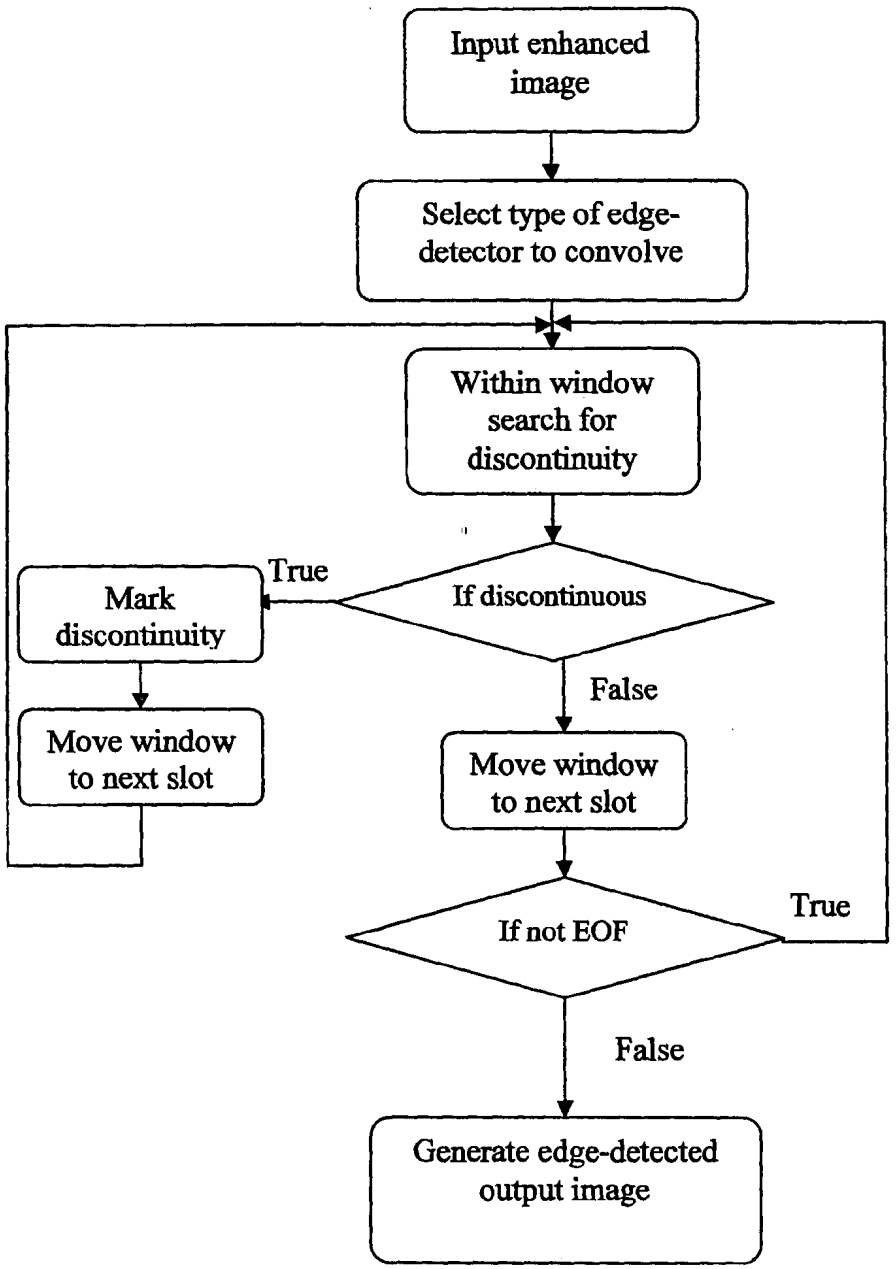

Flowchart to calculate threshold for binarization

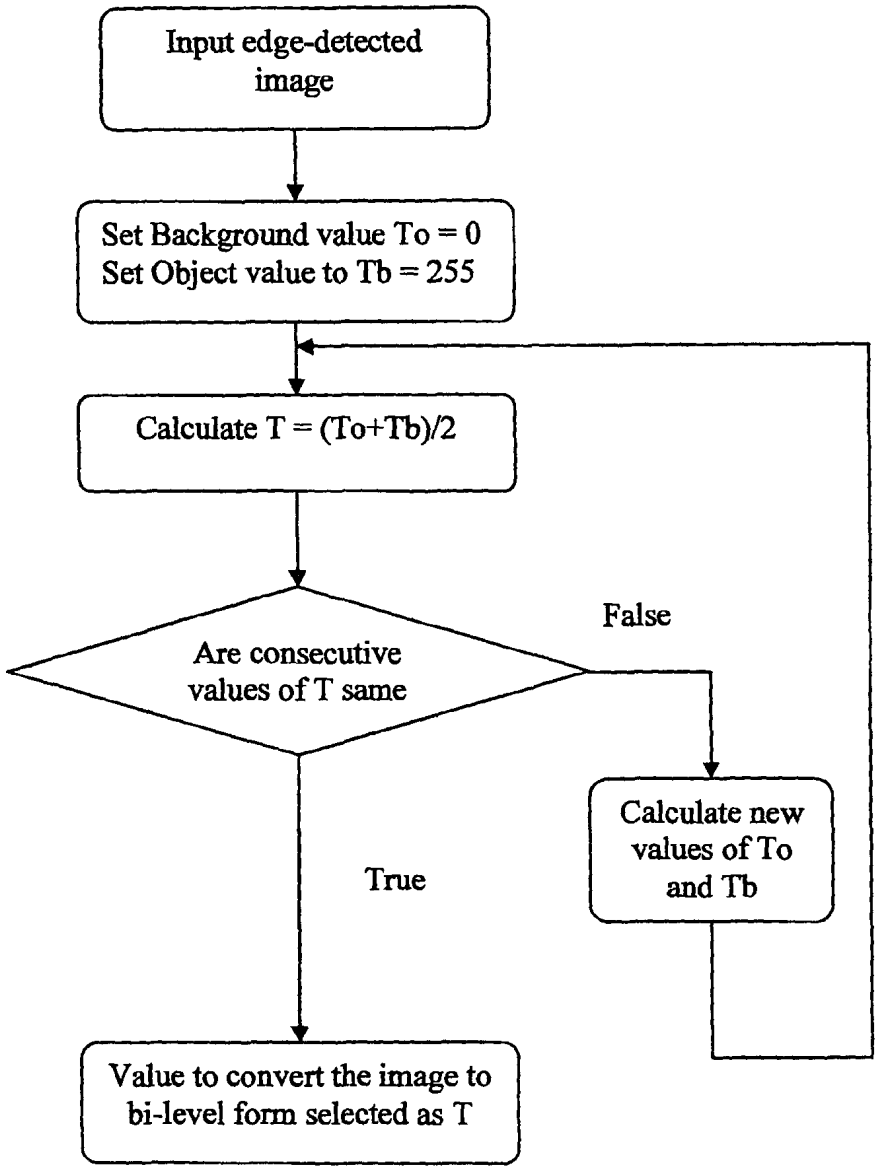

Flowchart to convert the image to a bi-level form

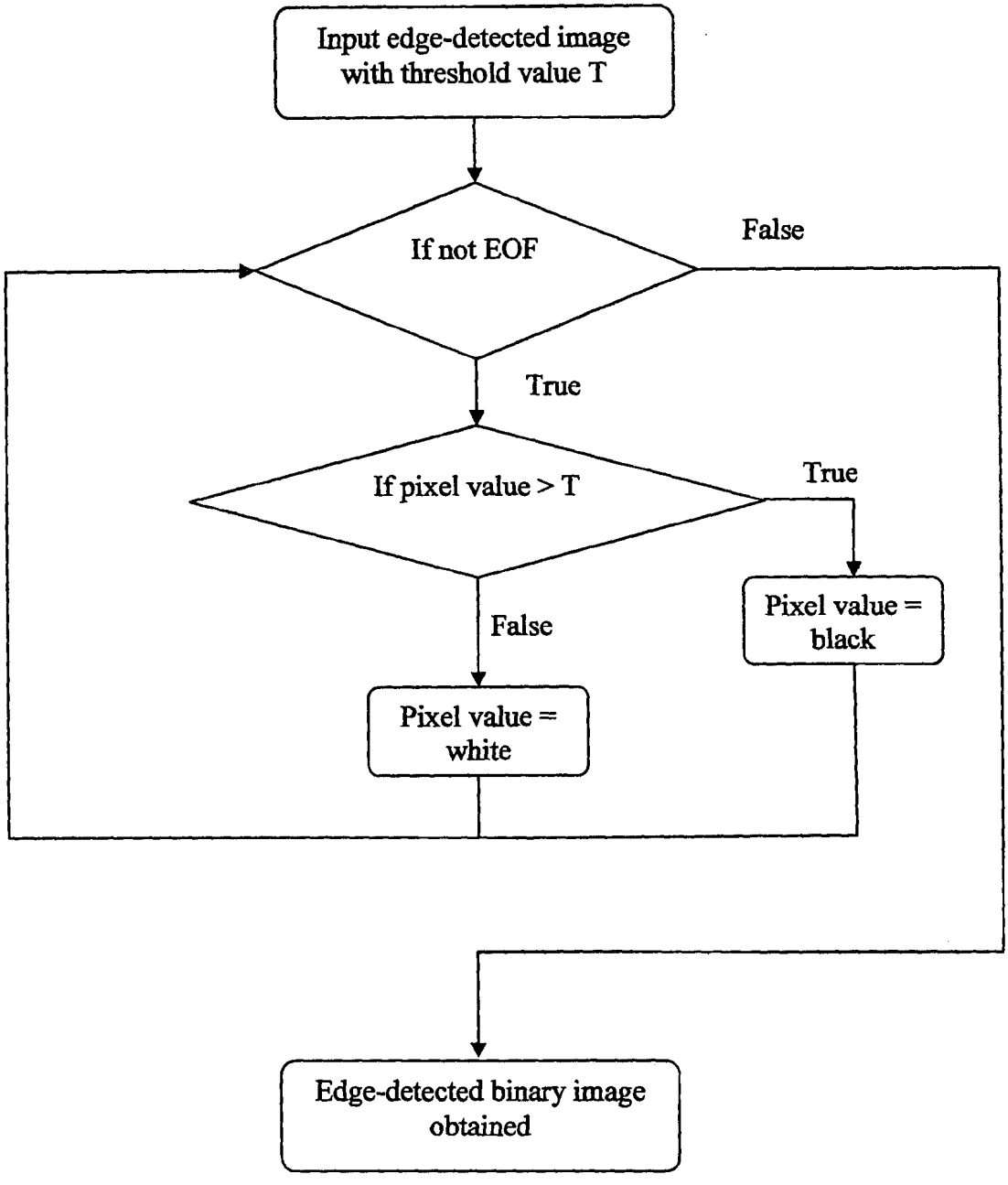

Flowchart to extract ferrule region

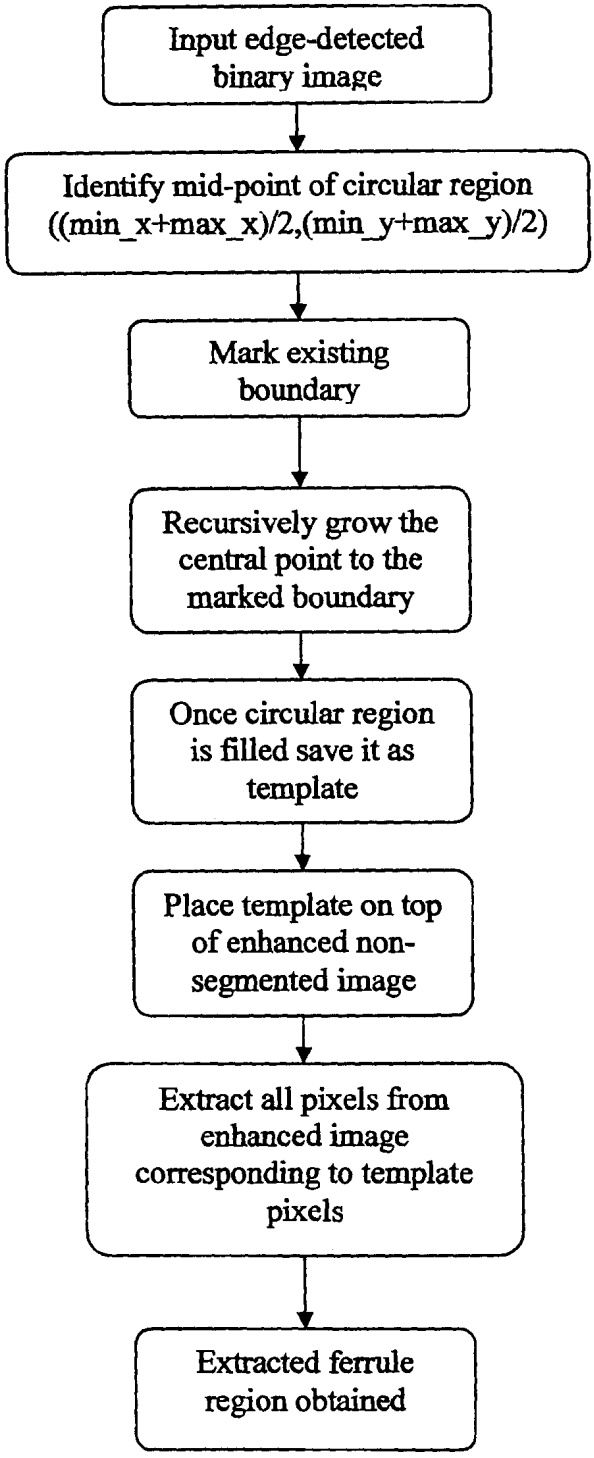

Flowchart describing the use of wavelets to identify defects

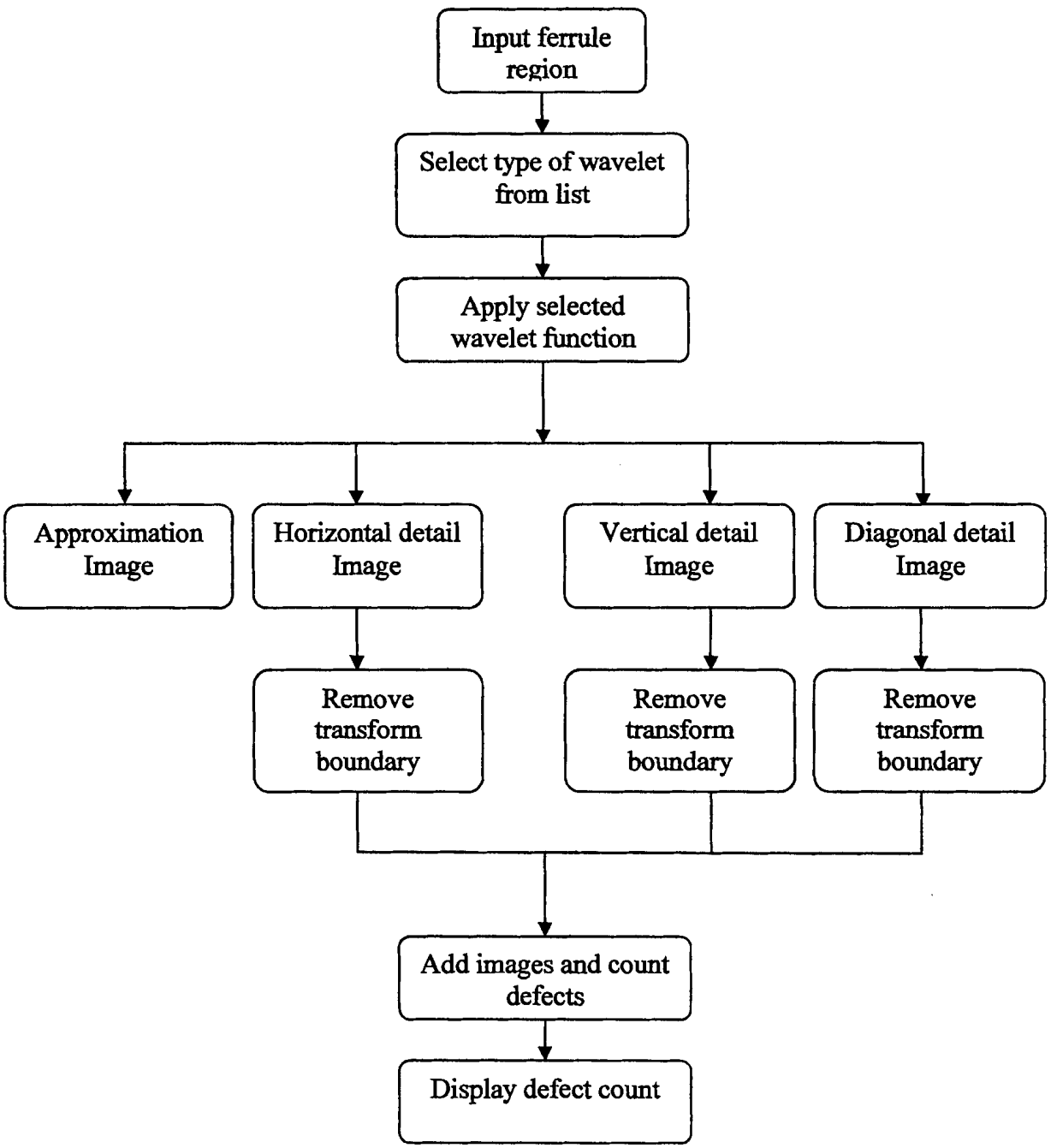

4.2 Image Enhancement

As mentioned earlier we used high-boost filtering method to sharpen the images. High-boost filtering is defined as

$$f_{hb}(x,y) = Af(x,y) - \bar{f}(x,y) \quad (4.2\text{-}1)$$

where $f_{hb}(x,y)$ is the sharpened image, $A \geq 1$, and $\bar{f}(x,y)$ is the blurred version of f(x,y).

The implantation of high-boost filtering is done in the file unsharp.cpp and its algorithm is shown below.

unsharp.cpp

```
for ( i = first row to last row ; i++) {
        for (j = first column to last column ; j++) {

                for (s = loop three times the rows of the kernel do) {
                        for (t = loop three times the columns of the kernel do) {

                        Average_Value[count] = Image[(i+s),(j+t)];
                        sum = sum + Average_Value[count];
                        count++;
                        }
                }
                count=0;
                Blurred_Image[i,j] = sum/(MASKROWS*MASKCOLUMNS);
                Sharpened_Image[i,j]=(2.1)*Image[i,j]-Blurred_Image[i,j];
                sum=0;
        }
}
```

Result of high-boost filtered image is shown in Fig. 4.1.

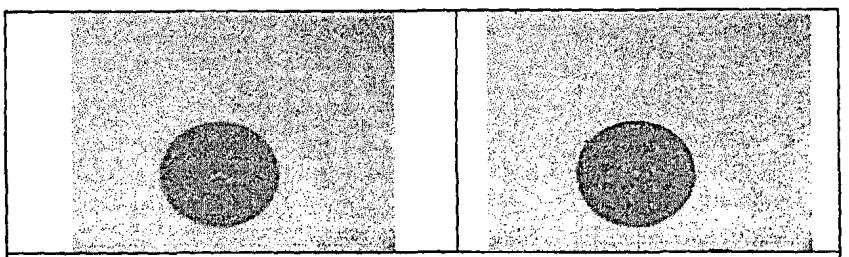

Figure 4.1: The original image on the left-hand side and the right-hand side image obtained after high-boost filtering.

4.3 Image Segmentation

After the enhancement the images are then segmented to separate the ferrule region from the main image.

This process in also implemented in C. It also involves more steps and functions. This is implemented in the file seg.cpp.

Seg.cpp

The image is first of all passed through an edge-detector to enhance the edges.

```
for ( i = first row to last row ; i++) {
        for (j = first column to last column ; j++) {

        Edge_Detected_Image[i,j] =
                        ((originalimage[(i-1),(j-1)] + originalimage[(i,j-1)] +
                                originalimage[(i+1,j-1)]) - (originalimage[(i-1,j+1)] +
                        originalimage[(i,j+1)] + originalimage[(i+1, j+1)] ))

                        +

                        ((originalimage[(i+1),(j-1)] + originalimage[(i+1,j)] +
                        originalimage[(i+1),(j+1)]) - (originalimage[(i-1),(j-1)] +
                                originalimage[(i-1,j)] + originalimage[(i+1),(j+1)]));
                }
}
```

This algorithm detects the edges horizontally and vertically. The edges of the regions in the image, that have just been identified, are then replaced with the values of the gray-levels that appear in the original image. This results in a more perked-up representation of the edge-enhanced image. This is shown below in Fig. 4.2.

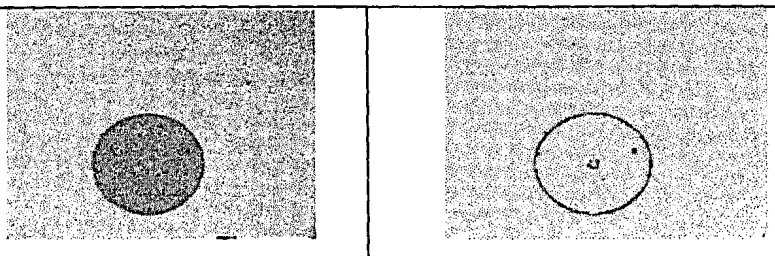

Figure 4.2: (a) Connector ferrule with central core and light colored background; and (b) The ferrules pronounced edges after convolving with an edge-detector

4.4 Binarization

The "edged" image is then converted to a black-and-white or binary form. Here a threshold value is chosen iteratively. Values greater than the iterative threshold are converted to white or made part-of-the-background, and values of gray-levels below the threshold are converted to black; in other words are made part of the object.

The histogram is initially segmented into two parts using a starting threshold range such as 0-127 and 128-255 (these are the ranges we have assumed in our technique, they may however be different depending on the application at hand); i.e. half the maximum dynamic range. The mean of the gray values associated with the foreground pixels and the sample mean of the gray values associated with the background pixels are computed. A new threshold value is then computed as the average of these two sample means. The process is repeated, based upon the new threshold, until the threshold value does not change any more.

1. An initial threshold value (T) is chosen, this can be done randomly or according to any other method desired but is usually chosen as T=(max_value+min_value)/2.

2. The image is segmented into object and background pixels as described above, creating two sets:

   a. G_1 = {f(m,n):f(m,n)<T} (object pixels)
   b. G_2 = {f(m,n):f(m,n)≥ T} (background pixels) (note, f(m,n) is the value of the pixel located in the m^{th} column, n^{th} row)

3. The average of each set is computed.

   a. m_1 = average value of G_1
   b. m_2 = average value of G_2

4. A new threshold is created that is the average of m_1 and m_2

   a. $T' = (m_1 + m_2)/2$

5. Go back to step two, now using the new threshold computed in step 4, keep repeating until the new threshold matches the one before it.

The above sequence is shown in a pictorial form in Fig. 4.3.

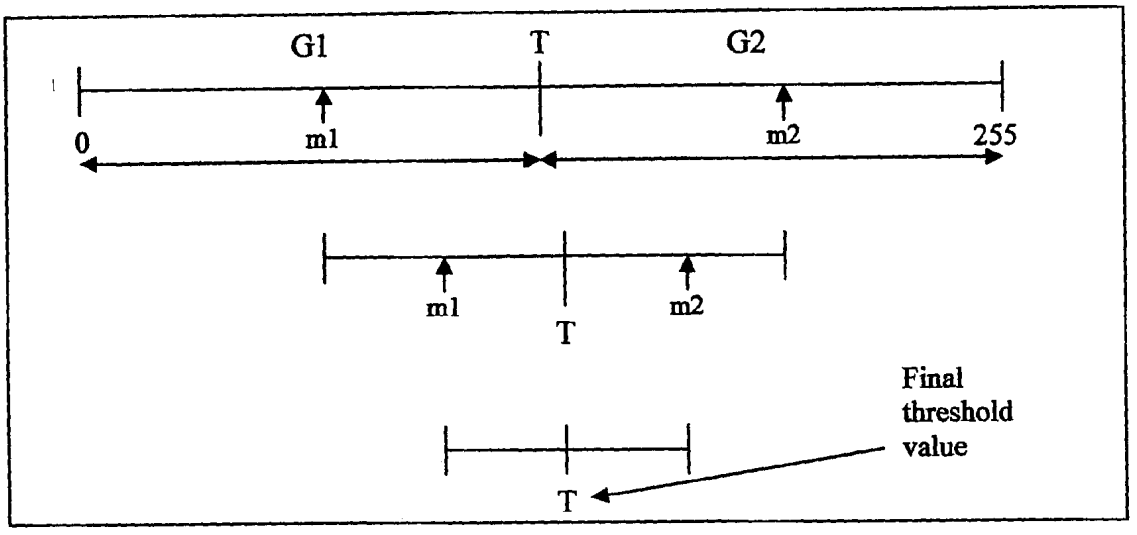

Figure 4.3: Threshold value selection based on the iterative method. Final threshold value results when two successive iterations produce the same value of T.

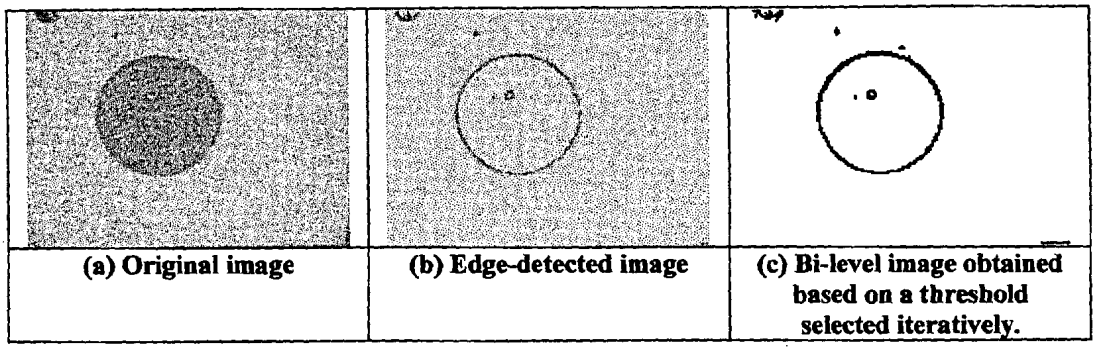

(a) Original image	(b) Edge-detected image	(c) Bi-level image obtained based on a threshold selected iteratively.

Figure 4.4: Obtaining the bi-level image

Fig. 4.4 (c) shows a binary image obtained based on the threshold value (T) that was selected iteratively. The binary image however still contains other objects in the image that are not part of the ferrule region and hence need to be discarded. This is the next step in the process of ferrule-region extraction.

4.5 Circularity Based Region Extraction

Extra information (small irregular objects other than the ferrule) in the bi-level image is highlighted and removed on the basis of their overall area. Other auxiliary information available from the image aids this process. The unique circular shape of the ferrule region provides important information that is characteristic of circular regions. Here the circularity property is used to check if the region is round enough to be

considered circular. If the circularity value is 1 or close to 1, the region is circular. And if the area of the object is also within the limits of the range set by our application, for that of a ferrule region, then we have a successful hit. Other elements are eliminated from the image since these would not qualify based on our set criteria.

In the meantime, the area of the object that is selected as a ferrule-region candidate is grown into a template recursively. The area is calculated and center of mass value established.

Center of mass and circularity is calculated as described in section 4.5.1 and 4.5.2

4.5.1 Center of Mass

The center of mass *C* is also calculated as (*Cr*, *Cc*), where *Cr* is the center row and *Cc* is the center column of the circular object. *Cr* and *Cc* can be computed as described in equation 3.4-1 and 3.4-2 in section 3.4. The *area (F)* described therein is the number of pixels of the object [2].

4.5.2 Circularity

Before we proceed to the formula please note that the ratio P^2/A for a circle is always 4π. The minimum value for a circular region is 1. This value will increase as the object becomes more complicated. And it is defined as [2]

$$C = \frac{P^2}{4\pi A} \tag{4.5-1}$$

Where P is the perimeter of the object, and A is the area (which is the actual count of an objects pixels).

We then have a template that will help in the extraction of the ferrule-region from the main, enhanced image. This template is shown in Fig. 4.5a.

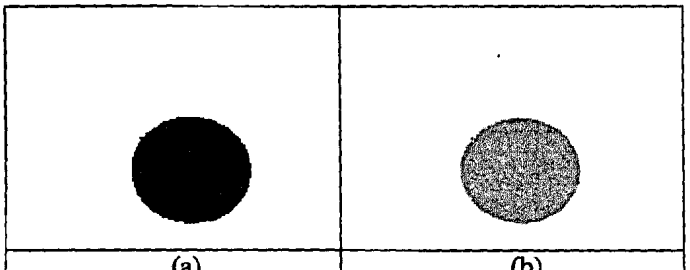

Figure 4.5: (a) bi-level template that has been grown; and (b) ferrule obtained based on the grown template.

Based on the template that has just been grown, the ferrule segment of the image is successfully obtained. Fig. 4.5b shows a successfully segmented ferrule region.

4.6 Defect Detection Based on Wavelet Coefficients

Once the images are segmented they are then passed through a Matlab application that calculates wavelet coefficients of different genre and type. The application displays the results of the coefficients into different place holders where an assessment of the transform can be had.

The application is a GUI and is implemented using Matlabs GUIDE tool. This tool allows for rapid GUI rendering, where the backend can be programmed using the syntax that the Matlab program supports.

We have applied different Matlab functions to carry out the demonstration. We used Haar, Daubechies, Coiflet and the Symlet wavelet transform.

These different function each carry out and display the approximation, horizontal, vertical, and diagonal details of the ferrule image.

5 RESULTS & CONCLUSION

5.1 Image Enhancement Results

High-boost filtering was used to enhance the images. We used a multiplication factor of 2.1 before subtracting the blurred image from it. More detail on high-boost filtering is provided in section 4.1. Following images labeled (a) – (r) have been arranged in a manner that the original images appear in the left hand-side column under the heading Original Image and their respective enhanced images appear in the right hand-side column under the heading Enhanced Image.

Original Image	Enhanced Image
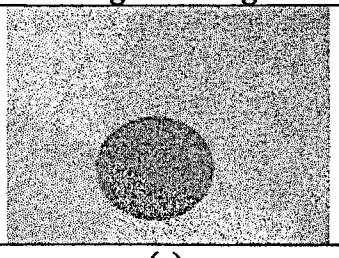	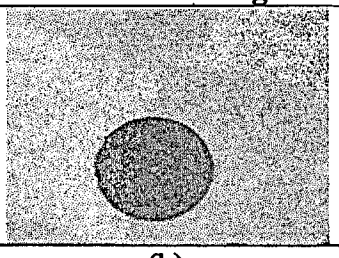
(a)	(b)
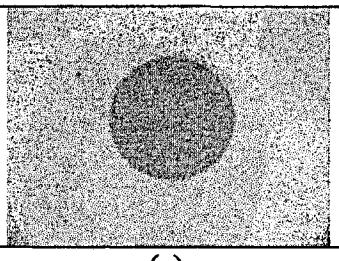	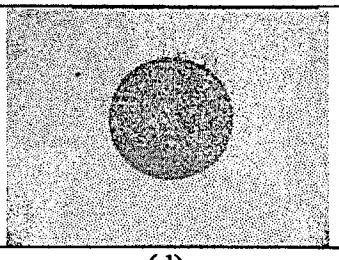
(c)	(d)
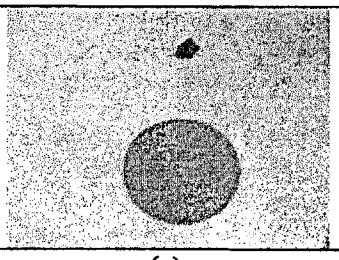	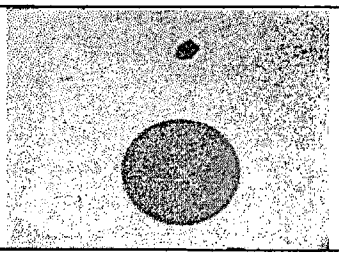
(e)	(f)
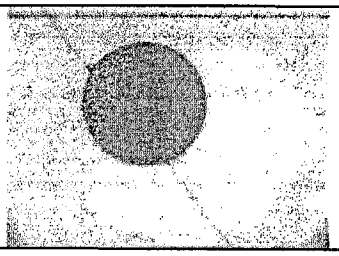	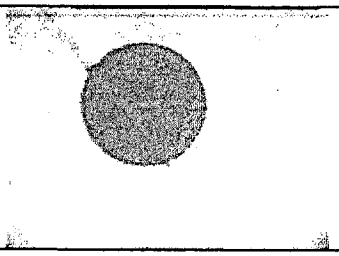
(g)	(h)

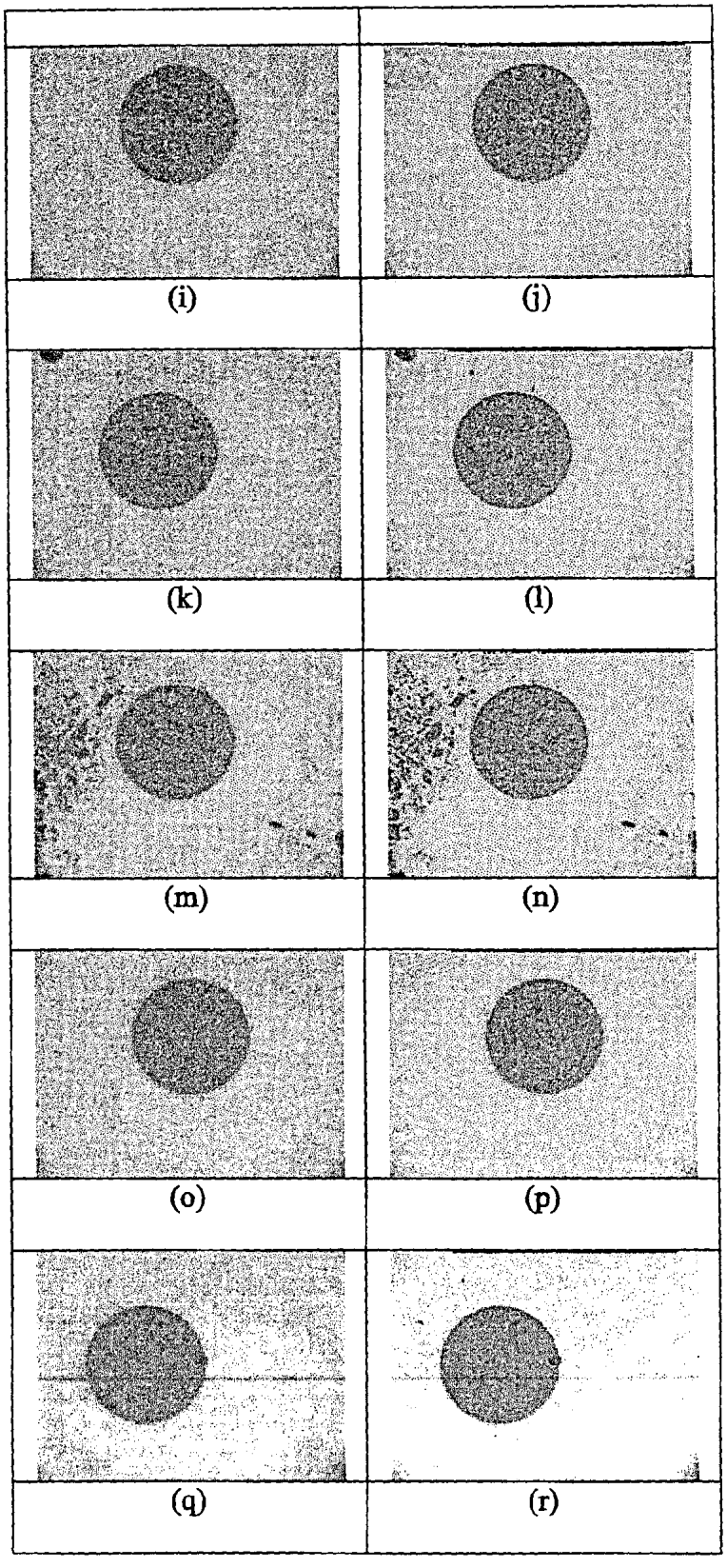
(i)
(j)
(k)
(l)
(m)
(n)
(o)
(p)
(q)
(r)

5.2 Segmentation Results

The following images, s-(a) to s-(r) have been arranged in a manner that enhanced images appear in the left hand-side column and their respective segmented ferrule regions appear in the right hand-side column.

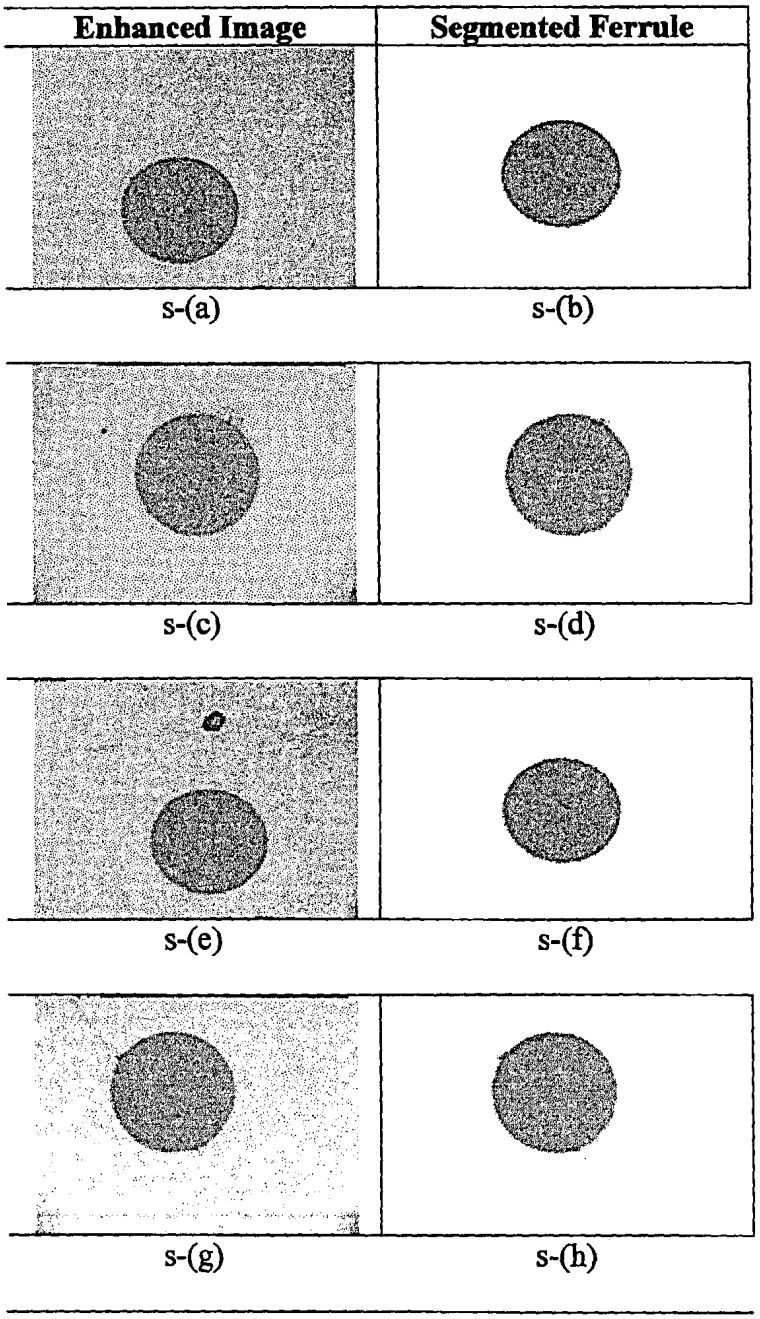

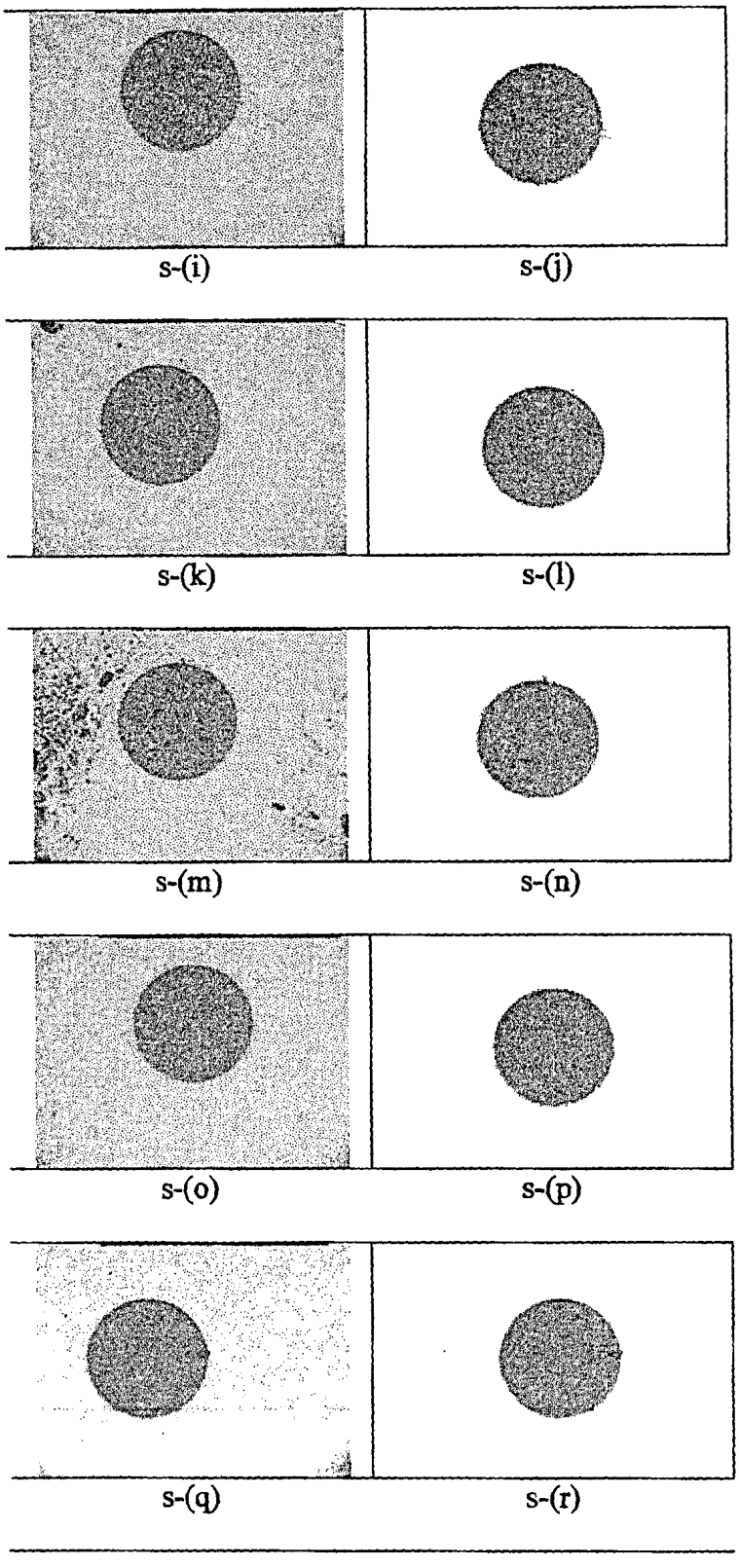

5.3 Wavelet Results

Wavelet transformed detail images are shown below. These are level 1 transforms. The results are in the form as shown in Fig W-W:

Approximation Detail	Horizontal Detail
w-(a)	w-(b)
Vertical Detail	Diagonal Detail
w-(c)	w-(d)

Figure W-W: w-(a) Approximation image of segmented ferrule region, w-(b) Horizontal detail image, w-(c) Vertical detail and w-(d) Diagonal detail obtained using the Haar transform

And have been computed using the Haar transform. Defects are clearly visible in the detail coefficients.

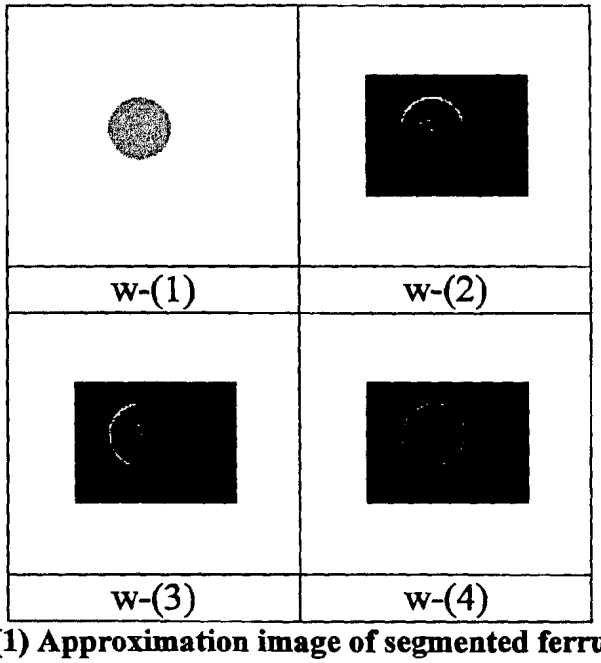

Figure W-A: w-(1) Approximation image of segmented ferrule region of image shown in Fig. s-(I), w-(2) Horizontal detail image, w-(3) Vertical detail and w-(4) Diagonal detail obtained using the Haar transform

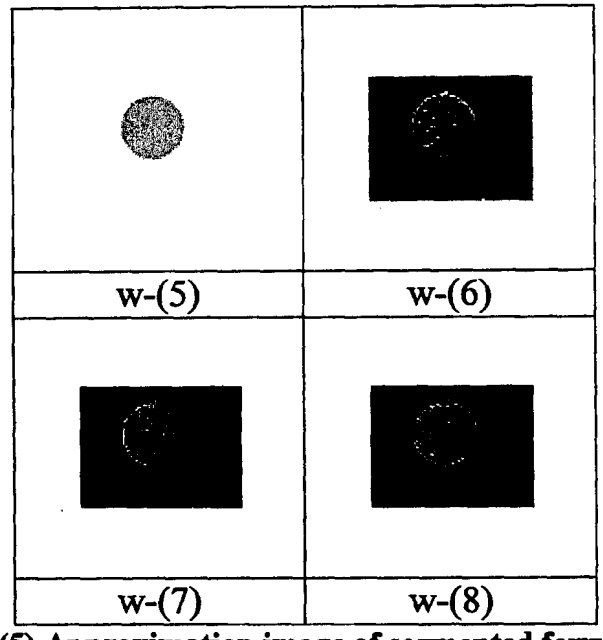

Figure W-B: w-(5) Approximation image of segmented ferrule region of image shown in Fig. s-(n), w-(6) Horizontal detail image, w-(7) Vertical detail and w-(8) Diagonal detail obtained using the Haar transform

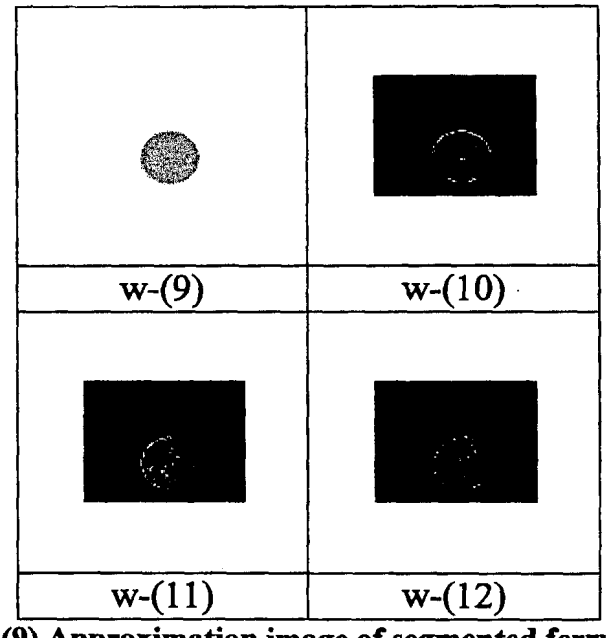

Figure W-C: w-(9) Approximation image of segmented ferrule region of image shown is Fig. s-(f), w-(10) Horizontal detail image, w-(11) Vertical detail and w-(12) Diagonal detail obtained using the Haar transform

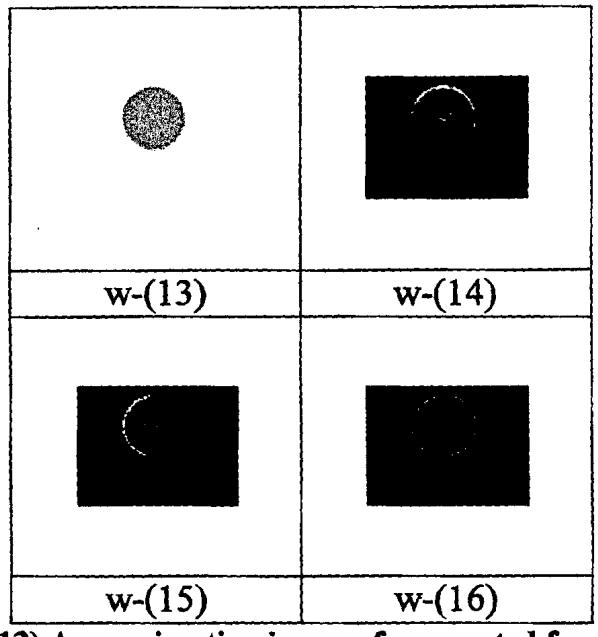

Figure W-D: w-(13) Approximation image of segmented ferrule region of image shown in Fig. s-(j), w-(14) Horizontal detail image, w-(15) Vertical detail and w-(16) Diagonal detail obtained using the Haar transform

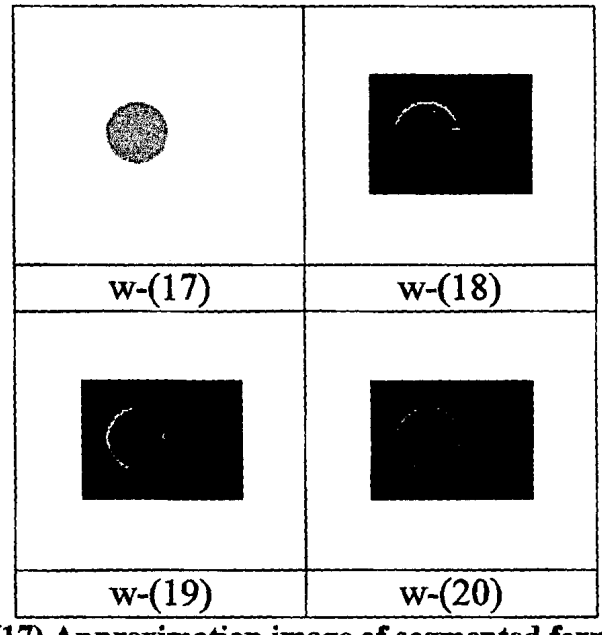

Figure W-E: w-(17) Approximation image of segmented ferrule region of image shown in Fig. s-(r), w-(18) Horizontal detail image, w-(19) Vertical detail and w-(20) Diagonal detail obtained using the Haar transform

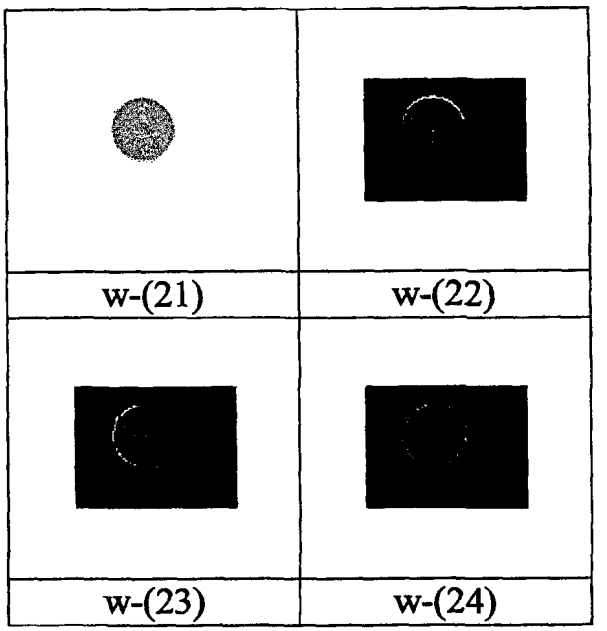

Figure W-F: w-(21) Approximation image of segmented ferrule region of image shown in Fig. s-(h), w-(22) Horizontal detail image, w-(23) Vertical detail and w-(24) Diagonal detail obtained using the Haar transform

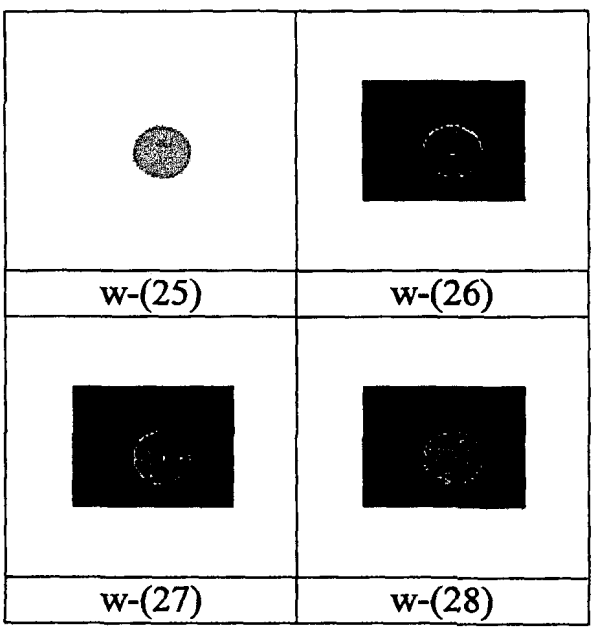

Figure W-G: w-(25) Approximation image of segmented ferrule region of image shown in Fig. s-(p), w-(26) Horizontal detail image, w-(27) Vertical detail and w-(28) Diagonal detail obtained using the Haar transform

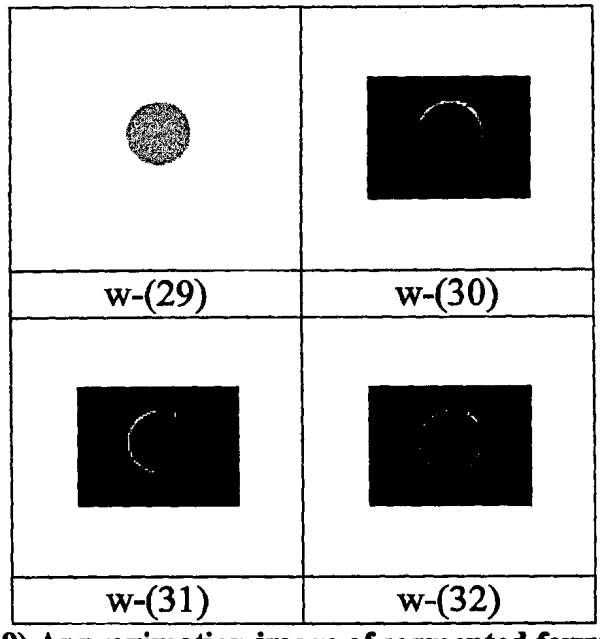

Figure W-H: w-(29) Approximation image of segmented ferrule region of image shown in Fig. s-(d), w-(30) Horizontal detail image, w-(31) Vertical detail and w-(32) Diagonal detail obtained using the Haar transform

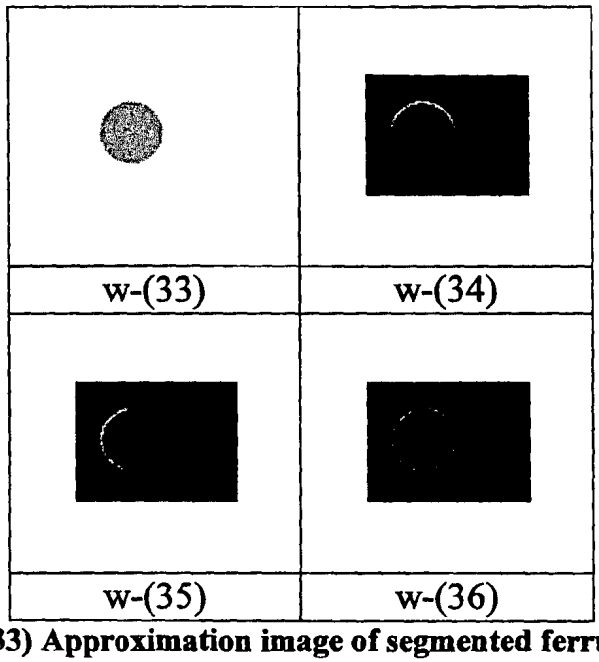

Figure W-I: w-(33) Approximation image of segmented ferrule region of one of the other images, w-(34) Horizontal detail image, w-(35) Vertical detail and w-(36) Diagonal detail obtained using the Haar transform

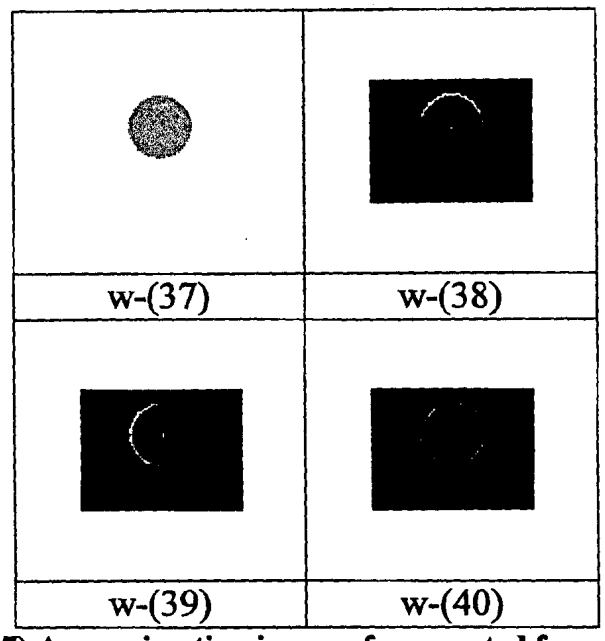

Figure W-J: w-(37) Approximation image of segmented ferrule region of another one of the images, w-(38) Horizontal detail image, w-(39) Vertical detail and w-(40) Diagonal detail obtained using the Haar transform

The three detail images, namely the horizontal, vertical and diagonal images produced by the wavelet transform, out of the four images are used together to determine the defects on the surfaces of the ferrule regions. Initially the images produced by the wavelet transform produce very strong reactions to outer boundary regions demarcated against the white background (it visible in all the transformed images). This is due to the sharp contrast in the gray-level values of both the foreground region and the white background and the wavelets tendency to highlight such changes. As a result the detail approximations highlight the boundary regions as defects. Calculating a defect based on the severity as would be determined by a higher gray-level value for a severe defect would classify most of the boundary-region as defective. Most of the boundary region gray-level coefficients highlighted in these approximation images lay well over 200 in value (or whitish in appearance for an 8-bit gray-level image). Majority of the boundary pixels, in these approximation images, had a gray-level value of 255.

The actual ferrule-region defects also produced good reactions in the transformed approximations. The more severe the defect the greater in value the gray-level would appear in the transformed image. A severe defect would have a high gray-level value accompanied with lower gray-level pixels in its immediate neighborhood.

The findings have been such that in most cases the transformed approximations did not highlight the defects in unison. In fact, for instance, a defect not picked up in the horizontal approximation would either be highlighted in the vertical or the diagonal approximation or both. Same could be the case the other way round. It was a rarity to see all of the three approximations highlighting a more severe defect simultaneously.

The approximations, however, highlighted defects individually. A horizontal approximation highlighted its own set of defects as did a vertical approximation or a diagonal approximation. Together these images would highlight most of the defects across the domain as a whole.

Here we describe two approaches which we have used to highlight the defects from these approximations.

First Approach

The first approach deals with the removal of the highlighted boundary region of the transformed images based on gray-level values. With this possibility the three approximations other than the approximation detail image are combined to form a single image with all the defects made prominent. This single image contained all the pronounced defects from all the three images along with the highlighted boundary region. The boundary presence caused the presence of pseudo-defects in this new image. This heavily skewed any result data out of the image analysis that this team was wishing to work on.

Therefore, image synthesis of detail approximations (horizontal, vertical and diagonal detail images) was delayed till after the exclusion of the highlighted boundary regions from these images (the detail images). This was done based on the gray-level values of the pronounced boundary regions. To minimize any losses gray-levels with a value of 255 were chosen and removed from the approximation images. Choosing a single value preserved the surrounding region gray-levels of defects whose values were close to 255. A range of values was not chosen as it would have eroded most of the surrounding lesser-valued gray-level pixels of a defect.

This process greatly removed most of the boundary region pixels from detail approximation images. It, however, did not completely eradicate all such pixels. The synthesized new image contained several boundary-region pixels with high gray level values albeit very small in number. Different wavelet transforms had different number of defect pixels. Some of the defect pixels accounted for pseudo-defects that were present due to the boundaries. These defects were always present in all images and had an average number of pseudo-defect pixels presence in all synthesized images. An average value, therefore, was calculated to determine the pre-presence of such pixels. To determine the least possible number of defects an average pixel count was determined based on five most clean defect-free ferrule image. The acceptable average defect values for different wavelet transforms was found as under:

Images on which the averages were based are labeled below from Fig C1 to C5.

			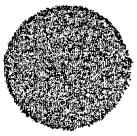	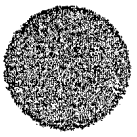
Figure C1	Figure C2	Figure C3	Figure C4	Figure C5

Wavelet name	Defects Per Image	Acceptable average defect number	Standard deviation of defects per image	Maximum acceptable no of defect points
Haar	Image C1 - 38 Image C2 - 27 Image C3 - 31 Image C4 - 26 Image C5 - 47	34	8.75	42.75
Daubechies	Image C1 - 34 Image C2 - 32 Image C3 – 41 Image C4 - 43 Image C5 - 40	38	4.74	42.74
Coiflet*	Image C1 - 51 Image C2 - 49 Image C3 – 50 Image C4 - 52 Image C5 - 45	49	2.70	51.70
Symlet*	Image C1 - 39 Image C2 - 38 Image C3 – 42 Image C4 - 37 Image C5 - 43	40	2.58	42.58

Table 5.1: Results using the first technique. The average acceptable defect number for its respective wavelet is shown in the third column.

• Values are for horizontal detail only. Image integration in these cases generated too much data for them to be of any practical use.

Most of these values represent pseudo-defects present because of the boundary-region pixels.

A ferrule-end with defects found that totaled greater than these values for that respective transform would be rejected as being too deficient to be acceptable for packaging and would be turned back for another round of polishing.

Another observation made was that of defect severity based on gray-level values returned by the transforms in the detail approximations. Using this information a color-

based synthesized image was given shape to aid in the identification of sever defects. Gray-level values representing mild defects having values between 120 and 160 were given the color blue. Similarly intermediate-type defects with values between 160 and 200 were given the color green and values over 200 till 255 were represented with the color red that signified a severe defect. These colors were added only to aid the decision making ability of an individual who would, eventually, determine the products acceptability as a polished end.

The following image (Fig. 5a) show the detail images of a wavelet transform. The horizontal, vertical and diagonal detail images are combined to form a synthesized image. This synthesized image is shown in fig 5b. Fig 5c shows its respective color based image.

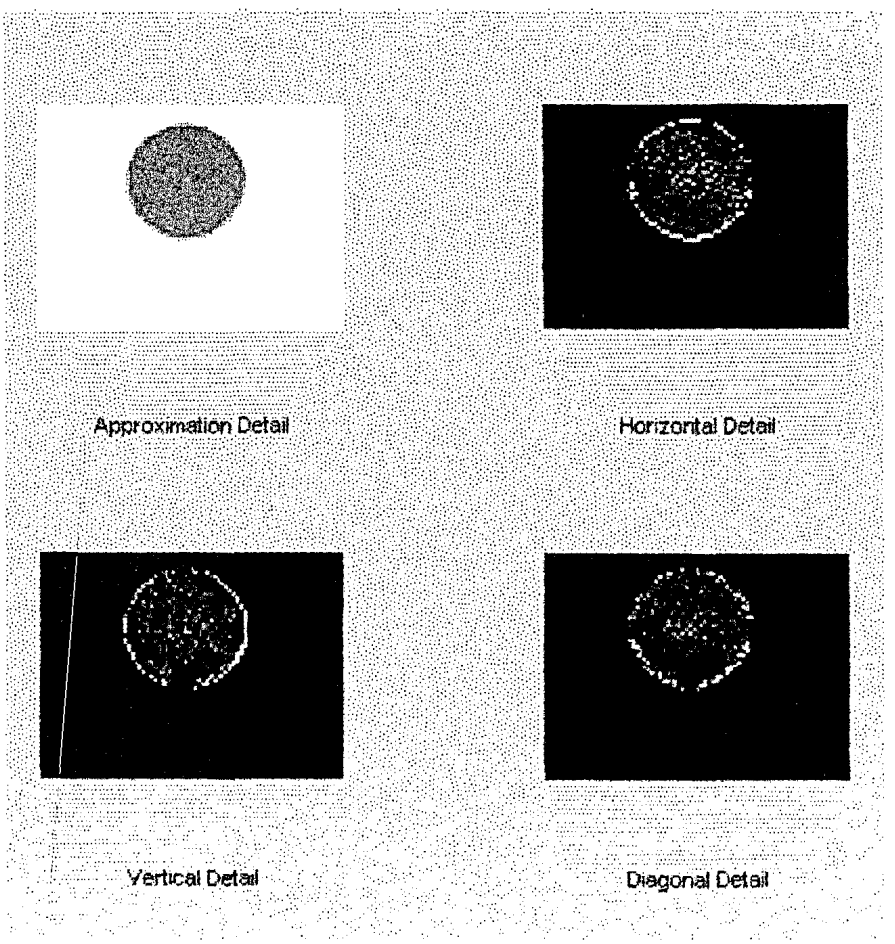

Figure 5a: Daubechies approximation, horizontal, vertical and diagonal details images of the image shown in Fig s-(j).

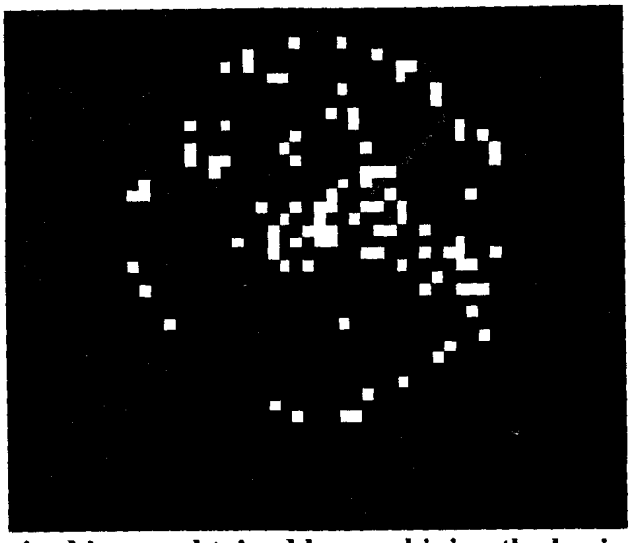

Figure 5b: Synthesized image obtained by combining the horizontal, vertical and diagonal details of images shown in Fig 5a after boundary reduction. Total defect points in this image are 99.

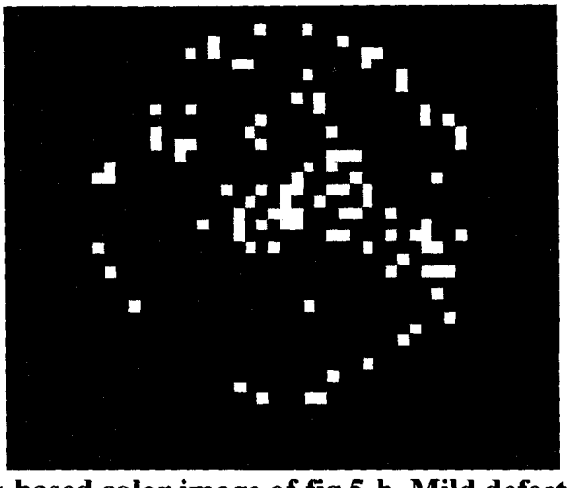

Figure 5c: Severity-based color image of fig 5-b. Mild defects are blue in color, defects of intermediate nature are green and sever defects as red. Notice that the boundary-region pseudo-defects are also visible in red.

Second Approach

The second approach, however, yields better outputs in terms of the number of the boundary pseudo-defects that appear in an output image. In this approach we proceed with the usual wavelet transform of a ferrule image and at the same time take another transform of only the corresponding ferrule boundary area. With both the transforms available, the wavelet transformed boundary images are subtracted from the ferrule image detail images. In other words, the horizontal detail transform of the boundary area is subtracted from the horizontal detail transform of the ferrule image. Similarly the vertical

and diagonal detail transforms of the boundary region are subtracted from their respective ferrule transforms.

Followed by this, and like in the previous approach gray-levels equal to 255 in value are removed as are any pixels with values less than 100. The resultant subtracted detail images are integrated. The results are then displayed. Color codes and schemes used in the previous approach are kept the same. And as summary are categorized below:

Pixel Color	Meaning
■	signifying a sever defect
■	signifying an intermediate defect
■	signifying a mild defect

Results of the new approach are demonstrated below. Image of the ferrule region shown is Fig. s-(j) is subjected to the Daubechies transform. The approximation and detail images of this transform are shown in Fig. 5d.

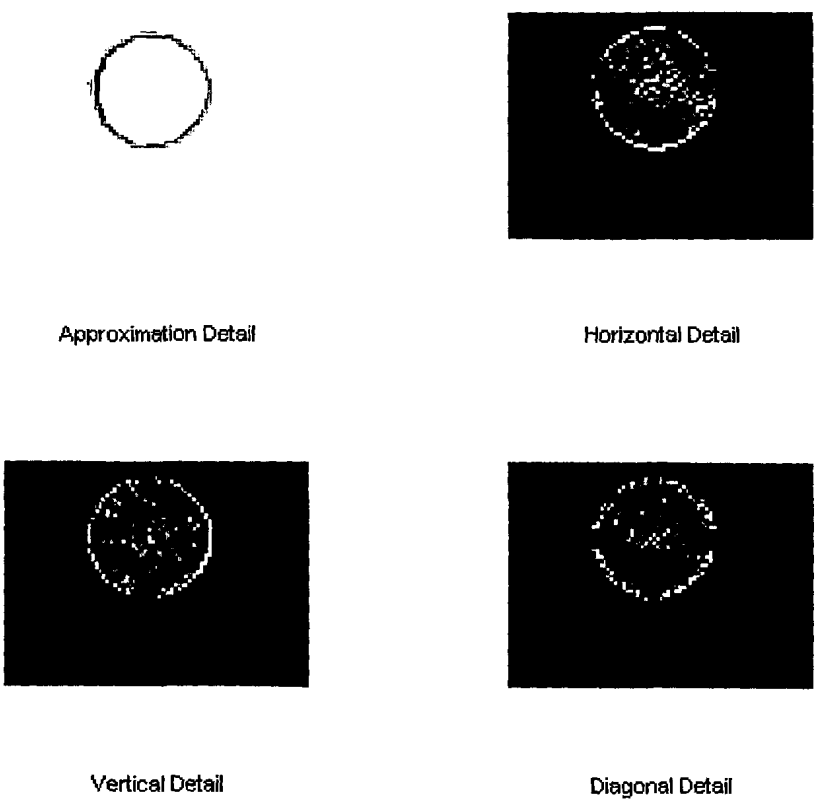

Figure 5d: Daubechies approximation, horizontal, vertical and diagonal detail images of the image shown in Fig s-(j).

The integrated image of the horizontal, vertical and diagonal detail using the new approach is shown in Fig. 5e.

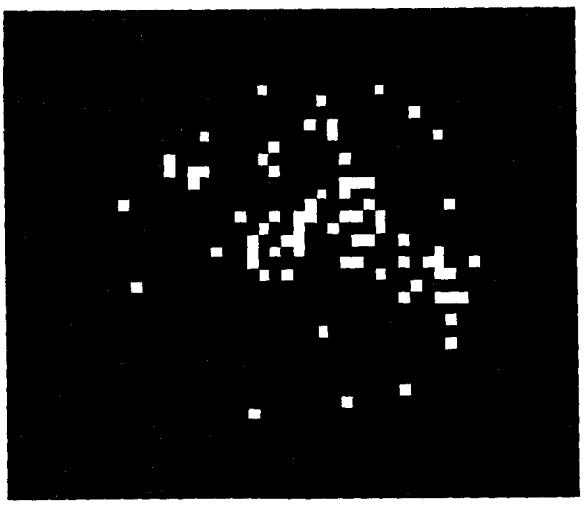

Figure 5e: Synthesized image obtained by combining the border-subtracted horizontal, vertical and diagonal details of images shown in Fig 5d. Total defect points in this image are 73.

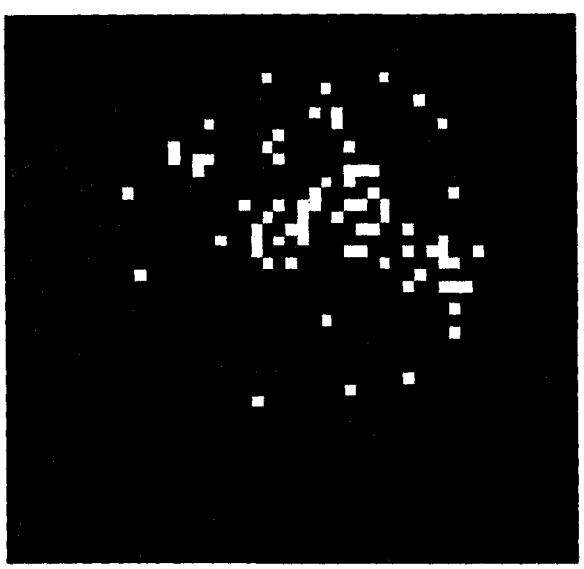

Figure 5f: Severity-based color image of fig 5e. Notice how the boundary pseudo-defects have diminished in number compared to the integrated color image of the transform in Fig 5c. The defect pixels have been successfully retained.

Based on the images labeled C1 to C5 is table 5.2 below. The results are tabulated in a similar manner and contain the defects figures obtained by applying the second approach of border-transform subtraction from the main ferrule wavelet transform.

Wavelet name	Defects Per Image	Acceptable average defect number	Standard Deviation of defects per image	Maximum acceptable no of defect points
Haar	Image C1 - 13 Image C2 - 9 Image C3 - 10 Image C4 - 21 Image C5 – 19	14	5.37	19.37
Daubechies	Image C1 - 9 Image C2 - 13 Image C3 – 16 Image C4 - 21 Image C5 – 10	14	4.87	18.87
Coiflet	Image C1 - 29 Image C2 - 28 Image C3 – 30 Image C4 - 35 Image C5 – 21	29	5.03	34.03
Symlet	Image C1 - 27 Image C2 - 23 Image C3 – 14 Image C4 - 37 Image C5 – 28	26	8.35	34.35

Table 5.2: Results obtained using the second technique. The average acceptable defect number for every respective wavelet is shown in the third column. Notice the decrease in average acceptable defect count from that of Table 5.1.

Table 5.3 shows some results of defective and clean images taken after the application of the second approach.

Image	Wavelet	Defects	Standard Deviation	Max Allowed	Outcome
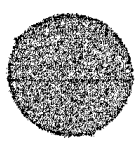	Haar	58	5.73	19.37	Fail
	Daubechies	52	4.87	18.87	Fail
	Coiflet	46	5.03	34.03	Fail
	Symlet	60	8.35	34.35	Fail
	Haar	23	5.73	19.37	Fail
	Daubechies	23	4.87	18.87	Fail
	Coiflet	46	5.03	34.03	Fail
	Symlet	47	8.35	34.35	Fail

	Haar	93	5.73	19.37	Fail
	Daubechies	73	4.87	18.87	Fail
	Coiflet	102	5.03	34.03	Fail
	Symlet	89	8.35	34.35	Fail
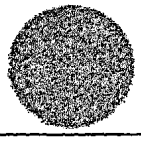	Haar	19	5.73	19.37	Pass
	Daubechies	10	4.87	18.87	Pass
	Coiflet	21	5.03	34.03	Pass
	Symlet	28	8.35	34.35	Pass
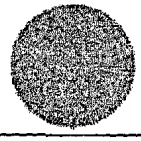	Haar	10	5.73	19.37	Pass
	Daubechies	16	4.87	18.87	Pass
	Coiflet	30	5.03	34.03	Pass
	Symlet	14	8.35	34.35	Pass

Table 5.3: Results of the chosen technique. Images with defects fail the tests while the clean images have passed.

5.4 Conclusion

As is visible from figures 5b, 5c, 5e and 5f, the techniques applied identify defects effectively. And the notable difference between the two approaches is the number of pseudo-defect pixels related to the boundary regions. The results from the two approaches are summarized in Table 5.3 detailing the degree to which the pseudo-defects have been reduced with the use of the second approach.

The first approach involved taking the transform of a ferrule region and combining the detail subbands to get a single image. However, pseudo-defects appeared in the image because of the boundary. This heavily skewed any result data out of the image analysis that this team was wishing to work on. It was also noticed that the boundary pixels in particular had gray-level values well over 200 and as a result were removed. But pseudo-defects still remained and that too in large numbers.

A second approach involved taking a transform of the boundary pixels separately. These respective detail subbands of the boundary were subtracted from the detail subbands of the main ferrule transform. Another interesting aspect to note is that, though the second approach reduced the number of pseudo-defects significantly, it maintained the pixels corresponding to actual defects. There was no handicap of the second approach in terms of effective identification of defects when compared to the first approach.

Another interesting aspect to note is that, though the second approach reduced the number of pseudo-defects significantly, it maintained the pixels corresponding to actual defects. There was no handicap of the second approach in terms of effective identification of defects when compared to the first approach.

Data from Tables 5.1 and 5.2 is compared and summarized in Table 5.3

Wavelet Name	Average acceptable defect number using technique 1	Average acceptable defect number using technique 2	% change for technique 2 (decrease)
Haar	34	14	58.82
Daubechies	38	14	63.16
Coiflet	49	29	40.82
Symlet	40	26	35

Table 5.3: Summary of the results obtained using the first and the second technique. The average acceptable defect numbers for their respective wavelet transforms are shown in the second and third columns. The fourth column lists the % change in terms of pseudo-defects using the two techniques. Notice the significant decrease as a percentage in the number of pseudo-defects obtained by using the second approach.

Based on these results we adopted the second technique. The number of boundary pseudo-defects has significantly been reduced using the second technique. And this approach continues to identify defects effectively.

Different wavelets have given different results. Different wavelets work on images in different ways. Based on information from tables 5.2 and 5.3 we can conclude that the Daubechies wavelet provides more accurate results. It also takes into account greater level of detail. But overall from the techniques applied we have seen that all the wavelets successfully failed the erroneous ends and passed the clean ones.

Appendix A Types of optical fiber connectors

The schemes that we have used here are done on straight/flat tip ferrule connectors. There are however other types of connectors available commercially. A description of these connectors is provided below. These are some of the popular connectors and there is a whole range of other connectors available from different manufacturers.

Short name	Long form
LC	Lucent Connector / Local Connector
ST	Straight Tip
SC	Subscriber Connector / Standard Connector
FC	Ferrule Connector
MT-RJ	Mechanical Transfer Registered Jack
FDDI	Fiber distributed data interface

Obsolete

NEC D4
Optimate
Biconic
SMA
Deutsch 1000

LC (Lucent/Local Connector)

This interface was developed by Lucent Technologies (hence, Lucent Connector). LC is a small form factor connector that uses a 1.25 mm ferrule. It is a standard ceramic ferrule connector, easily terminated with any adhesive. Good performance, highly favored for singlemode. It uses a push-pull mechanism, similar to the SC, and the connector body resembles the squarish shape of SC connectors as well. LC connectors can also be held together in a duplex configuration with a plastic clip.

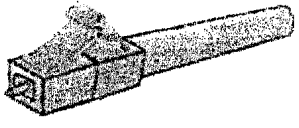

Figure A-1: An LC Connector

ST (Straight Tip Connector)

The ST connector was one of the first connector types widely implemented in fiber optic networking applications. It was developed by AT&T, and for Straight Tip

connector. The connector stays in place with a "twist-on/twist-off" bayonet-style mechanism. ST connectors have ferrule sizes or 2.5 mm and can be mixed and matched to each other using hybrid mating adapters. This makes it convenient to test, since you can have a set of multimode reference test cables with ST or SC connectors and adapt to all these connectors. Although extremely popular for many years, the ST connector is slowly being replaced by smaller, denser connectors.

Figure A-2: a straight tip connector

SC (Subscriber/Standard Connector)

SC connectors use a round 2.5 mm ferrule to hold a single fiber. They use a push-on/pull-off mating mechanism which is generally easier to use. The connector body of an SC connector is squarish, and two SC connectors are usually held together with a plastic clip (this is referred to as a duplex connection). The SC connector was developed in Japan by NTT (telecommunications company)

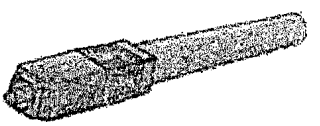

Figure A-3: An SC connector

FC (Fiber Connector)

The FC is one of the most common connector types. The FC is the connector of choice for single-mode, SM & PMF fiber optic components and applications, and in high-speed fiber optic data transfer links. This very precise, ceramic ferrule connector has been equipped with an antirotation key that prevents rotational sensitivity and fiber end face damage. The FC connector is also available in multimode versions.

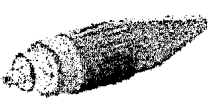

Figure A-4: A FC connector

MT-RJ (Mechanical Transfer Registered Jack)

The MT-RJ connector closely resembles an RJ-style modular plug, even getting part of its name from the resemblance. MT-RJ is a duplex connector with both fibers in a single ferrule. It uses pins for alignment and has male and female versions. The body and ferrule are normally made from plastic or plastic composite, and lock into place with a

tab (just like a modular RJ-style plug). MT-RJ are difficult connectors to test, as most test sets do not allow direct adaptation to the connector.

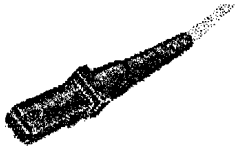

Figure A-5: a MT-RJ connector

FDDI (Fiber Distributed Data Interface)

FDDI stands for Fiber Distributed Data Interface, and it actually refers to a local area network standard such as Ethernet or Token Ring and hence FDDI connectors mate to their specific networks. They are generally used to connect to the equipment from a wall outlet, but the rest of the network will have ST or SC connectors. Since they both use 2.5 mm ferrules, they can be mated to SC or ST connectors with adapters. It may be worthy to note that the FDDI connector is now considered by many to be heading towards obsolescence if not already out-of-date.

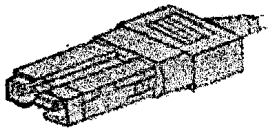

Figure A-6: An FDDI connector

These were some of the more popular connectors and below is a brief description of some of the popular connectors that were considered revolutionary in their times but have since become obsolete.

Obsolete Connectors

NEC D4

The NEC D4 was probably the first connector to use ceramic or hybrid ceramic/stainless steel ferrules. It uses a smaller ferrule than SCs or FCs. It was widely used in telco networks in the 80s to early 90s and some may still be in use.

Optimate

It was developed by AMP and was popular in the early 80s. It used a conical plastic ferrule and screw-on nut. It was available for every fiber size including plastic fiber. Some may still be in use in old military and industrial systems.

Biconic

This connector was developed at Bell Labs. The Biconic was molded from a glass-filled plastic that was almost as hard as ceramic. Since it was not keyed and could rotate in the mating adapters, it had an airgap between the ferrules when mated resulting is sever signal attenuation and hence could not become very popular.

SMA (SubMiniature A)

It was developed by Amphenol and is in use mainly in old military and industrial systems.

Deutsch 1000

Deutsch 1000 was probably the first commercially successful fiber optic connector. It was a "pin vise" holding a stripped fiber. This connector was state of the art in the late 70s for optical fiber systems and has since been rendered obsolete.

The Ferrule

The ferrule is a thin structure (often cylindrical) that actually holds the glass fiber. It has a hollowed-out center that forms a tight grip on the fiber. Ferrules are usually made from ceramic, metal, or high-quality plastic, and typically will hold one strand of fiber. The ferrule also acts as a fiber alignment mechanism. The ferrule is bored through the center at a diameter that is slightly larger than the diameter of the fiber cladding. The end of the fiber is located at the end of the ferrule. Diagrams are shown in figures A-11 and A-12.

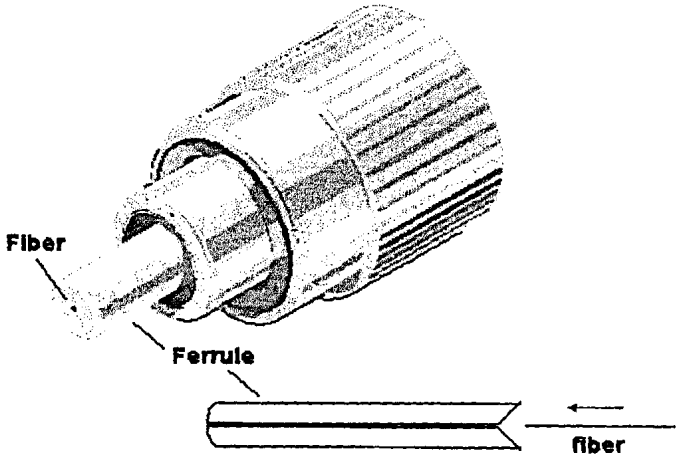

Figure A-11: A typical connector

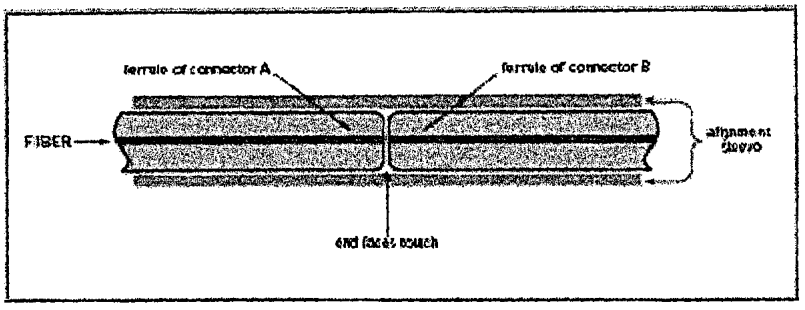

Figure A-12: Cross sectional view of connectors

Ferrule tip-end face preparation

When a connector is terminated on the end of a fiber the end face of the fiber will be shaped.

When one of the standard connectors from the previous section is used the fiber is placed in a ferrule and is polished. There are several ways of polishing. This determines the return loss (RL) or back reflection of the connector.

Flat Polish

The connector tip will be flat which can be a problem when two fibers are mated because even the slightest contamination of the connector tip will result in optical loss. A flat polish of the connector surface will result in a back reflection of about -14.7 dB (4%), when two connectors are mated the RL will be in the area of -11.7 dB.

PC Polish

The Physical Contact (PC) polish gives a slightly curved connector tip forcing the fiber ends of mating connector pairs into physical contact with each other The return loss is around 14.7 dB. This results in back reflections of -30 to -40 dB when mated. The PC polish is the most popular connector end face polish and used in most applications.

SPC Polish

The Super PC (SPC) polish also called ultra polish (UPC), is the result of improved polishing processes and verifying measurements. These connectors have a smoother surface resulting in back reflections of -40 to -55 dB when mated. Unmated the RL is again 14.7 dB. This polish is used in highspeed, digital fiber optic transmission systems, for single mode fiber.

APC Polish

The Angled PC (APC) polish, adds an eight or nine-degree angle to the connector end face. Back reflections of <-60 dB can routinely be accomplished with this polish. Other angles are possible but not standard. This polish is not intermatable with the others.

Etching

It is possible to alter the NA of a conventional fiber with the use of an etching process. With etching one can create a lens at the fiber tip and therefore improve the coupling parameters of a fiber.

Laser cleaving

Polishing is a time consuming process so to reduce the time needed to produce connectors manufactures are looking for alternatives. The use of a laser is a very promising alternative. The laser allows one to create a scratchs and digs free fiber end face due to the fact that the quartz is vaporized. Also, it is possible to create a cylindrical lens on the fiber end face and improve the diode-laser fiber coupling efficiency [15].

Different shapes are shown in Fig A-13.

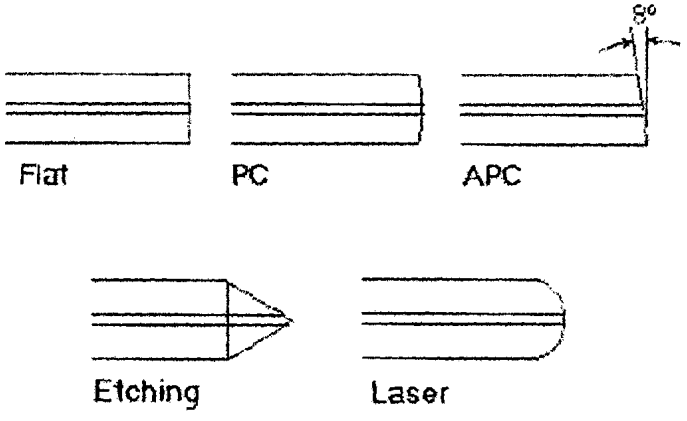

Figure A-13: Different end-face preparations

And the tip-ends of the ferrule types are shown in Fig. A-14.

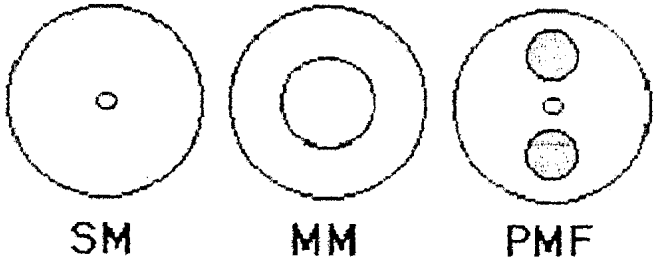

Figure A-14: Different types of ferrule-tip ends

References

[1] R. C. Gonzales and R. E. Woods, *Digital Image Processing* 2nd edition, Prentice-Hall, 2002.

[2] J. R. Parker, *Practical Computer Vision Using C*, John Wiley & Sons, 1993.

[3] http://www.corningcables.com

[4] William Stallings, *Data and Computer Communications*, 6th Edition, Prentice-Hall, 2000.

[5] Scott E. Umbaugh, *Computer Vision and Image Processing*, Prentice-Hall, 1999.

[6] R. Crandall, *Projects in Scientific Computation*, Springer-Verlag, New York, 1994.

[7] Robi Polikar Wavelet Tutorial
http://users.rowan.edu/~polikar/WAVELETS/WTtutorial.html

[8] G. Kaiser, *A Friendly Guide to Wavelets*, Birkhauser, Boston, 1994.

[9] G. Strang, "Wavelets", *American Scientist*, vol. 82, 1992, pp. 250-255.

[10] M. Vetterli and C. Herley, "Wavelets and Filter Banks: Theory and Design," *IEEE Transactions on Signal Processing*, Vol. 40, 1992, pp. 2207-2232.

[11] A. Graps, "An Introduction to Wavelets," *IEEE Computational Science and Engineering*, 1995, vol. 2, num 2, Los Alamitos.

[12] S. Mallat, "A compact Multiresolution Representation: The Wavelet Model," *Proc. IEEE Computer Society Workshop on Computer Vision*, IEEE Computer Society Press, Washington D.C., 1987, pp. 2-7.

[13] W. Press et al., *Numerical Recipes in Fortran*, Cambridge University Press, 1992.

[14] H. M. Elbehiery, A. A. Hefnawy and M. T. Elewa, "Visual Inspection for Fired Ceramic Tile's Surface Defects using Wavelet Analysis," *IEEE Trans.*, ICENCO, Cairo University, Cairo, Egypt, December 2004.

[15] I. P. Stroobach, *IPSE Ingenieursbureau.*, Eindhoven, 2005 IPSE uitgave.

[16] G. Strang and T. Nguyen, *Wavelets and Filter Banks*, Wellesley-Cambridge Press, 1996.

[17] P. J. Burt and E. H. Adelson, "The Laplacian Pyramid as a Compact Image Code," *IEEE Trans. Commun.*, no. 4, 1983.

[18] Jr. R. W. Tucker, S. W. Kercel and V. K. Varma, "Characterization of Gas Pipeline Flaws using Wavelet Analysis," *6th Int'l conf. on Quality Control by Artificial Vision*, Proceedings of the SPIE, 2003.

[19] H. Elbehiery, A. Hefnawy and M. Elewa, "Surface Defects Detection for Ceramic Tiles using Image Processing and Morphological Techniques," *Trans. On Engineering, Computing and Technology*, Enformatica, 2005.

[20] P. Meinlschmidt, "Thermographic detection of defects in wood and wood-based materials," *14th Int'l symposium on nondestructive testing of wood*, Hannover, 2005.

[21] Applications Engineering Note, Multimode Optical Fiber Connectors with Polymer Ferrules, revision 3, AEN 73, Oct. 2002.

[22] D. A. Karras, S. A. Karkanis, D. K. Lakovidis, D. E. Maoulis, B. G. Mertzios, "Improved Defect Detection in Manufacturing using Novel Multidimensional Wavelet Feature Extraction Involving Vector Quantization and PCA Techniques," *8th Panhellenic Conf. on Information*, 2001.

[23] P. F. Odgaard and M. V. Wicherhauser, "Discrimination between different kind of surface defects on compact discs," Accepted by proceedings of IECON, Busan, 2004.

[24] Serdaroglu, A., A. Ertuzun, and A. Ercil, "Defect detection in textile fabric images using wavelet transforms and independent component analysis," *Pattern Recognition and Image Understanding: New Technologies, PRIA-7-2004,* Oct. 18-23, 2004, St. Petersburg, Russia.

[25] P. F. Odgaard, J. Stoustrup and M. V. Wickerhauser, "Wavelet Packet Based Detection Of Surface Faults On Compact Discs," *6th (IFAC) Symposium on Fault Detection, supervision and Safety of Technical Processes,* 30 Aug. 2006, pp. 1165–1170, Beijing, China.

Optical Fiber Connector Surface Defect Detection Using Wavelets

Atique Rehman*‡, Waheed Bin Mozaffar*‡‡
*International Islamic University, Islamabad
‡atique.rehman@gmail.com, ‡‡waheed.bin.mozaffar@gmail.com

Abstract

In this paper, a wavelet-based surface defect detection of optical fiber ferrules is proposed. Surface defects on optical fiber connectors can be damaging to passing signals when coupled with other connectors. Our quality control enhancement work is a visual control stage, using magnified images, whereby morphological operations segment the image and wavelet transforms then detect defects on optical fiber connector surfaces to improve the overall acceptability of the manufactured components.

1. Introduction

Optical fiber connector surfaces have received very little attention in terms of defects that can and do appear over them due to mandatory undergoing of a process called polishing. Optical fiber itself has gone through a continuing evolution of several decades now but, without splices and connectors would not be of much practical use. Much like any other communication media, optical fibers have to be cut and connected to other optical fiber ends. This introduces the role of the connector.

The connector has an alignment mechanism, which also mounts the fiber, in a long, thin cylindrical shape, called the ferrule. The ferrule of the connector (with the fiber housed) is then polished using specialized equipment to achieve a good optical finish. This processing of the end-face is one of the most important steps in the process of preparing a connector for coupling. It will determine the ferrule-end geometry and will set the characteristics of the connector like return loss performance, physical contact, dome radius, dome offset, fiber protrusion or undercut and angle [5]. Diagram of a typical connector and its ferrule part is shown in Fig 1.

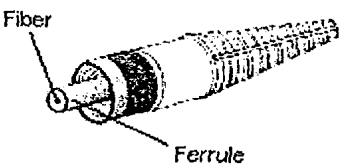

Figure 1. A typical singlemode flat ST (straight tip) connector.

Incorrect polishing will result in lips and hackles, blobs and scratches and other forms of defects on the surface-tip of the ferrule. Fiber cores inside the connectors are coupled very precisely to other connecting fibers to minimize attenuation as light propagates between the cores of two separate connectors. It is important to note that fiber cables transmit pulses of light instead of electrical signals, so the terminations must be more precise. Instead of allowing metal pins to make metal-to-metal contact, fiber optic connectors must align microscopic glass fibers perfectly. Attenuation of a coupled connector pair is directly related to the polish, contact area and alignment of the cores. Hence, these defects are detrimental to the signal that passes through the coupled pair [1][4][5]. A polished multimode ferrule end is shown in Fig 2.

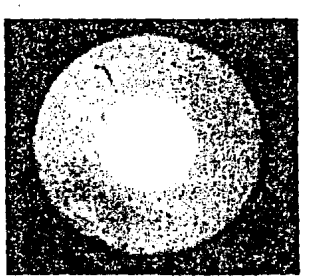

Figure 2. Polished multimode ferrule end with large central core.

These ferrule ends are very miniscule and, for them to be of any use in terms of defect detection, require magnification of the scale beyond the capabilities of the human eye. Specialized equipment captures and magnifies images of the ferrule-end to a size that is easily discernable by human beings. These images can then be fed to visual systems for desired processing.

Therefore, in this paper, we aim to create a visual system that is capable of detecting defects on the connectors' ferrule surface, once the ferrule region has been segmented from the main image.

Moreover, the presented inspection procedures have been implemented and tested on a number of connectors using real and mock defects. Examining such tasks can of course be uninteresting, skewed and expensive, but it is based on the unparalleled recognition abilities of the human brain. However, with the use of automated systems, production and quality control teams can specify the test criteria and quality management teams may then decide which connector ends to filter out and ones which to keep. One of its advantages is that the automated systems are flexible in regard to production changes and testing criteria. That makes them simple to operate and give a good overview. By looking at the results, we found them highly suitable for providing a rapid feedback in the production process.

This paper has two major sections that follow this introduction; sections 3 and 4. Section 3 discusses image segmentation using morphological techniques and section 4 discusses use of the wavelet transform to detect defects on the surfaces of these connectors.

2. Image acquisition

Images have been acquired using specialized cameras used in industrial quality control departments. Image acquisition of these connector surfaces is unfazed by gloss-related problems that may appear due to polishing or glazing operations that hamper the accurate detection of surface defects of certain items in the industry [3]. The captured images are converted to grayscale and binary forms to be suitable for use with various algorithms that are used to segment areas of interest in such images. There are other such similar tools that may be used to acquire these images [5].

3. Image segmentation

The flowchart of the ferrule region extraction is shown in Fig 3. The images in question have a special range of colors, distinctive from most other natural images (Fig. 4a.) Their contrasting colors give the images two very distinct segments – the foreground and the background. The foreground consists of the circular ferrule, which is grayish and darker in color and also contains the central core (fiber.) The background, which is relatively much lighter in color, is part of the polishing machine and holds the connector tip in place during the actual polishing. Because the image contains such distinctive segments, it also has very pronounced edges (see Fig 4b.)

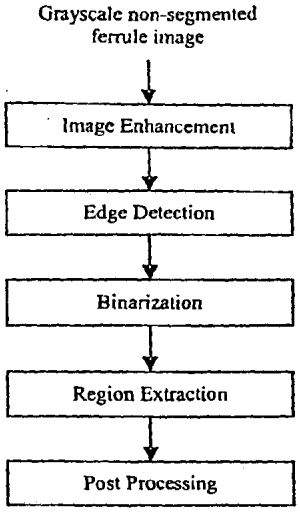

Figure 3. Image segmentation flowchart.

However, before the image is segmented, we apply a spatial image enhancement filter. We tried several filters but the best results were obtained when we applied the spatial high-boost filter to enhance this image as is also described in [1].

The image was then passed through an edge detection algorithm to highlight the edges of the segments with a kernel size of 3x3.

The edge-detection algorithm successfully highlights the desired boundary-area of the ferrule, as can be seen in Fig. 4b.

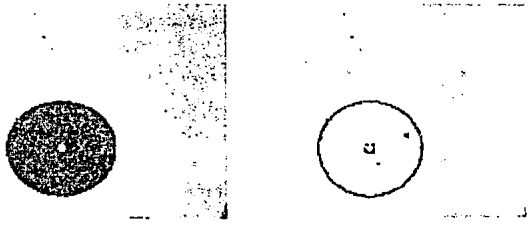

Figure 4. (a) Connector ferrule with central core and light colored background; and (b) The ferrules pronounced edges after convolving with an edge-detector

The shape of the ferrule region is unique and consistent. Therefore, the outline of the ferrule region can therefore be approximated by a circle and attributes associated with circles can be used to obtain useful information about the circular region. Once the edges are detected, machine vision techniques are used to convert the image to a bi-level form from grayscale, using a threshold value calculated using the iterative method.

The idea here is to provide an estimate of the average grey level of both, the background (Tb) and the objects (To), and to use the average of these two levels as the threshold: T=(To+Tb)/2. Because the properties of the image are known (darker foreground and lighter background), initial values chosen are To=0, and Tb=255.

Once the bi-level image is obtained, the area of the region inside the circular region is calculated using the technique, as mentioned in [2]. The center of mass C is also calculated as (Cr, Cc), where Cr is the center row and Cc is the center column of the circular object. Cr and Cc can be computed as:

$$Cr = \frac{\sum_{Row=1}^{NR} \sum_{Col=1}^{NC} F(row,col).row}{area\ (F)} \quad (1)$$

$$Cc = \frac{\sum_{Row=1}^{NR} \sum_{Col=1}^{NC} F(row,col).col}{area\ (F)} \quad (2)$$

(where *area (F)* is the number of pixels of the object. NR and NC are the Number or Rows and Number of Columns of the object, respectively.)

The unique property of the central core (being very small in area) is that it is also the very center of the ferrule region that encloses it. This information is used in conjunction with the center of mass value to establish the central point of the circular region (which is also aided by the fact that the core is much lighter in color than the ferrule region that encloses it). A seed pixel is chosen that is then grown outwards, recursively, towards the boundary from the center. Once the central circular region is fully grown, it is able to provide a form of template that is then used to extract the circular region from the main image (Fig. 5b).

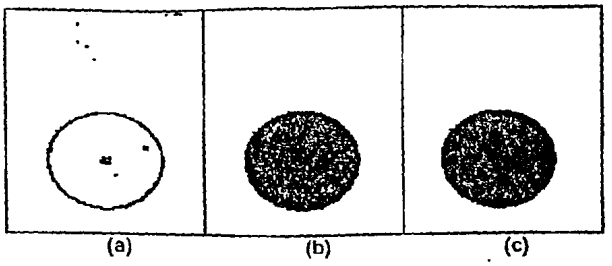

Figure 5. (a) Binary image obtained based on an iterative threshold; (b) template that has been grown; and (c) ferrule obtained based on the grown template.

Other segments that appear in the background area are highlighted and removed from the image on the basis of their overall area (see Fig. 5b).

Based on the template that has just been grown, the ferrule segment of the image is successfully obtained. Fig. 5c shows a successfully segmented ferrule region.

Fig. 6 shows some more results obtained by applying our technique.

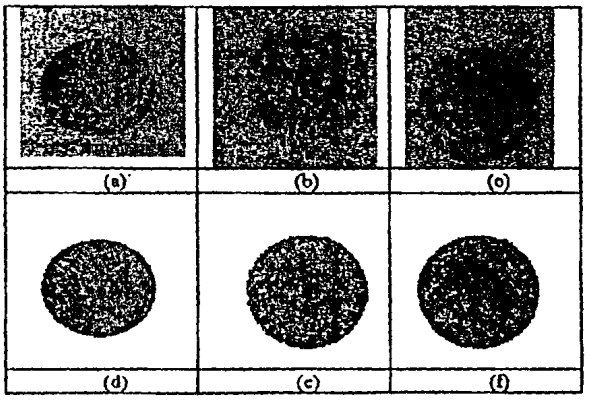

Figure 6. Ferrule tips of varying size with respective segmented ferrule regions (a-d,b-e,c-f)

4. Defect detection based on wavelet coefficients

Wavelets are mathematical functions that cut up data into different frequency components, and then study each component with a resolution matched to its scale. They have advantages over traditional Fourier methods in analyzing physical situations where the signal contains discontinuities and sharp spikes [3].

It is possible to find the surface faults from the disturbances in time and/or frequencies only, but the wavelet transform provides added benefits that elude one or the other domains. It might be useful to use a

joint time and frequency method [10]. Here we use different wavelet transforms to identify the surface faults from the other features of the ferrule, and, thereby, detect the surface defects.

Unlike Fourier transform, whose basis functions are sinusoids, wavelet transforms are based on small waves called wavelets of varying frequency and limited duration. Wavelets take advantage of the image pyramid, which is a conceptually simple structure representing an image at more than one resolution, and the multiresolution theory (Mallat [1987]). The appeal of such an approach is obvious – features that might go undetected at one resolution may be easy to spot at another. At every level, the image is down sampled and decomposed. Optimal decomposition is eventually determined by the Heisenberg Uncertainty Principle [14].

Wavelet transform, in our method, is used for a more obvious reason – little impulsive reaction to similar data, i.e., the regions of little variation in the original data manifest themselves as small or zero elements in the wavelet transformed version. Therefore an irregularity in the image will have a more pronounced effect in the outcome of the wavelet transform.

Use of Wavelet Packets

The decomposition of a signal can be done via the conventional method of wavelet transform and is called as *pyramid structured wavelet transform* [8]. Each time the low frequency band is split, the other bands are not used. This is suitable for signals with most of their energy concentrated in the low frequency regions. However, for some signals, energy is concentrated at the middle frequencies. In this case, we have to split all the bands. This is called as *wavelet packet decomposition* [9].

The wavelet bases constructed by Haar, Daubechies became the foundation for one of the most popular techniques for signal analysis and representation in a wide range of applications [3]. We applied two kinds of wavelet decomposition types (Haar and Daubechies) on different connectors to identify the defects on the surface of the polished ferrule, with the eventual aim of identifying defects on the surfaces using wavelet transforms.

Before we analyze the results of the wavelets that we used, a brief description of wavelets is provided below.

A. The Continuous Wavelet Transform

The continuous wavelet transform (CWT) is defined as the sum over all time of the signal, multiplied by scaled, shifted versions of the wavelet function ψ:

$$CO(scale, position) = \int f(t)\psi(scale, position, t)dt \qquad (3)$$

The results of the CWT are many wavelet coefficients *CO*, which are a function of scale and position. Multiplying each coefficient by the appropriately scaled and shifted wavelet yields the constituent wavelets of the original signal [6]. Wavelet analysis for the signals to different scales and positions is shown in Fig 7.

If the signal is a function of a continuous variable and a transform that is a function of two continuous variables is desired, then the continuous wavelet transform (CWT) can be defined by (equation 4):

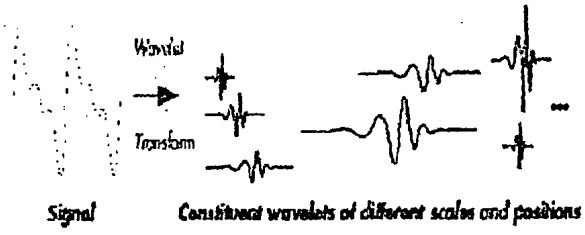

Figure 7. Wavelet analysis for signals

$$F(a,b) = \int f(t)\omega((t-a)/b) \qquad (4)$$

With an inverse transform of,

$$f(t) = \iint F(a,b)\omega((t-a)/b)dadb \qquad (5)$$

Where $\omega(t)$ is the basic wavelet and (a, b *belong to* R) are real continuous variables.

B. Discrete Wavelet Transform Algorithms

An awful lot of data is generated and quite a fair amount of work is required if wavelet coefficients are to be calculated at every possible scale. (What if we choose only a subset of scales and positions at which to make our calculations?) It turns out, rather remarkably, that if we choose scales and positions based on powers of two, so called dyadic scales and positions, then our analysis will be much more efficient and just as accurate. We obtain such decomposition from the discrete wavelet transform (DWT) [7]. Decomposition is usually large enough to provide enough discrimination power but not so large as to make the computation time prohibitively large.

Given a signal s of length N, the DWT consists of $\log_2 N$ stages at most. Starting from s, the first-step produces two sets of coefficients: approximation coefficients cA_1, and detail coefficients cD_1. These vectors are obtained by convolving s with the low-pass filter Lo_D for approximation, and with the high-pass

filter Hi_D for detail, followed by dyadic decimation. This is shown in Fig 8.

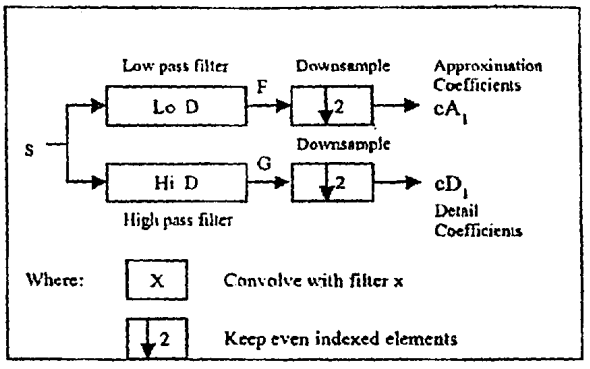

Figure 8. General algorithm for discrete wavelet transforms

The next step splits the approximation coefficients cA_1 in two parts using the same scheme, replacing s by cA_1 and producing cA_2 and cD_2, and so on. Therefore, the wavelet decomposition of the signal s analyzed at level j has the following structure: $[cA_j, cD_j, ..., cD_1]$ (Fig. 9). This way the structure will also contain terminal nodes in the form of a tree [6][11][12].

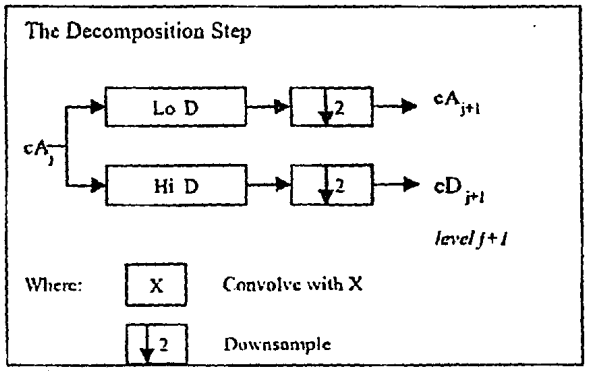

Figure 9. One dimensional DWT

C. Fast Wavelet Transform (FWT)

In 1988, Mallat produced a fast wavelet decomposition and reconstruction algorithm. The Mallat algorithm for discrete wavelet transform is, in fact, a classical scheme in the signal processing community, known as a two-channel sub-band coder using conjugate quadrature filters or quadrature mirror filters (QMF). The decomposition algorithm starts with signal s, next calculates the coordinates of A_1 and D_1, and then those of A_2 and D_2, and so on. The reconstruction algorithm, called the inverse discrete wavelet transform (IDWT), starts from the coordinates of A_j and D_j, next calculates the coordinates of A_{j-1}, and then, using the coordinates of A_{j-1} and D_{j-1}, calculates those of A_{j-2}, and so on [13].

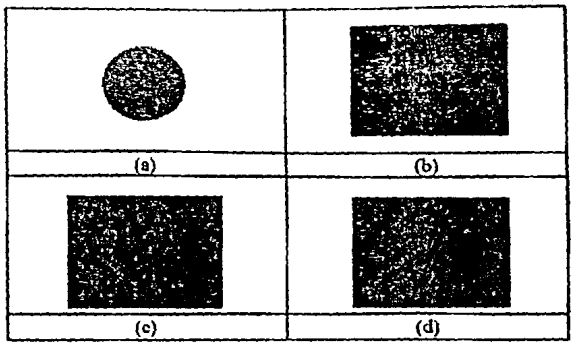

Figure 10. (a) Approximation image of the ferrule part shown in Fig. 6f, (b) Horizontal detail image, (c) Vertical detail and (d) Diagonal detail obtained using the Haar transform

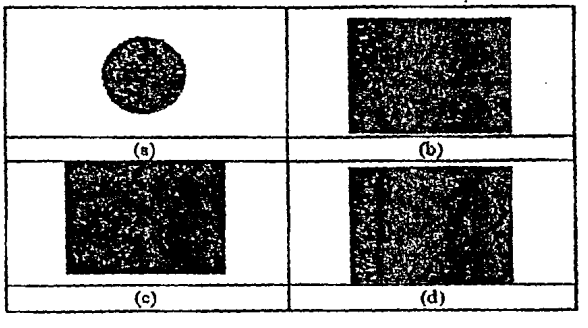

Figure 11. (a) Approximation image of the ferrule part shown in Fig. 6f, (b) Horizontal detail image, (c) Vertical detail and (d) Diagonal detail obtained using the Daubechies 4-tap transform

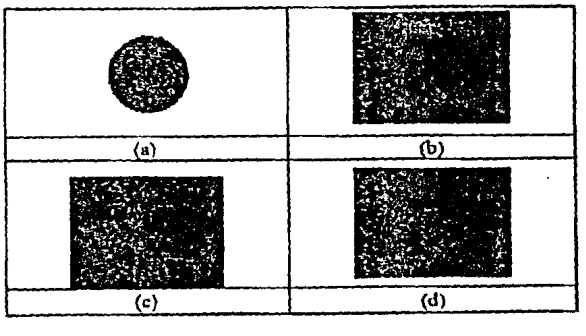

Figure 12. (a) Approximation image of the ferrule part shown in Fig. 6e (b) Horizontal detail image, (c) Vertical detail and (d) Diagonal detail obtained using the Haar transform

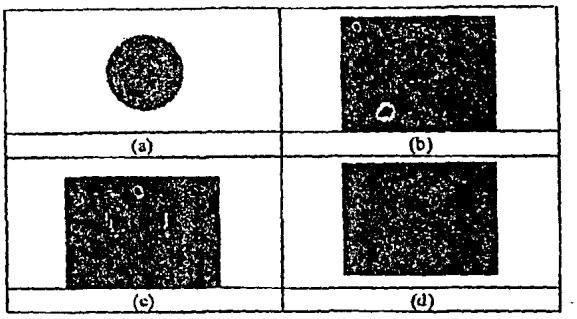

Figure 13. (a) Approximation image of the ferrule part shown in Fig. 6e, (b) Horizontal detail image, (c) Vertical detail and (d) Diagonal detail obtained using the Daubechies 4-tap transform

5. Results

We applied the Haar and Daubechies wavelets to our segmented images using Matlab. Both effectively identified the defects with the Daubechies giving the better of the two results. However, there is one thing to note. Although the results obtained identified the defects pretty successfully, outer boundary areas of the ferrule region also produced sharp discontinuities in the transformed version. Since these are farthest from the central core, they may be eliminated based on their radius value from the center of the ferrule.

Figures 10 through 13 show some results. Fig. 10 and Fig. 12 show the coefficients obtained using the Haar wavelet transform, while Fig. 11 and Fig. 13 do the same for the Daubechies transform.

The results of this project have basically been achieved with some major simplifications compared to the solutions that might be required for a commercial product. An automated system's main advantage, compared with a manual system, is in its ability to speed up the testing process.

We used our techniques on 12 images with different defects. Some of the images were without the central core. Some were plain and flawless. We found that different types of wavelets provided different results. In our scenario the Daubechies filters provided the best results. Detail coefficients of Fig. 10 and Fig. 12 (horizontal, vertical and diagonal details) were calculated using the Haar wavelets. Similarly detail coefficients of Fig. 11 and Fig. 13 were calculated using the Daubechies 4-tap wavelets. The latter have provided better results and have to quite a good extent been able to identify the defects. Image analysis was done using the Matlab software (version 7).

6. Acknowledgment

The authors would like to acknowledge the support of Dr. Muid Mufti of University of Engineering and Technology, Taxila for the images.

7. References

[1] R. C. Gonzales and R. E. Woods, *Digital Image Processing* 2nd ed., Prentice-Hall, 2002.

[2] J. R. Parker, *Practical Computer Vision Using C*, John Wiley & Sons, 1993.

[3] H. M. Elbehiery, A. A. Hefnawy and M. T. Elewa, "Visual Inspection for Fired Ceramic Tile's Surface Defects using Wavelet Analysis," *IEEE Trans.*, ICENCO, Cairo University, Cairo, Egypt, December 2004.

[4] Applications Engineering Note, Multimode Optical Fiber Connectors with Polymer Ferrules, revision 3, AEN 73, Oct. 2002.

[5] I. P. Stroobach, *IPSE Ingenieursbureau.*, Eindhoven, 2005 IPSE uitgave.

[6] J. Benedetto and M. Frazier, "Wavelets: Mathematics and Applications." CRC, 1993, Japanese translation of selected by M. Yamaguti, M. Yamada, Springer, 1996

[7] S. Liapis, N. Alvertos, and G. Tziritas, "Maximum likelihood texture classification and Bayesian texture segmentation using Discrete Wavelet Frames," Institute of computer Science, and Department of Computer Science, University of Crete, Greece press, 1994.

[8] T. Chang, J. Kuo, "Texture Analysis and Classification with Tree-Structured Wavelet Transform," *IEEE Transactions on Image processing*, Vol.2, No.4, pp. 429-441, October, 1993.

[9] Serdaroglu, A., A. Ertuzun, and A. Ercil, "Defect detection in textile fabric images using wavelet transforms and independent component analysis," *Pattern Recognition and Image Understanding: New Technologies, PRIA-7-2004,* Oct. 18-23, 2004, St. Petersburg, Russia.

[10] P. F. Odgaard, J. Stoustrup and M. V. Wickerhauser, "Wavelet Packet Based Detection Of Surface Faults On Compact Discs," *6th (IFAC) Symposium on Fault Detection, supervision and Safety of Technical Processes,* 30 Aug. 2006, pp. 1165-1170, Beijing, China.

[11] P. J. Laurent, and A. K. Peter, "Wavelets, Images and Surface fitting," Pattern Recognition Letters, Vol. 15, pp337-339, 1994.

[12] E.J. Stollnitz, T. DeRose, and D. Salesin," *Wavelets for Computer Graphics*," Morgan Kaufmann Publishers, 1996.

[13] M. Kobayashi, "Wavelets and their Applications," Case Studies, SIAM Press (Society for Industrial and Applied Mathematics), 1998.

[14] G. Strang and T. Nguyen, *Wavelets and Filter Banks*, Wellesley-Cambridge Press, 1996